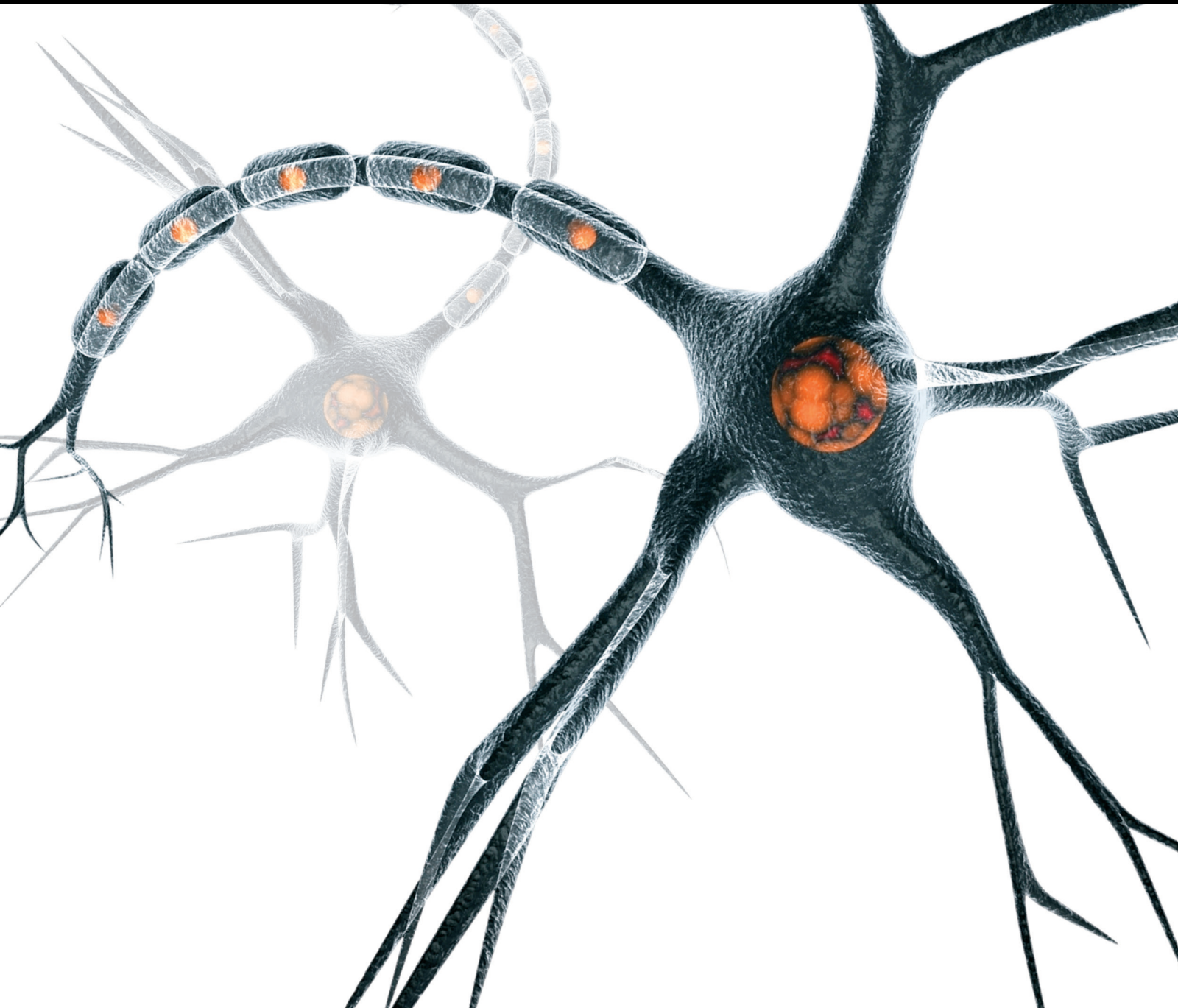


Synaptic Plasticity in Age-Related Disorders

Lead Guest Editor: Luca Marsili

Guest Editors: Marco Canevelli and Tommaso Schirizzi



Synaptic Plasticity in Age-Related Disorders

Neural Plasticity

Synaptic Plasticity in Age-Related Disorders

Lead Guest Editor: Luca Marsili

Guest Editors: Marco Canevelli and Tommaso Schirinzi



Copyright © 2020 Hindawi Limited. All rights reserved.

This is a special issue published in "Neural Plasticity" All articles are open access articles distributed under the Creative Commons Attribution License, which permits unrestricted use, distribution, and reproduction in any medium, provided the original work is properly cited.

Chief Editor

Michel Baudry, USA

Associate Editors

Nicoletta Berardi , Italy
Malgorzata Kossut, Poland

Academic Editors

Victor Anggono , Australia
Sergio Bagnato , Italy
Michel Baudry, USA
Michael S. Beattie , USA
Davide Bottari , Italy
Kalina Burnat , Poland
Gaston Calfa , Argentina
Martin Cammarota, Brazil
Carlo Cavaliere , Italy
Jiu Chen , China
Michele D'Angelo, Italy
Gabriela Delevati Colpo , USA
Michele Fornaro , USA
Francesca Foti , Italy
Zygmunt Galdzicki, USA
Preston E. Garraghty , USA
Paolo Girlanda, Italy
Massimo Grilli , Italy
Anthony J. Hannan , Australia
Grzegorz Hess , Poland
Jacopo Lamanna, Italy
Volker Mall, Germany
Stuart C. Mangel , USA
Diano Marrone , Canada
Aage R. Møller, USA
Xavier Navarro , Spain
Fernando Peña-Ortega , Mexico
Maurizio Popoli, Italy
Mojgan Rastegar , Canada
Alessandro Sale , Italy
Marco Sandrini , United Kingdom
Gabriele Sansevero , Italy
Menahem Segal , Israel
Jerry Silver, USA
Josef Syka , Czech Republic
Yasuo Terao, Japan
Tara Walker , Australia
Long-Jun Wu , USA
J. Michael Wyss , USA

Lin Xu , China



Contents

Aging Alters Olfactory Bulb Network Oscillations and Connectivity: Relevance for Aging-Related Neurodegeneration Studies

A. Ahnaou , D. Rodriguez-Manrique, S. Embrechts, R. Biermans, N. V. Manyakov , S. A. Youssef, and W. H. I. M. Drinkenburg




Research Article (17 pages), Article ID 1703969, Volume 2020 (2020)

Memory and Cognition-Related Neuroplasticity Enhancement by Transcranial Direct Current Stimulation in Rodents: A Systematic Review

Carla Cavaleiro, João Martins, Joana Gonçalves , and Miguel Castelo-Branco 


Review Article (23 pages), Article ID 4795267, Volume 2020 (2020)

Electroacupuncture Improved Chronic Cerebral Hypoperfusion-Induced Anxiety-Like Behavior and Memory Impairments in Spontaneously Hypertensive Rats by Downregulating the ACE/Ang II/AT1R Axis and Upregulating the ACE2/Ang-(1-7)/MasR Axis

Peipei Feng, Zemin Wu, Hao Liu, Yafang Shen , Xu Yao, Xinwei Li , and Zui Shen 



Research Article (12 pages), Article ID 9076042, Volume 2020 (2020)

The Long-Term Effects of Acupuncture on Hippocampal Functional Connectivity in aMCI with Hippocampal Atrophy: A Randomized Longitudinal fMRI Study

Hui Li, Zhiqun Wang, Haikuo Yu, Ran Pang, Hong Ni, Chiang-shan R. Li, and Kuncheng Li 

Research Article (9 pages), Article ID 6389368, Volume 2020 (2020)

Changes in the Fluorescence Tracking of NaV1.6 Protein Expression in a BTBR T+Itpr3tf/J Autistic Mouse Model

Musaad A. Alshammari, Mohammad R. Khan, Fawaz Alasmari , Abdulaziz O. Alshehri, Rizwan Ali, Mohamed Boudjelal, Khalid A. Alhosaini, Abdurahman A. Niazy, and Tahani K. Alshammari 

Research Article (12 pages), Article ID 4893103, Volume 2019 (2019)

Research Article

Aging Alters Olfactory Bulb Network Oscillations and Connectivity: Relevance for Aging-Related Neurodegeneration Studies

A. Ahnaou ¹, D. Rodriguez-Manrique,¹ S. Embrechts,¹ R. Biermans,¹ N. V. Manyakov ¹, S. A. Youssef,² and W. H. I. M. Drinkenburg¹

¹Department of Neuroscience, Janssen Research & Development, a Division of Janssen Pharmaceutica NV, Turnhoutseweg 30, B-2340 Beerse, Belgium

²Department of Non-Clinical Safety, Janssen Research & Development, a Division of Janssen Pharmaceutica NV, Turnhoutseweg 30, B-2340 Beerse, Belgium

Correspondence should be addressed to A. Ahnaou; aahnaou@its.jnj.com

Received 6 December 2019; Revised 27 January 2020; Accepted 12 February 2020; Published 2 May 2020

Guest Editor: Luca Marsili

Copyright © 2020 A. Ahnaou et al. This is an open access article distributed under the Creative Commons Attribution License, which permits unrestricted use, distribution, and reproduction in any medium, provided the original work is properly cited.

The aging process eventually cause a breakdown in critical synaptic plasticity and connectivity leading to deficits in memory function. The olfactory bulb (OB) and the hippocampus, both regions of the brain considered critical for the processing of odors and spatial memory, are commonly affected by aging. Using an aged wild-type C57B/6 mouse model, we sought to define the effects of aging on hippocampal plasticity and the integrity of cortical circuits. Specifically, we measured the long-term potentiation of high-frequency stimulation (HFS-LTP) at the Shaffer-Collateral CA1 pyramidal synapses. Next, local field potential (LFP) spectra, phase-amplitude theta-gamma coupling (PAC), and connectivity through coherence were assessed in the olfactory bulb, frontal and entorhinal cortices, CA1, and amygdala circuits. The OB of aged mice showed a significant increase in the number of histone H2AX-positive neurons, a marker of DNA damage. While the input-output relationship measure of basal synaptic activity was found not to differ between young and aged mice, a pronounced decline in the slope of field excitatory postsynaptic potential (fEPSP) and the population spike amplitude (PSA) were found in aged mice. Furthermore, aging was accompanied by deficits in gamma network oscillations, a shift to slow oscillations, reduced coherence and theta-gamma PAC in the OB circuit. Thus, while the basal synaptic activity was unaltered in older mice, impairment in hippocampal synaptic transmission was observed only in response to HFS. However, age-dependent alterations in neural network appeared spontaneously in the OB circuit, suggesting the neurophysiological basis of synaptic deficits underlying olfactory processing. Taken together, the results highlight the sensitivity and therefore potential use of LFP quantitative network oscillations and connectivity at the OB level as objective electrophysiological markers that will help reveal specific dysfunctional circuits in aging-related neurodegeneration studies.

1. Introduction

Aging is the leading risk factor, which promotes a large class of neurodegenerative brain diseases that are particularly feared such as Alzheimer's disease (AD) and Parkinson's disease (PD) [1–3]. As the brain ages, both functional and structural changes result in a natural slow decline of cognitive processes. The aging impacts functional aspects of all the organs and biological pathways resulting in protein aggrega-

tions, early synapse damage, and selective neural network dysfunction. These changes make the brain more susceptible to augmenting amyloidogenic metabolism of APP, promoting the toxicity of A β oligomers, enhancing the hyperphosphorylation of tau, and accelerating the formation of neurofibril tangles or synucleopathy [4–6]. Other changes associated with loss of brain volume include atrophy of white matter, accumulation of damage in nuclear and mitochondrial DNA, epigenetic alterations, mitochondrial dysfunction, loss of proteostasis, stem

cell exhaustion, and altered intracellular communication and neuroinflammation [5].

The process of aging may have detrimental effects on neural activities, leading to a breakdown in critical synaptic plasticity and connectivity. Synaptic plasticity, which is the ability of synapses to strengthen (long-term potentiation LTP) and weaken (long-term depression LTD) over time in response to increases and decreases in their activity, plays a major role in the persistent long-term changes associated with learning, memory, and cognitive functions. The intricate balance between LTP and LTD processes plays a major role in the encoding and storage of new, incoming information [7]. The natural processes of aging damage and destroy synaptic connectivity, leading to a decline in normal synaptic plasticity mechanisms and providing a likely neural basis for the decline in memory and cognition associated with age [8].

The hippocampus, the epicenter of memory function and a highly plastic structure, is the first to degenerate in both normal aging and AD/PD brains, leading to a breakdown in the trisynaptic circuit, in which the CA1 region is a key part. Atrophy of these areas will lead to a significant decline in synaptic transmission and plasticity within the trisynaptic circuit and detrimental to declarative and spatial memory functions which rely on synaptic plasticity to consolidate and encode new incoming information [9]. This process is heightened in AD/PD patients, accounting for the symptomatic loss in memory. The age-related impairments in memory processes have been linked to modulation of activity-dependent forms of synaptic plasticity (Schaffer collateral/commissural fiber synapses) in the CA1 region of the hippocampus. This LTP is typically induced by brief trains of high-frequency synaptic stimulation (HFS), which is dependent on NMDA receptor activation and synapse specificity. Several studies have described deficits in activity-dependent forms of synaptic plasticity in the hippocampal CA1 region of aged animals, which is believed to be underlying physiological mechanisms that might represent a physiological basis for age-dependent deficits in memory. Most of those studies have used induction protocols to examine whether LTP is altered in hippocampal slices from aged animals [10–13].

However, a growing view argues against ubiquitous neuronal loss and brain atrophy during aging [14, 15]. Accordingly, subtle regional abnormalities of neural structure and synaptic connectivity were observed in the sensory cortex and hippocampus, which may be underlying cognitive decline associated with aging. Sensory olfaction processing such as odor identification, odor memory formation, and discrimination is sensitive to aging [16–19]. Ultrastructural observations showed that the cellular organization of the olfactory bulb remained stable during aging; however, discrete region and layer-specific neuronal loss were revealed in the glomerular layer resulting in a disorganized olfaction function [20].

The waking electrooculogram (EEG) in aged mice is characterized by slowing of the theta frequency rhythm, which is a prevalent activity during exploratory motor activity events [21]. The leftward shift of high frequency to slow EEG oscillations has been confirmed in epidural cortical

recordings of passive waking in aged mice [22]. Higher theta and gamma frequency activities have been related to higher cognitive functioning, learning, and memory processing [23–25], whereas lower theta and gamma network oscillations are two hallmarks associated with aging-related cognitive deficits [26–28].

The present study used young adult and aged wild-type C57Bl/6 mice to describe the circuit-level mechanisms of age-related deficit in higher cognitive functioning. The olfactory bulb and hippocampus were chosen because of their wide connectivity and role in spatial learning and memory and odor sensory processing, which are compromised by aging.

2. Materials and Methods

2.1. Animals. All experiments were performed under strict adherence with the guidelines of the Association for Assessment and Accreditation of Laboratory Animal Care International (AALAC) and with the European Communities Council Directive of 22nd September 2010 (2010/63/UE) and were approved by the local ethical committee. Male C57BL/6 mice (Bl6) of 3 and 22–23 months ($n = 16$ in total: $n = 8$ young and $n = 8$ aged animals) obtained from Janvier were group housed with their litter mates in individually ventilated cages at a relative humidity of $55\% \pm 10$ and $22^\circ\text{C} \pm 2$ temperature. They were kept at a 12 h/12 h light/dark cycle and had standard food and water available ad libitum.

2.2. *In Vivo* Local Field Potential (LFP) Procedures

2.2.1. Surgery. Surgery was carried out in animals weighing between 20 g and 28 g at the time of electrode implantation. Animals were anesthetized with isoflurane and injected with piritramide (0.25 mg/kg). They were mounted in a stereotaxic frame (David Kopf Instruments), with the incisor bar around 5 mm beneath the centre of the ear bars. This was adjusted to ensure that the height of the skull surface was equal to bregma and lambda, according to the stereotaxic mouse brain atlas of Paxinos and Franklin [29]. A heating pad was placed under the animals to maintain their core body temperature at 38°C . Animals were then stereotaxically equipped with 8 stainless steel recording electrodes in the olfactory bulbs (OB) (AP: +4.3 mm from Bregma, ML: ± 1.2 mm, DV: -2 mm), frontal cortex (AP: +2 mm from Bregma, ML: ± 1.5 mm), the lateral entorhinal cortex (EC) (AP: -2.9 mm from Bregma, ML: -4 mm, DV: -4.5 mm), and the ventral hippocampus CA1 (AP: -1.7 mm from Bregma, ML: -1.5 mm, DV: -1.7 mm), the dorsal hippocampus CA1 (AP: -1.94 mm from Bregma, ML: +1 mm, DV: -1.25 mm), and the lateral amygdala (AP: -2.06 mm from Bregma, ML: +3.25 mm, DV: +3.2 mm). All electrodes were referenced to a ground screw electrode, placed above the midline of the cerebellum. Electrodes were connected to a pin with a small insert (Future Electronics: 0672-2-15-15-30-27-10-0) (Track pins; Dataflex: TRP-1558-0000) and were inserted into a 10-hole connector, which was carefully fixed to the skull with dental cement.

2.2.2. Experimental Design, Recording, and Analysis. After one-week recovery period and adaptation to recording conditions, EEG were recorded for 20 hours during the dark phase of the circadian cycle, under vigilance-controlled wake, as described elsewhere [30, 31]. Recordings were taken in the animal's home cages placed in a sound-attenuated Faraday cages. Motor activity was measured by a pair of passive infrared (PIR) detectors located above every recording cage. Motion levels were analyzed from the envelope of activity from both PIR detectors. Continuous EEG recordings were acquired with Biosemi ActiveTwo system (Biosemi, Amsterdam, Netherlands). Analogous signal was band-pass filtered between 1 and 256 Hz at a sampling rate of 512 Hz with a range of ± 500 mV.

2.2.3. EEG Spectra. EEG recordings were derived from eight brain regions under vigilance waking condition during the dark circadian phase. Artifact-free waking epochs with high to moderate body activities were considered in the analysis. Epochs with high-voltage slow cortical waves in the absence of locomotor activities were discarded. Powerline interference was removed using a filter described in the supplementary materials in [32]. Analysis was performed using a custom-made scripts in MATLAB toolbox described earlier [30, 31]. Briefly, spectral power density was calculated in 2 second sliding windows using a Welch's method with Hanning window, and the power spectra was expressed as relative power for each frequency over 1-256 Hz. Average across recording time relative power in each frequency bin of each location was averaged across animals for young and aged mice separately to visualize the grand averaged relative spectra. One young mouse was discarded from the analysis due to artefacts in the EEG signals. For the sake of clarity in presenting spectral data, graphs only shown the frequency range between 1 and 7 Hz and from 30 to 80 Hz, and box plots only show results for delta (1-4 Hz) and gamma (30-80 Hz) bands.

2.2.4. Coherence. Longitudinal effects of aging on the integrity of cortical neural pathways and the functional coupling between different cortical structures at various frequency oscillations were estimated according to the procedure described earlier [30, 31]. The coherency function, which gives information on the stability of the similarity at each frequency bin between the time series in different electrodes, was quantified at different time points by the normalization of the cross-spectrum by the square root of the product of the autospectra: $\text{Coherency}(f) = S_{AB}(f) / \sqrt{(S_{AA}(f)S_{BB}(f))}$, where S_{AB} is the cross-spectrum between the signals A and B, S_{AA} is the autospectrum of the signal A, and S_{BB} is the autospectrum of the signal B. To characterize the strength of the interaction between signals A and B, magnitude-squared coherence was used. It is quantified as $\text{Coh}(f) = |\text{Coherency}(f)|^2$ and is reported as normalized values between 0 and 1: A low value indicates no similarity between the two signals, whereas values close to 1 indicate a high similarity between two time series signals up to near constant phase shift. It is known that coherence estimation is highly influenced by volume conductance effect

[33]. To reduce volume conductance effect, an imaginary part of coherency was used [34].

2.2.5. Phase-Amplitude Cross-Frequency Coupling. To estimate whether high frequency EEG amplitudes are modulated by low frequency phase variations of the same electrode site signals, phase-amplitude coupling (PAC) was calculated using the algorithm based on modulation index (MI) [35, 36]. MI is estimated as a mean (a long time t) absolute value of the signal $z(t) = A_H(t) \cdot \exp(i \cdot \varphi_L(t))$, $i = \sqrt{-1}$, using instantaneous phase $\varphi_L(t)$ around low frequency f_L , and instantaneous amplitude envelope $A_H(t)$ around high frequency f_H . In order to extract time-varying frequency band-specific amplitude $A_H(t)$ and phase $\varphi_L(t)$, a raw nonfiltered EEG signal was convoluted with complex Morlet wavelets. For PAC estimation, f_L was varied in an interval of 2-12 Hz with a step of 2 Hz, and all f_H taken from interval 10-200 Hz with a step of 5 Hz were considered.

2.3. In vivo Long-Term Potentiation (LTP) Procedures

2.3.1. Anesthesia. Mice were anesthetized using sodium pentobarbital [37–39]. The mice received a first bolus intraperitoneal administration of the anesthetic, at 60 mg/kg formulated in H₂O and NaCl solvent and after 10 min a second bolus of 10 mg/kg. Throughout the experimental procedure, mice were placed on the heated pad, and the depth of anesthetic state was checked by pedal reflex and was maintained by hourly administration of the anesthetic (10 mg/kg, 0.1 ml for 10 g body weight).

2.3.2. Surgery. Following observation of an adequate depth of anesthesia, the mice were placed in a stereotaxic frame. Core body temperature was maintained using a thermostatically controlled heating pad. An incision was made along the midline of the head, and bregma was defined. Additionally, it was checked that the skull was not tilted at any axis. A bipolar stimulating electrode of tungsten wire with 0.5 M Ω impedance and 1-2 μ m tip diameter (World Precision Instruments) was inserted into the Schaffer collateral and a monopolar recording electrode of Teflon-coated tungsten wire with a 75 μ m outer diameter (World Precision Instruments) was inserted into the stratum pyramidale layer of the CA1. The coordinates for the Schaffer collateral are AP: -2,0; ML: -2,0; and DV: \sim 1.2 and for the stratum pyramidale layer are AP: -1,7; ML: -1,5; and DV: \sim 1.1 from dura. Two holes were drilled to insert reference and ground screws.

2.3.3. Basal Synaptic Activity. Single square pulses (200 μ s, 3000 mV) were delivered, while descending the recording and stimulating electrodes (at 0.2 mm/min), to confirm their location in the brain. Labview homemade oscilloscope software was used to visualize the evoked field excitatory post synaptic potentials (fEPSPs). The electrode's dorsal-ventral position was measured from the dura before piercing it with a small needle.

Recordings of fEPSPs were made from the stratum pyramidale in the CA1 area of the right hippocampal hemisphere

in response to stimulation of the ipsilateral Schaffer collateral-commissural pathway. Axon excitability was tested by generating an input/output curve that measured the amplitude of the curve compared to the slope of the fEPSP responses across a range of stimulation voltages.

2.4. Inclusion and Exclusion Criteria. fEPSPs recorded in the Labview oscilloscope software need to meet the inclusion and exclusion criteria prior to engaging in an input/output (I/O) curve: The latency to peak negative deflection of fEPSPs is within 6-10 ms, the maximum amplitude between 1500 μ V and 2500 μ V and its maximum slope must lie between 400 μ V/ms and 900 μ V/ms at 200 μ s stimulus duration. Once the response met the preset criteria, a functional input/output (I/O) curve is generated using neuroscience measurement custom-designed software. Stimulation at intensities ranging from 1000 to 10000 mV in steps of 1000 mV at 0.033 Hz frequency and 200 μ s duration was delivered, and 3 responses were recorded at each intensity. The curve was drawn using the mean of the 3 responses at each time point. The stimulus which evoked an fEPSP slope of 50% of the maximum response was selected as a test stimulus for the LTP induction procedure. All I/O curves followed a sigmoid curve distribution, and the calculated test stimulus fits between 3300 mV and 4700 mV for all experiments.

2.4.1. LTP Induction. The procedure consists of calculating the change in magnitude of the evoked response at constant test stimuli before and after high frequency stimulation. Stimulation settings are put into neuroscience measurement custom-designed software and sent to the stimulation electrode via a data acquisition board linked to a constant current isolator unit (Multichannel System MC SRG4002). EEG and fEPSPs are recorded using a Biosemi Active Two amplifier (Differential amplifier, Netherlands) at a sample rate of 3 kHz. For each time point measured during the experiment, five records of evoked responses at the frequency 0.033 Hz and 200 μ s duration were averaged. The duration of the experiment is 30-60 min baseline followed by 90-120 min of posttetanisation. The last 30 min of the baseline recording (6 time points) was averaged and used as control for LTP induction. Custom-made analysis toll software normalizes data points and expresses them as a percentage of the last 30 min of baseline.

The high frequency stimulation (HFS) protocol that was used to induce LTP response, consisted of two trains of 50 pulses at 200 μ s pulse duration with an intertrain interval of 30 s and 100 Hz frequency [40–42].

2.5. Histological Marker of DNA Damage. After euthanasia, olfactory bulbs (OB) were collected from the brains of four young and four aged mice and fixed immediately in 10% neutral buffered formalin. Fixed tissues were processed with routine paraffin embedding technique and stained immunohistochemically with antibody (Anti-gamma H2A.X. Cat No. ab26350, Abcam, Cambridge, United Kingdom) against H2AX (histone 2 a family X), which is a standardized

marker for DNA damage [43] and double stranded breaks at dilution of 1/500 (2 μ g/ml).

2.6. Data Analysis. Result for described EEG metrics and for groups of aged and young Bl6 mice are presented as mean values with 95% confidence intervals (CI). Between group difference in means was assessed using two-sample *t*-test, and in case of significance, it is indicated by asterisks on box plots (**p* value < 0.05, ***p* value < 0.01). In order to deal with multiple comparisons and account for strong relations of estimates at neighbouring frequencies, for spectra and coherence data, threshold-free cluster enhancement (TFCE, $H = 2$, $E = 0.5$, $\alpha = 0.05$) was also used [44], which is based on *t*-statistics and provides threshold-independent advancement to cluster permutation test [45].

All LTP data were expressed as percentage of change from baseline and were presented as means \pm SEM%. The slope of the fEPSP was calculated from least square linear fit performed on the 80% interval between the artefact end and the negative peak. fEPSP slopes were obtained every 2.5 min as an average of 5 responses at 0.033 Hz and were then expressed as mean percentage change from baseline (defined as the last 30 min prior tetanisation) \pm SEM. Analysis of variance (ANOVA) followed by a post hoc test (Dunnett's test) were used to correct for multiple comparisons. Difference in means between groups was considered significant, if *p* value is below 0.05.

3. Results

3.1. Histology. The olfactory bulbs of older mice exhibited mild increase in the numbers of H2ax-positive neurons when compared to the OB of younger mice as shown Figures 1(a) and 1(b). The few positive H2AX-neurons in the OB of young mice were present mainly in the granular cells layer (Figure 1 top panel); however, in the OB of older mice, they were mainly present in the mitral cell layer and to lesser extent the granular cell layer (Figure 1 bottom panel).

3.1.1. Attenuation of Wake LFP Gamma Oscillations in Aged Mice. Wake LFP recorded from the OB of both young and aged animals showed a peak in the gamma frequency oscillations; however, aged mice showed significant reduction in relative power at cluster correspondent to this peak, driven by frequencies between 48 and 73 Hz (threshold-free cluster enhancement [TFCE] analysis) (Figure 2(a), bottom middle curve plot), which also could be seen using more traditional two-sample *t*-test for a total relative gamma power in the interval of 30-80 Hz (*p* = 0.01, Figure 2(a), bottom right bar plot). Using TFCE analysis at the EC network, a decrease with age in the relative power was found at clusters, driven by frequencies between 49-54 Hz, 60-67 Hz, 68-72 Hz, 75-76 Hz, and 78-80 Hz (Figure 2(b), bottom middle curve plot), which could also be seen in a reduction in total relative gamma power in the interval of 30-80 Hz with two-sample *t*-test (*p* = 0.02, Figure 2(b), bottom right bar plot).

No significant alteration was found in the gamma oscillatory pattern in the CA1 and BLA areas (Figures 2(c) and 2(d), bottom middle curve and right bar plots, respectively).

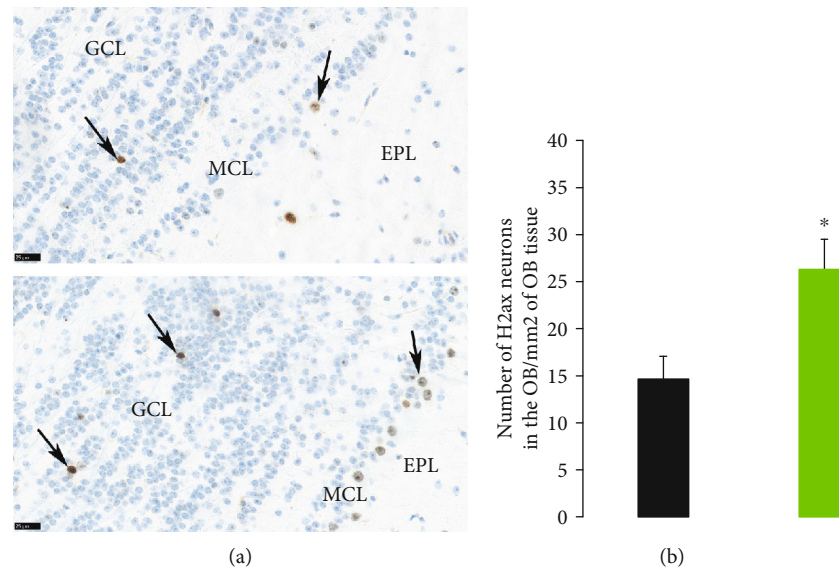


FIGURE 1: (a) Histological overview of the olfactory bulbs (OB) from 1 young mouse (top panel) and old mouse (bottom panel) stained for H2AX and taken at same magnification (scale bar = 25 microns). The OB of the old mouse exhibited significant increase in the numbers of H2AX-positive neurons particularly in the mitral cell layer (MCL) and the granular cell layer (GCL). H2AX-positive neurons are depicted by arrows. EPL: external plexiform layer. (b) Numbers of H2AX neurons in the olfactory bulbs of young and aged mice/mm² of olfactory bulb tissue. Data are presented as mean values \pm SEM for young (black, $n = 4$) and aged C57BL/6 mice (green, $n = 4$). Two-sample t -test.

3.1.2. Attenuation of Theta Oscillations and Shift towards Slow Rhythm Oscillations in Aged Mice. The age-dependent alterations in network oscillations appeared in the shift of the relative power into slow oscillatory rhythm (TFCE analysis with difference driven by oscillations below 3.5 Hz) at the OB network (Figure 2(a), top middle curve plot), which could also be identified by two-sample t -test in delta band ($p = 0.03$, Figure 2(a), top right bar plot). Increases in total relative power of the delta band were also observed in the EC area ($p = 0.04$, two-sample t -test; and correspondent TCFE analysis) (Figure 2(b), right top bar plot). Spectral analysis of LFP signals revealed that the activity in the theta frequency range, a correlate of arousal, was different between groups in the CA1 area (Figure 2(c), top middle curve plot), suggesting that aging also reduces vigilance during the active period. No alteration was observed in the slow frequency oscillatory pattern at BLA network (Figure 2(d), top middle curve and right bar plots).

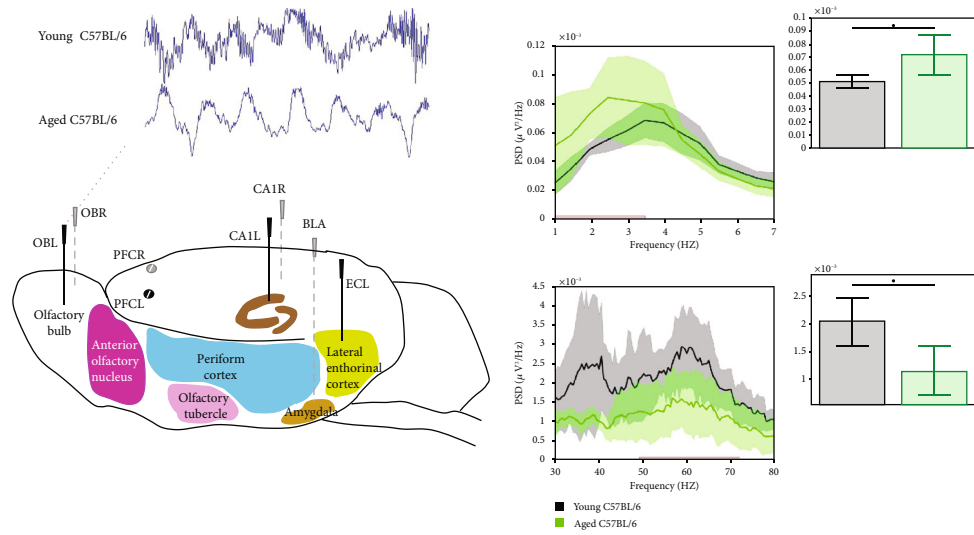
3.1.3. Attenuation of Theta-Gamma Phase-Amplitude Coupling in Aged Mice. The functional relevance of temporal interaction between superimposed network oscillations, estimated by the strength of cross-frequency coupling between the phase of slow and the amplitude of fast oscillations (PAC), has been associated with information processing in the brain. We examined whether aging altered the relationship between the gamma amplitude and the theta phase. The estimated mean PAC values in different recording sites at the OB and CA1 regions are qualitatively shown in the form of comodulation heat maps for young and aged mice.

As depicted in Figure 3, top left panel, young mice animals exhibit high phase-amplitude coupling in the OB

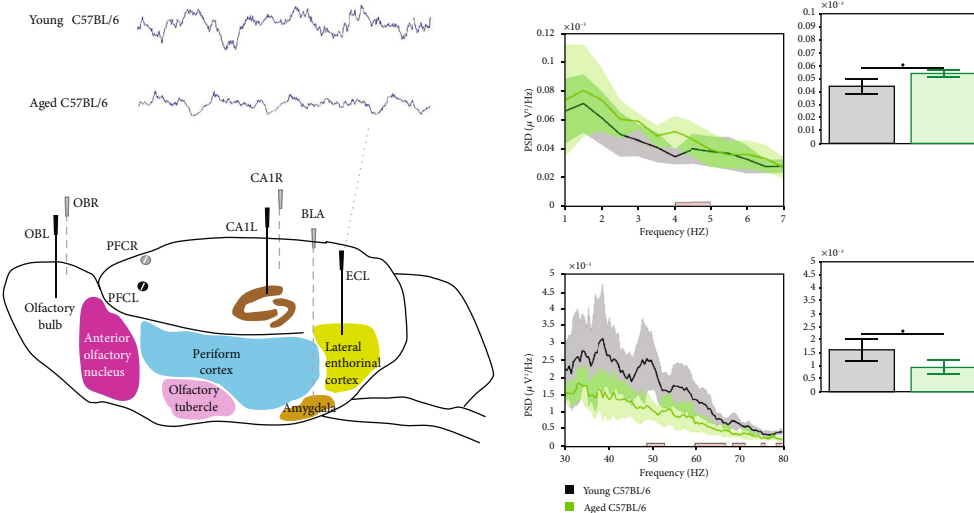
region. This high coupling peaks around a phase frequency of 7 Hz and amplitude frequency of around 57.5 Hz, in the theta-gamma range. Aged mice demonstrate reduced PAC in the OB area, whereas PAC comodulation heat maps in the CA1 areas of aged mice appear to be not affected (Figure 3, bottom panels). Quantification in the form of bar charts showed a significantly ($p < 0.05$, two-sample t -test) reduced mean theta-gamma PAC in the OB region in the aged group as compared to young mice (Figure 3, top right panels), respectively. The strength of theta-gamma coupling was weak in the CA1 area and did not differ between aged and young mice (Figure 3, bottom panels).

3.1.4. Attenuation of Coherent Activity in the OB Area in Aged Mice. We addressed whether aging affects network connectivity by measuring pairwise coherence and imaginary part of coherency in different networks during waking state (Figures 4(a) and 4(b)). Using threshold-free cluster enhancement (TFCE), we found significant between group difference in imaginary part of coherency in olfactory networks, driven by frequencies between 25 and 38 Hz (top right panel), which is also visualized in box plots for frequency interval 25-35 Hz ($p = 0.04$, two-sample t -test) (Figure 4(a)). No significant differences were found in OBL-CA1L (Figure 4(b)), CA1L-BLA (Figure 4(c)), ECL-CA1L (Figure 4(d)), and ECL-BLA (Figure 4(e)).

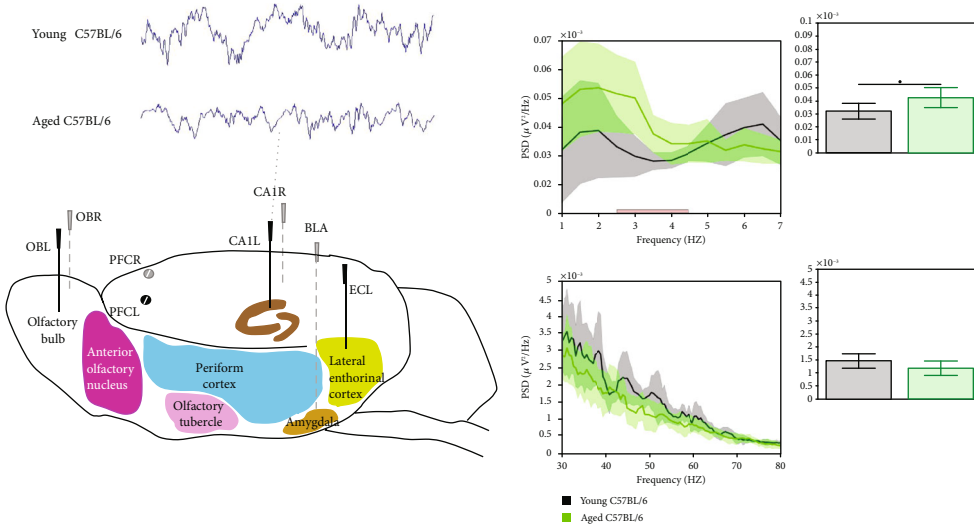
3.1.5. Impairment of LTP Response to HFS in Aged Bl6 Mice. To examine whether aging affects plasticity mechanisms, we studied the plasticity response to HFS at the Shaffer collateral-CA1 stratum pyramidale synapse (Figure 5 top scheme), in aged and young C57BL/6 mice (Figure 5(a)). As revealed by I/O curves of fEPSP responses, a slight



(a)

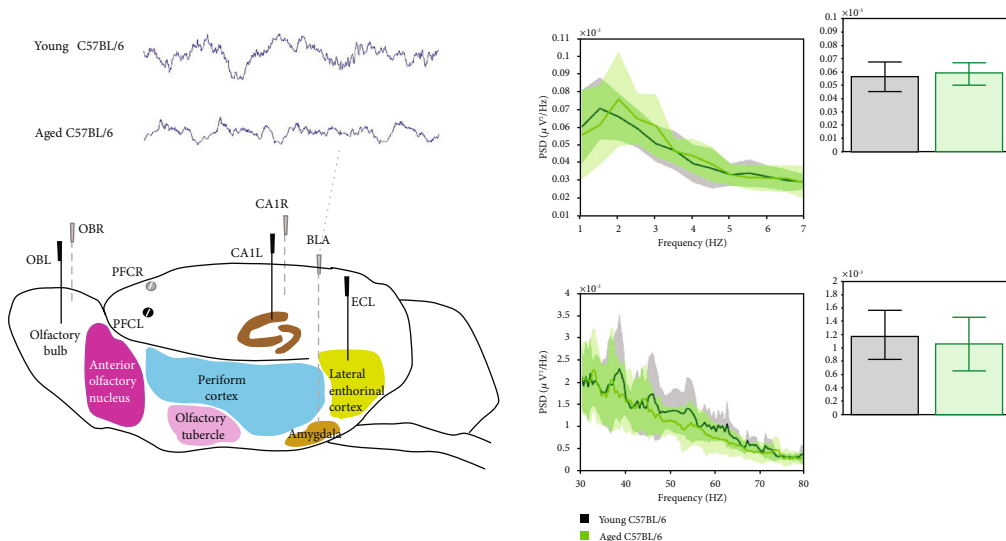


(b)



(c)

FIGURE 2: Continued.



(d)

FIGURE 2: Relative power spectra data of wake LFP signals in low (1-7 Hz) and high (30-80 Hz left panels) frequencies for recordings performed in left hemisphere. (a) Olfactory bulb (OBL), (b) entorhinal cortex (ECL), (c) hippocampal CA1 (CA1L), and (d) basolateral amygdala (BLA) for young (black, $n = 7$) and aged (green, $n = 8$) C57BL/6 mice. Data are presented as mean values \pm 95% confidence intervals for young (black, $n = 7$), and aged C57BL/6 mice (green, $n = 8$). Bars on the horizontal axis indicate clusters, which drive significant between group differences using threshold-free cluster enhancement (TFCE, $\alpha = 0.05$). Right bar and whiskers panels show relative power in delta frequency 1-4 Hz (top) and gamma frequency 30-80 Hz (bottom). Lines above bar plots with asterisks indicate presence of significant between group difference, * p value < 0.05 (two-sample t -test), * p value < 0.05 .

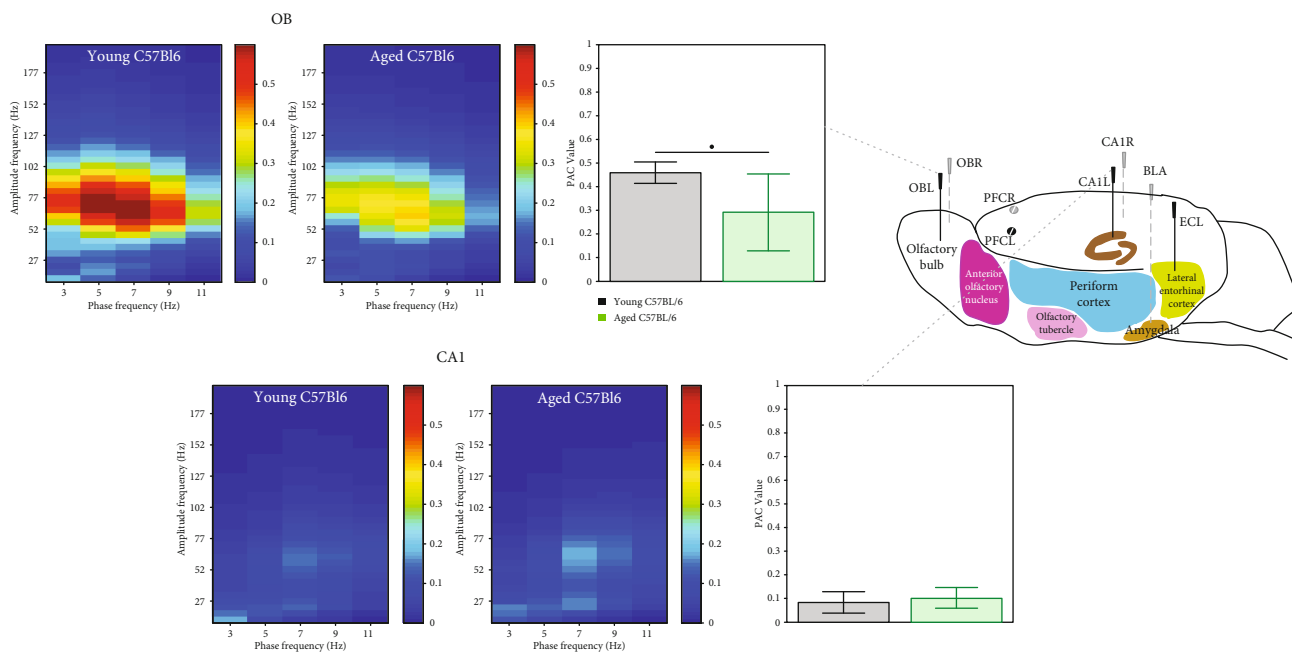


FIGURE 3: Heat maps showing the mean phase amplitude coupling (PAC) modulation index at the OB and CA1 recording electrodes for young (left panels in each frame) and aged (right panels in each frame) C57BL/6 mice. As shown by the color scale, “hotter” colors indicate high coupling values while “colder” colors indicate low or no coupling. Bar graphs showing the mean (across animals) theta-gamma PAC (with 95% CI) at the OB, EC, and CA1 electrodes for young (black, $n = 7$) and aged (green, $n = 8$) Bl6 mice. These means along animals’ PAC values were computed as the average PAC for the large window of phase frequency: 2–12 Hz, and amplitude frequency: 10–200 Hz. Right bar charts show estimated mean PAC index phase 4-8 Hz and amplitude 40-100 Hz, and horizontal lines above bar plots with asterisks indicate presence of significant difference between genotypes (* p value < 0.05). Data are presented as mean values (with 95% CI).

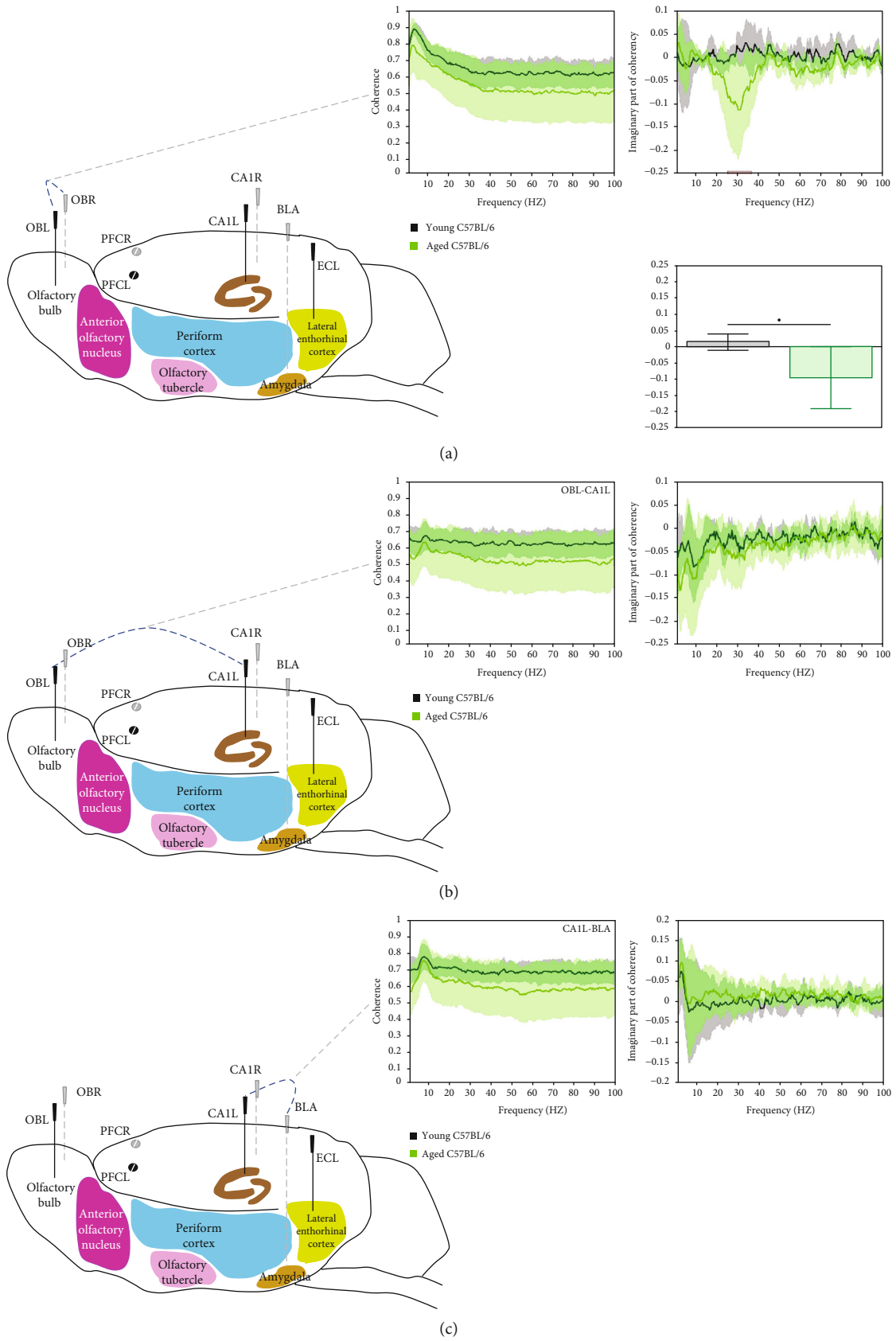


FIGURE 4: Continued.

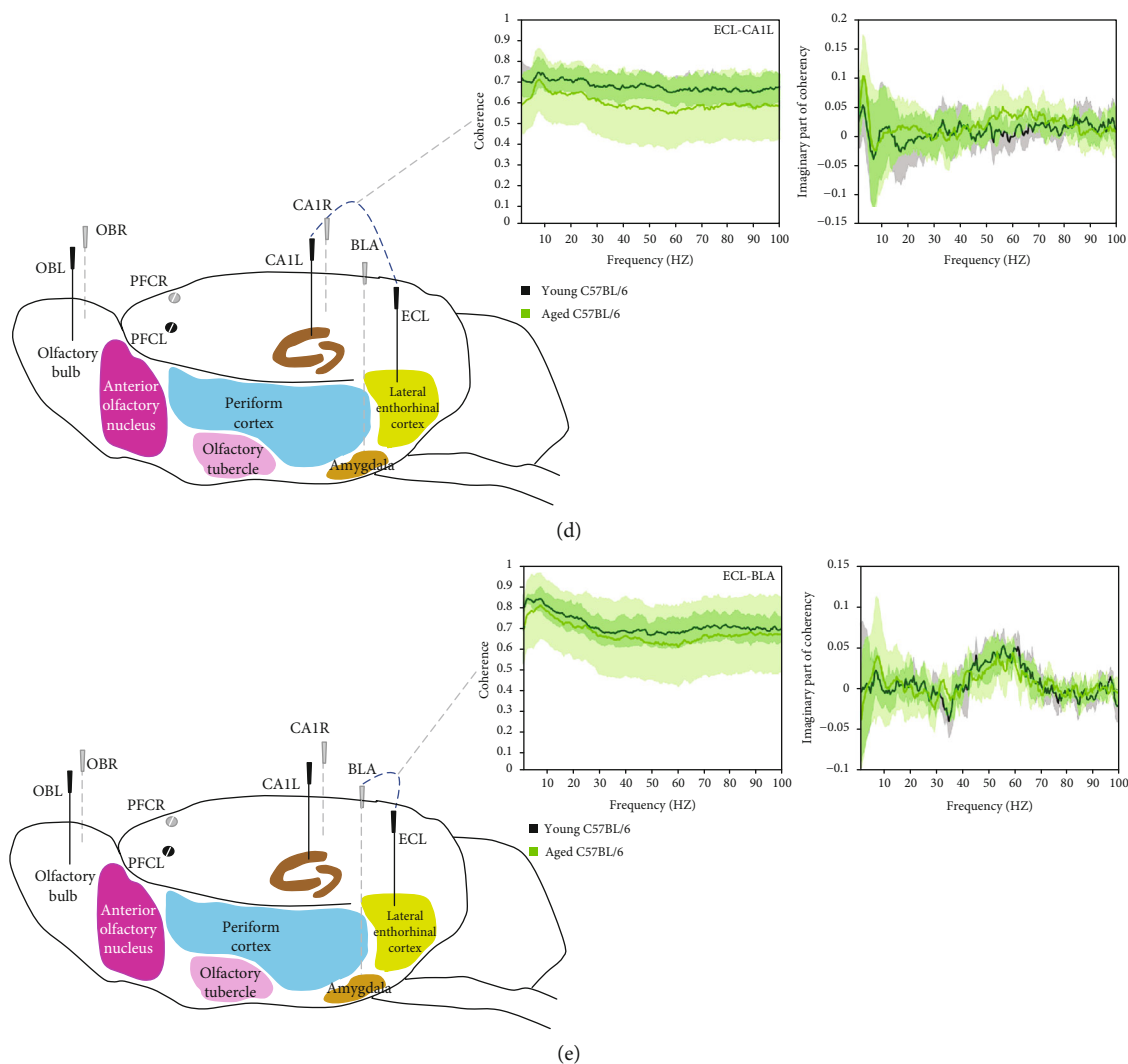


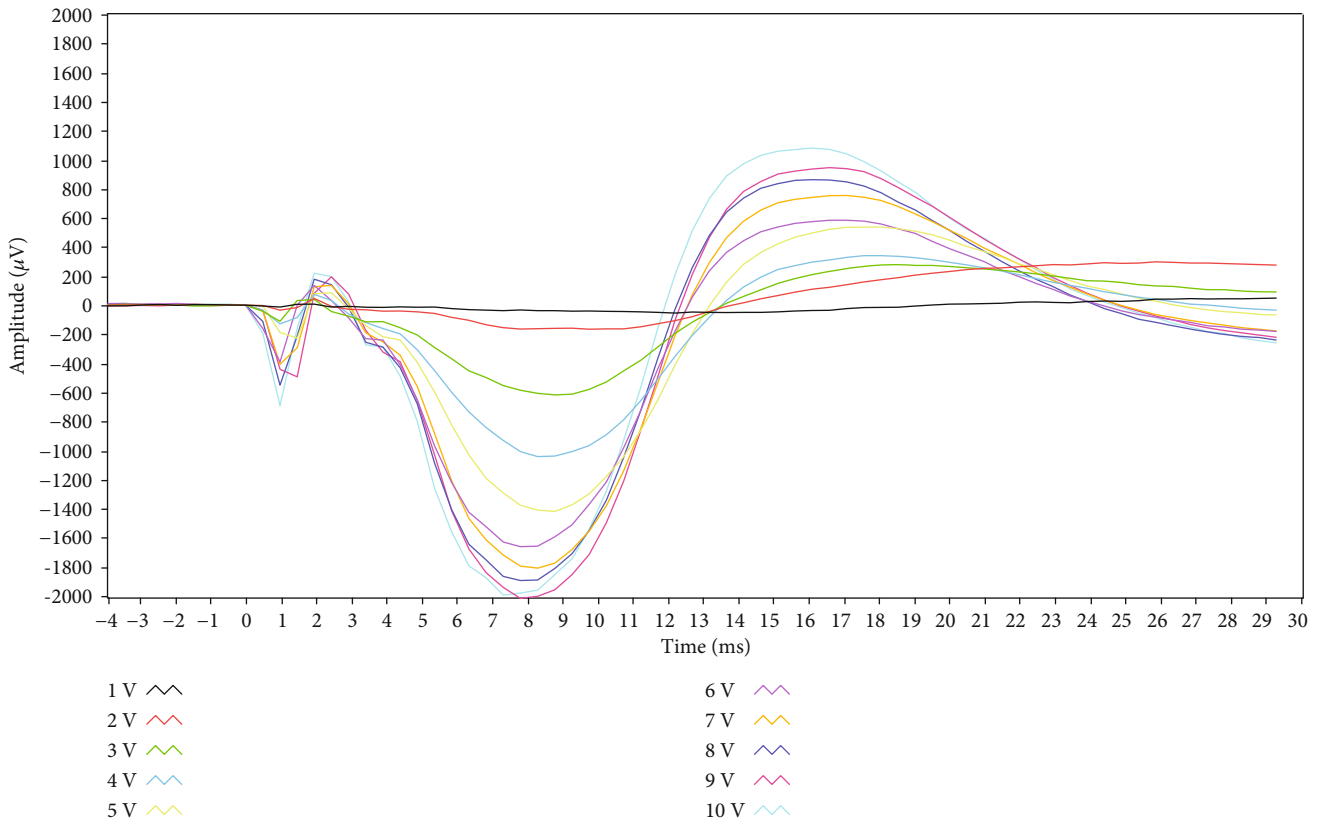
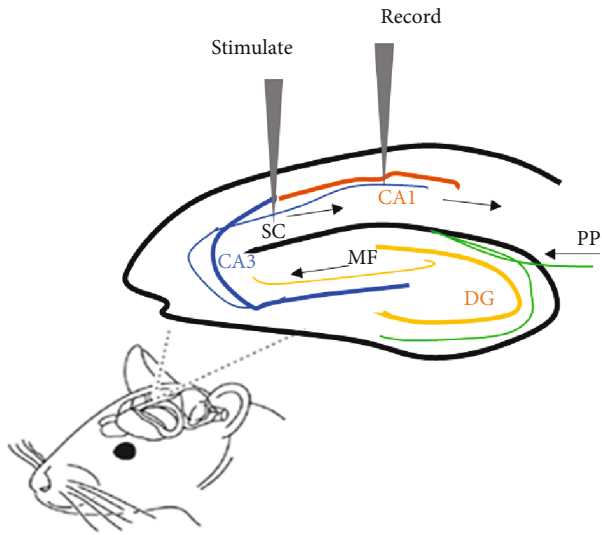
FIGURE 4: Coherence and imaginary part of coherency patterns between recording pairs (a) olfactory bulb left and right (OBL-OBR), (b) olfactory bulb left and CA1 left (OBL-CA1L), (c) CA1 left and basolateral amygdala (CA1L-BLA), (d) entorhinal cortex left and CA1 left (ECL-CA1L), (e) entorhinal cortex left and basolateral amygdala (ECL-BLA), in young (black, $n = 7$) and aged (green, $n = 8$) C57BL/6 mice. Graphs show mean values ($\pm 95\%$ CI) as a function of frequency in 1-100 Hz range. Bars on the horizontal axis indicate clusters, which drive significant between group differences using threshold-free cluster enhancement (TFCE, $\alpha = 0.05$). In panel (a), bar and whiskers panels show imaginary part of coherency for interval 25-35 Hz. Lines above bar plot with asterisks indicate presence of significant difference between groups, * p value < 0.05 (two-sample t -test).

decrease was observed in basal synaptic activity of aged mice; however, there was no significant differences between the study groups (Figure 5(b) top panel). Similarly, no difference was observed in collective I/O curves of PSA, suggesting no overall difference in the basal synaptic activity between the study groups (Figure 5(b) bottom panel). However, aged mice exhibited declines in both fEPSPs and PSA values, suggesting impairments in the synaptic strength in response to HFS stimulation (Figure 5(c), top and bottom panels). A borderline significant difference was observed in fEPSPs of the early- and late-LTP phases (-33% and -18%, $p = 0.05$). PSA response values showed significant differences in early phase (-38%; $p = 0.02$) and late phase of LTP (-20.5%; $p = 0.02$) (Figure 5(c)).

4. Discussion

The data of the present experiments confirm the age-associated deficits in plasticity mechanisms. We demonstrate that aged C57BL/6 mice exhibited significant increase in DNA damage as a marker of neurodegeneration, deficits in HFS-induced changes in synaptic strength as compared to young aged mice. The results further extend previous studies by showing age-related abnormalities in network oscillations and connectivity patterns that were particularly pronounced at OB circuit.

4.1. Aged Mice Exhibit Deficits in Hippocampal LTP Response to HFS, While no Alteration Was Observed in Basal Synaptic Activity. Aging plays a central role in age-related cognitive



(a)

FIGURE 5: Continued.

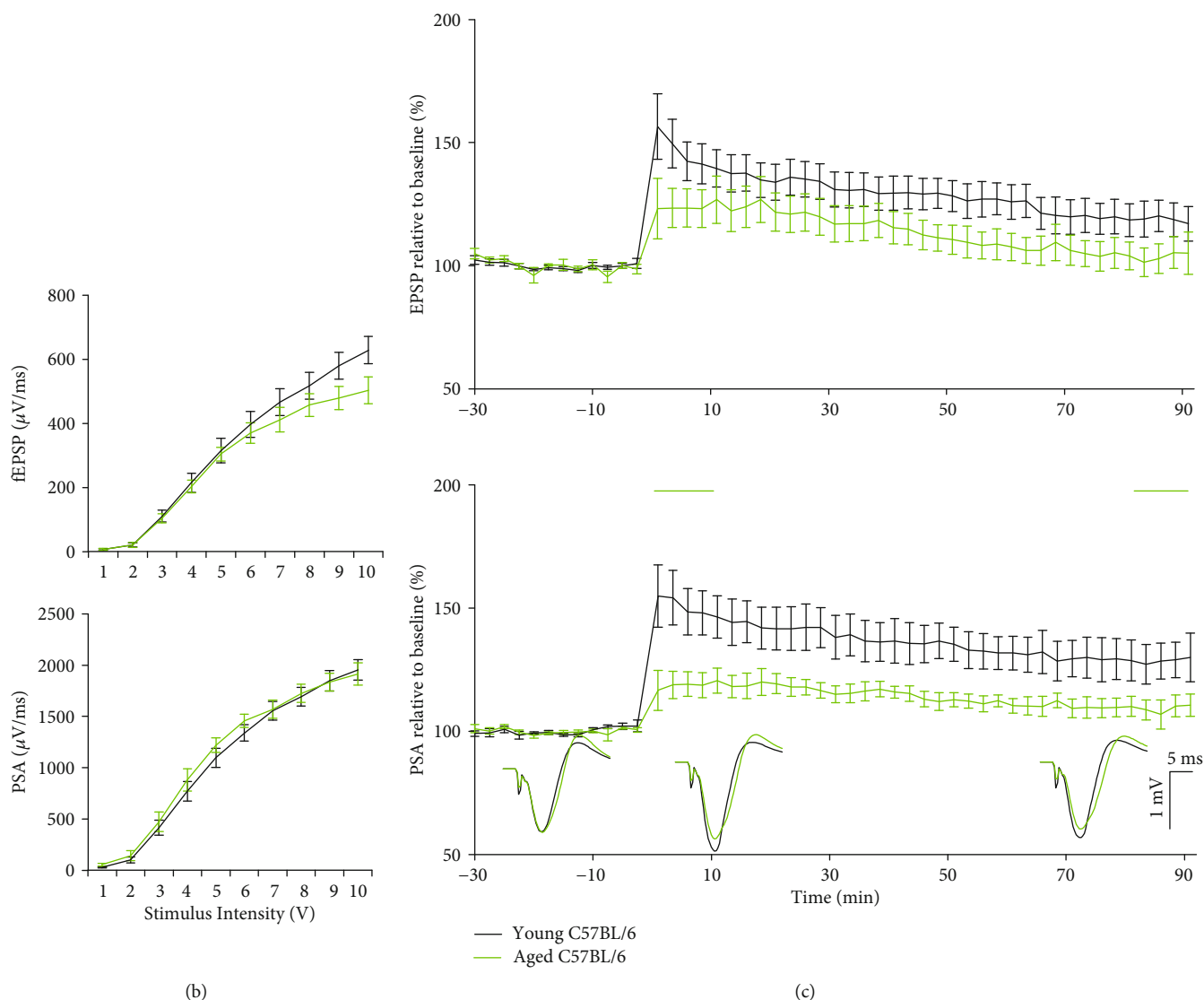


FIGURE 5: (a) Placement of the stimulation-recording electrodes at the Schaffer collateral-CA1 stratum pyramidale synapses in anesthetized mice (top panel), and a typical waveform spaghetti curves where the latency to peak negative deflection of fEPSPs is within 6-10 ms and the maximum amplitude between 1500 μ V and 2500 μ V. (b) Collective I/O curves of stimulation voltage and fEPSP slope (top panel) or PSA (bottom panel) values relative to baseline are plotted for young (black, $n = 9$) and aged (green $n = 8$) C57BL/6 mice. There was no significant alteration in baseline synaptic response, (c) A decline in synaptic response to HFS was observed in normalized EPSP and PSA values and was maintained throughout the recording session. No difference was observed in the average wave form during the 30 min baseline interval prior tetanisation, whereas smaller waveform was observed in aged mice during 0-30 min and 60-90 min posttetanisation. Data are presented as means \pm SEM (%). Line above indicates statistical significance between groups, repeated ANOVA.

deficits [46], where synapses are particularly vulnerable sites of attack. Most mechanistic studies of memory storage have focused on the hippocampus, due to its critical role in learning and memory [47]. There is a high degree of overlap between the atrophy and degeneration of brain structures seen in normal aging and of that seen in AD brains [5]. The hippocampus is an early target for neurodegeneration and atrophy, which could be down to hippocampal hyperactivity and overactivation, with the CA1 subfield being one of the main targets for degeneration.

LTP has been used as an experimental model for studying mechanisms of memory and brain plasticity. It has been suggested that age-related impairments in learning and memory

may be due to age-related deficits in LTP of glutamatergic synaptic transmission. Age-dependent effects on synaptic function are regionally heterogeneous [46]. In old rats, the synaptic density declines in the dentate gyrus, but not in the CA1, and electrophysiological studies using minimal stimulation suggest declines of the basal synaptic potency in CA1 but not in the dentate gyrus of aged animals [48]. In young animals, NMDA receptor-dependent LTP in the stratum radiatum of hippocampal area CA1 is thought to underlie memory formation [49-51]. Several plasticity studies in aged animals have reported alterations in activity-dependent forms of synaptic plasticity in the hippocampal CA1 region, which might underlie age-dependent deficits in

learning and memory processes [10–12]. Aging causes a deficit in LTP induction, which can be overcome with strong electrical stimulation [46, 52]. In most cases, hippocampal slices from aged animals were used to show abnormalities in the LTP response [10–12, 53]. However, it has become increasingly important to progress electrophysiology research from *in vitro* brain slices to *in vivo* study of the intact brain. As it may be more physiologically representative of the processes occurring in the human brain, accounting for the inputs from different brain regions which may influence the synaptic response. In the present study, we found that aged mice have reduced response, which sustained over the recording period. Decreased LTP with aging was not accompanied by significant alteration in basal synaptic excitability as the I/O curves were not different in young and aged mice.

Ultrastructural and molecular analysis have been used to study synaptic basis of hippocampal memory alterations underlying LTP in young and aged mice during contextual fear memory formation [54]. Unlike young mice, aged mice did not show an increase in mushroom spines and complex PSD, which are characteristics of structural LTP [55, 56]. Although we detected declines in functional LTP in aged mice indicating changes in synapse morphology, there was still a response to HFS suggesting that aged mice could still use NMDA receptor-dependent LTP in hippocampal area CA1. However, NMDA receptor-independent component of LTP has been shown to occur more predominantly in the hippocampus of aged animals and involves high activation of L-type voltage-gated calcium channels (VGCC) [5, 8], likely owing to the increases in density of functional VGCC in CA1 hippocampal neurons during aging [57–59]. In addition, aging is accompanied with Ca^{2+} dysregulation and loss of input specificity in LTP, which may contribute to diminished NMDA-dependent component of LTP [60–62].

4.2. Aged Mice Exhibit Deficits in Network Oscillations at the OB Circuit. The olfactory system, which has a high degree of organization and connectivity, is an attractive brain region for neurobiological studies of sensory and cognitive functions in aging [16, 63]. Odor information is encoded by sensory neurons in the olfactory epithelium and then relayed to the olfactory bulb (OB) for processing before distribution to olfactory cortex via the lateral olfactory tract. In the OB region where olfactory information is first processed in the brain, GABAergic inhibitory neurons greatly outnumber principal mitral cells [64], suggesting that odor representations in the olfactory bulb are strongly shaped by local inhibition. The dense connectivity of PV cells with mitral cells [65, 66], and the reciprocal dendro-dendritic signaling between mitral and Fast-spiking cells, indicates that PV+ interneurons play an important role in the processing of sensory information in the olfactory bulb [67].

Rhythmic neural activity has been proposed to play a fundamental role in cognition, and both healthy and pathological aging are characterized by frequency-specific changes in oscillatory activity. Neural activity that oscillates at the gamma rhythm results from the interplay of local inhibitory neurons and excitatory neurons [68, 69], as well as their interactions with local excitatory neurons [70–73].

The firing of fast-spiking PV+ interneurons plays a key role in the generation of gamma oscillations (30–100 Hz), considered as a fundamental mechanism underlying information sensory processing, behavioral control, and memory formation. Olfactory dysfunction has also been reported in aging rodents [17, 18, 69, 74–76]. Age-related degeneration of PV-immunoreactive neurons was observed in the OB of middle-aged and aged dogs [77] and rats [78], likely associated with the rise in the cerebral metabolic rate of oxygen and reduced calcium activity of PV interneurons [79]. Therefore, an alteration of PV interneuron function may be a neurobiological basis underlying impairments of fast network oscillations and thus higher olfactory functions in old adult mice.

4.3. Aged Mice Exhibit a Leftward Shift in Network Oscillations at the OB Circuit. Brain aging is markedly characterized by a shift in oscillatory rhythms from higher to lower frequencies, which can be captured by spectral data in higher and slow delta/theta and higher frequencies. The so-called slowing of resting state EEG rhythms observed in humans across physiological and pathological aging has also been observed in aged mice [30]. Some other studies have reported no effect of aging process on the amplitude of hippocampal theta oscillations while decreases in its frequency was observed [80, 81]. Hippocampal theta oscillations play an essential role in learning and memory and much evidence to this theory related theta activity to mnemonic task performance [23, 82], and decline or slowing of the hippocampal theta rhythm in may indicate a decline in learning and memory processes. In the present study, no major alteration was found in theta rhythm in LFP derived from EC and frontal cortical areas; however, a leftward shift in the power towards slow delta oscillations has been found in the OB and hippocampal CA1 area suggesting a decline in odor memory processing in aged animals.

The dynamic interactions between amygdala and hippocampus are critical for emotional memory. Anatomical studies demonstrated large interconnections between the amygdala and the hippocampus as well as with the prefrontal cortex [83–86]. The patterns of oscillatory activity have been studied in relation to fear behavior evoked by conditioned and indifferent sensory stimuli and contexts. Theta synchrony between these structures occurs during fear memory retrieval and may contribute to improvement in emotional and cognitive processes [87, 88]. Theta synchrony between amygdala and hippocampal CA1 nuclei increases during fear memory retrieval in rodents [86], and the degree of theta synchrony predicts memory performance after fear conditioning [89]. Experience-dependent molecular changes underlying synaptic plasticity during learning and memory can be impaired by aging [90, 91]. In the present work, there was no major changes in the theta or other oscillatory rhythms at the amygdala, and there was no entrainment of the amygdala nuclei to theta input as revealed by weak coherence with hippocampus and frontal cortex. This would be compatible with recordings performed under normal conditions where animals were not confronted with conditioned fear stimuli, thus future experiments in aged mice after

contextual fear might provide important mechanistic insights regarding oscillatory connectivity the hippocampus and amygdala.

4.4. Aged Mice Exhibit Deficits in Network Connectivity. In both humans and rodents, aging is linked to synaptic damage and aberrant functional circuitry leading to impairments in hippocampus dependent learning. Aged rats had lower coherence in theta and gamma frequency oscillations across dorsal CA1 pyramidal and radiatum layers [92]. The reduced coherence associated with pronounced weak strength of the theta-gamma PAC coupling in aged mice animals indicates that gamma is likely to be slower as a result of changes in the response of GABAergic neurons to glutamatergic signals. The neurobiological mechanisms underlying the deficit in high frequency oscillations may be related to age reduction in axon myelination, which may slow the conduction speed observed also in event related potentials [93, 94].

4.5. Implication of Current Work for Models of Aging-Related Neurodegeneration. Structural and pathophysiological studies revealed common deficits in the olfactory processing during senescence in humans and rodents, suggesting specific susceptibility of this brain circuit to aging processes [95]. In addition, the OB system appears to be particularly vulnerable to age-related neurodegenerative disease [96–98] and therefore offers a strong predictive utility of olfactory tests for progression from normal aging to MCI and to AD [99]. MCI patients display significant deficits in olfactory identification tests when compared to healthy elderly people [98–100]. At the functional level, late components of the olfactory event-related potential show increased latency with age, suggesting decline in odor processing [101]. Similarly, functional MRI during olfactory identification and discrimination tests demonstrated abnormal blood-oxygen-level-dependent (BOLD) responses in the piriform cortex and frontal and temporal lobes of older subjects [102, 103].

Olfactory dysfunction has also been observed in aging rodents [17, 74–76, 104], likely related to a decline in the density of olfactory receptor neurons [105, 106]. Aged mice showed deficits to learn two-odor discrimination problems for positive reinforcement and failed to show improvement across multiple discrimination problems when compared to young mice [18]. Neuronal recordings from orbitofrontal cortex revealed aberrant responses to odors during reversal tasks in older rats [76], and deficits in olfactory specific learning have been reported in 2-year-old rodents [74, 105], as well as for odor long-term memory, which may be cortical-dependent [105]. Experimental studies have shown a link between gamma oscillations and odor discrimination [107–109]. Accordingly, blockade of gamma oscillations in honeybees resulted in poor performance on discrimination tasks between similar odors [110]. However, increases of gamma oscillations were observed in the OB of rats performing in discrimination tasks [111]. In the present study, aged mice exhibit impairments in high frequency network oscillations, a shift into slow oscillation and deficit in connectivity at the OB circuit, which likely represent neurobiological bases

underlying odor deficits olfactory memory deficits. The use of quantitative sleep EEG analysis has been established as a promising biomarker for aging people at risk of cognitive decline [112]. Olfactory decline with normal aging in humans appears to localize to the olfactory epithelium and higher cortical areas and therefore changes in EEG recordings predisposed the early onset of mild cognitive impairment. From the translational perspective, the olfactory bulb and hippocampus were chosen because of their wide connectivity and role in spatial learning, memory, and odor sensory processing, known to be compromised by aging and in age-related neurodegeneration. While basal synaptic activity was not altered, the decline of hippocampal synaptic transmission was only observed in response to HFS. However, the age-dependent alterations in network gamma oscillations and connectivity under spontaneous conditions appeared to be specific to the OB circuit, suggesting the neurophysiological basis of synaptic deficits underlying odor sensory processing. The findings highlight the potential use of LFP quantitative network oscillations and connectivity at the OB neural network as a sensitive electrophysiological marker that will help reveal specific dysfunctional circuits in neurodegeneration studies related to aging.

Data Availability

All relevant data within the paper are fully available.

Conflicts of Interest

None of the authors has any conflict of interest to disclose with respect to the present work.

References

- [1] Alzheimer's Association, "2017 Alzheimer's disease facts and figures," *Alzheimer's Dement*, vol. 13, no. 4, pp. 325–373, 2017.
- [2] Y. Hou, X. Dan, M. Babbar et al., "Ageing as a risk factor for neurodegenerative disease," *Nature Reviews Neurology*, vol. 15, no. 10, pp. 565–581, 2019.
- [3] R. H. Swerdlow, "Is aging part of Alzheimer's disease, or is Alzheimer's disease part of aging?," *Neurobiology of Aging*, vol. 28, no. 10, pp. 1465–1480, 2007.
- [4] M. E. S. Ferreira, A. S. de Vasconcelos, T. da Costa Vilhena et al., "Oxidative stress in Alzheimer's disease: should we keep trying antioxidant therapies?," *Cellular and Molecular Neurobiology*, vol. 35, no. 5, pp. 595–614, 2015.
- [5] G. A. Kerchner and T. Wyss-Coray, "The role of aging in Alzheimer's disease," in *Advances in Geroscience*, F. Sierra and R. Kohanski, Eds., pp. 197–227, Springer, Cham, 2016.
- [6] Y. C. Wong and D. Krainc, " α -synuclein toxicity in neurodegeneration: mechanism and therapeutic strategies," *Nature Medicine*, vol. 23, no. 2, pp. 1–13, 2017.
- [7] T. Takeuchi, A. J. Duzskiewicz, and R. G. M. Morris, "The synaptic plasticity and memory hypothesis: encoding, storage and persistence," *Philosophical Transactions of the Royal Society of London Series B: Biological Sciences*, vol. 369, no. 1633, article 20130288, 2014.

- [8] K. Boric, P. Munoz, M. Gallagher, and A. Kirkwood, "Potential adaptive function for altered long-term potentiation mechanisms in aging hippocampus," *The Journal of Neuroscience*, vol. 28, no. 32, pp. 8034–8039, 2008.
- [9] A. R. Patten, S. Y. Yau, C. J. Fontaine, A. Meconi, R. C. Wortman, and B. R. Christie, "The benefits of exercise on structural and functional plasticity in the rodent hippocampus of different disease models," *Brain Plasticity*, vol. 1, no. 1, pp. 97–127, 2015.
- [10] T. C. Foster, "Involvement of hippocampal synaptic plasticity in age-related memory decline," *Brain Research Brain Research Reviews*, vol. 30, no. 3, pp. 236–249, 1999.
- [11] T. C. Foster and C. M. Norris, "Age-associated changes in Ca^{2+} -dependent processes: relation to hippocampal synaptic plasticity," *Hippocampus*, vol. 7, no. 6, pp. 602–612, 1997.
- [12] A. M. Watabe and T. J. O'Dell, "Age-related changes in theta frequency stimulation-induced long-term potentiation," *Neurobiology of Aging*, vol. 24, no. 2, pp. 267–272, 2003.
- [13] S. Sajikumar, S. Navakkode, and J. U. Frey, "Protein synthesis-dependent long-term functional plasticity: methods and techniques," *Current Opinion in Neurobiology*, vol. 15, no. 5, pp. 607–613, 2005.
- [14] D. L. Dickstein, D. Kabaso, A. B. Rocher, J. I. Luebke, S. L. Wearne, and P. R. Hof, "Changes in the structural complexity of the aged brain," *Aging Cell*, vol. 6, no. 3, pp. 275–284, 2007.
- [15] S. N. Burke and C. A. Barnes, "Senescent synapses and hippocampal circuit dynamics," *Trends in Neurosciences*, vol. 33, no. 3, pp. 153–161, 2010.
- [16] W. S. Cain and J. C. Stevens, "Uniformity of olfactory loss in aging," *Annals of the New York Academy of Sciences*, vol. 561, pp. 29–38, 1989.
- [17] E. Enwere, T. Shingo, C. Gregg, H. Fujikawa, S. Ohta, and S. Weiss, "Aging results in reduced epidermal growth factor receptor signaling, diminished olfactory neurogenesis, and deficits in fine olfactory discrimination," *The Journal of Neuroscience*, vol. 24, no. 38, pp. 8354–8365, 2004.
- [18] R. C. Patel and J. Larson, "Impaired olfactory discrimination learning and decreased olfactory sensitivity in aged C57Bl/6 mice," *Neurobiology of Aging*, vol. 30, no. 5, pp. 829–837, 2009.
- [19] N. E. Rawson, "Olfactory loss in aging," *Science of Aging Knowledge Environment*, vol. 2006, no. 5, article pe6, 2006.
- [20] M. B. Richard, S. R. Taylor, and C. A. Greer, "Age-induced disruption of selective olfactory bulb synaptic circuits," *Proceedings of the National Academy of Sciences of the United States of America*, vol. 107, no. 35, pp. 15613–15618, 2010.
- [21] M. E. Wimmer, J. Rising, R. J. Galante, A. Wyner, A. I. Pack, and T. Abel, "Aging in mice reduces the ability to sustain sleep/wake states," *PLoS One*, vol. 8, no. 12, article e81880, 2013.
- [22] C. Del Percio, W. Drinkenburg, S. Lopez et al., "On-going electroencephalographic rhythms related to cortical arousal in wild-type mice: the effect of aging," *Neurobiology of Aging*, vol. 49, pp. 20–30, 2017.
- [23] G. Buzsáki, "Theta oscillations in the hippocampus," *Neuron*, vol. 33, no. 3, pp. 325–340, 2002.
- [24] L. Chauvière, N. Raftafi, C. Thinus-Blanc, F. Bartolomei, M. Esclapez, and C. Bernard, "Early deficits in spatial memory and theta rhythm in experimental temporal lobe epilepsy," *The Journal of Neuroscience*, vol. 29, no. 17, pp. 5402–5410, 2009.
- [25] E. Olvera-Cortés, M. A. Guevara, and I. González-Burgos, "Increase of the hippocampal theta activity in the Morris water maze reflects learning rather than motor activity," *Brain Research Bulletin*, vol. 62, no. 5, pp. 379–384, 2004.
- [26] T. D. R. Cummins and S. Finnigan, "Theta power is reduced in healthy cognitive aging," *International Journal of Psychophysiology*, vol. 66, no. 1, pp. 10–17, 2007.
- [27] M. E. Olvera-Cortés, I. García-Alcántar, B. Gutiérrez-Guzmán, J. J. Hernández-Pérez, M. Á. López-Vázquez, and M. Cervantes, "Differential learning-related changes in theta activity during place learning in young and old rats," *Behavioural Brain Research*, vol. 226, no. 2, pp. 555–562, 2012.
- [28] N. Insel, L. A. Patron, L. T. Hoang et al., "Reduced gamma frequency in the medial frontal cortex of aged rats during behavior and rest: implications for age-related behavioral slowing," *The Journal of Neuroscience*, vol. 32, no. 46, pp. 16331–16344, 2012.
- [29] G. Paxinos and K. Franklin, *Paxinos and Franklin's the Mouse Brain in Stereotaxic Coordinates*, Elsevier Science, 2012.
- [30] A. Ahnaou, D. Moechars, L. Raeymaekers et al., "Emergence of early alterations in network oscillations and functional connectivity in a tau seeding mouse model of Alzheimer's disease pathology," *Scientific Reports*, vol. 7, no. 1, article 14189, 2017.
- [31] A. Ahnaou, C. Walsh, N. V. Manyakov, S. A. Youssef, and W. H. Drinkenburg, "Early Electrophysiological Disintegration of Hippocampal Neural Networks in a Novel Locus Coeruleus Tau-Seeding Mouse Model of Alzheimer's Disease," *Neural Plasticity*, vol. 2019, Article ID 6981268, 23 pages, 2019.
- [32] J. M. Schoffelen, R. Oostenveld, and P. Fries, "Neuronal coherence as a mechanism of effective corticospinal interaction," *Science*, vol. 308, no. 5718, pp. 111–113, 2005.
- [33] A. M. Bastos and J. M. Schoffelen, "A tutorial review of functional connectivity analysis methods and their interpretational pitfalls," *Frontiers in Systems Neuroscience*, vol. 9, p. 175, 2016.
- [34] G. Nolte, O. Bai, L. Wheaton, Z. Mari, S. Vorbach, and M. Hallett, "Identifying true brain interaction from EEG data using the imaginary part of coherency," *Clinical Neurophysiology*, vol. 115, no. 10, pp. 2292–2307, 2004.
- [35] N. Axmacher, M. M. Henseler, O. Jensen, I. Weinreich, C. E. Elger, and J. Fell, "Cross-frequency coupling supports multi-item working memory in the human hippocampus," *Proceedings of the National Academy of Sciences of the United States of America*, vol. 107, no. 7, pp. 3228–3233, 2010.
- [36] R. T. Canolty and R. T. Knight, "The functional role of cross-frequency coupling," *Trends in Cognitive Sciences*, vol. 14, no. 11, pp. 506–515, 2010.
- [37] A. B. L. Tort, R. W. Komorowski, J. R. Manns, N. J. Kopell, and H. Eichenbaum, "Theta-gamma coupling increases during the learning of item-context associations," *Proceedings of the National Academy of Sciences*, vol. 106, no. 49, pp. 20942–20947, 2009.
- [38] S. M. Huang, A. Mouri, H. Kokubo et al., "Nepriylisin-sensitive synapse-associated amyloid-beta peptide oligomers impair neuronal plasticity and cognitive function," *The Journal of Biological Chemistry*, vol. 281, no. 26, pp. 17941–17951, 2006.

- [39] Y. Yoshiyama, M. Higuchi, B. Zhang et al., "Synapse loss and microglial activation precede tangles in a P301S tauopathy mouse model," *Neuron*, vol. 53, no. 3, pp. 337–351, 2007.
- [40] A. Buschler, J. J. Goh, and D. Manahan-Vaughan, "Frequency dependency of NMDA receptor-dependent synaptic plasticity in the hippocampal CA1 region of freely behaving mice," *Hippocampus*, vol. 22, no. 12, pp. 2238–2248, 2012.
- [41] J. J. Goh and D. Manahan-Vaughan, "Synaptic depression in the CA1 region of freely behaving mice is highly dependent on afferent stimulation parameters," *Frontiers in Integrative Neuroscience*, vol. 7, pp. 1–13, 2013.
- [42] S. F. Cooke, J. Wu, F. Plattner et al., "Autophosphorylation of α CaMKII is not a general requirement for NMDA receptor dependent LTP in the adult mouse," *The Journal of Physiology*, vol. 574, no. 3, pp. 805–818, 2006.
- [43] U. Plappert-Helbig, S. Libertini, W. Friauff, D. Theil, and H.-J. Martus, "Gamma-H2AX immunofluorescence for the detection of tissue-specific genotoxicity *in vivo*," *Environmental and Molecular Mutagenesis*, vol. 60, no. 1, pp. 4–16, 2019.
- [44] S. M. Smith and T. E. Nichols, "Threshold-free cluster enhancement: addressing problems of smoothing, threshold dependence and localisation in cluster inference," *NeuroImage*, vol. 44, no. 1, pp. 83–98, 2009.
- [45] E. Maris and R. Oostenveld, "Nonparametric statistical testing of EEG- and MEG-data," *Journal of Neuroscience Methods*, vol. 164, no. 1, pp. 177–190, 2007.
- [46] S. N. Burke and C. A. Barnes, "Neural plasticity in the ageing brain," *Nature Reviews Neuroscience*, vol. 7, no. 1, pp. 30–40, 2006.
- [47] H. Eichenbaum, "On the integration of space, time, and memory," *Neuron*, vol. 95, no. 5, pp. 1007–1018, 2017.
- [48] C. F. Stevens and Y. Wang, "Changes in reliability of synaptic function as a mechanism for plasticity," *Nature*, vol. 371, no. 6499, pp. 704–707, 1994.
- [49] C. Rampon, Y. P. Tang, J. Goodhouse, E. Shimizu, M. Kyin, and J. Z. Tsien, "Enrichment induces structural changes and recovery from nonspatial memory deficits in CA1 NMDAR1-knockout mice," *Nature Neuroscience*, vol. 3, no. 3, pp. 238–244, 2000.
- [50] J. R. Whitlock, A. J. Heynen, M. G. Shuler, and M. F. Bear, "Learning induces long-term potentiation in the hippocampus," *Science*, vol. 313, no. 5790, pp. 1093–1097, 2006.
- [51] N. Matsuo, L. Reijmers, and M. Mayford, "Spine-type-specific recruitment of newly synthesized AMPA receptors with learning," *Science*, vol. 319, no. 5866, pp. 1104–1107, 2008.
- [52] T. C. Foster, "Dissecting the age-related decline on spatial learning and memory tasks in rodent models: N-methyl-D-aspartate receptors and voltage-dependent Ca^{2+} channels in senescent synaptic plasticity," *Progress in Neurobiology*, vol. 96, no. 3, pp. 283–303, 2012.
- [53] M. R. P. Elmore, L. A. Hohsfield, E. A. Kramár et al., "Replacement of microglia in the aged brain reverses cognitive, synaptic, and neuronal deficits in mice," *Aging Cell*, vol. 17, no. 6, article e12832, 2018.
- [54] W. Aziz, I. Kraev, K. Mizuno et al., "Multi-input synapses, but not LTP-strengthened synapses, correlate with hippocampal memory storage in aged mice," *Current Biology*, vol. 29, no. 21, pp. 3600–3610.e4, 2019.
- [55] M. Matsuzaki, N. Honkura, G. C. Ellis-Davies, and H. Kasai, "Structural basis of long-term potentiation in single dendritic spines," *Nature*, vol. 429, no. 6993, pp. 761–766, 2004.
- [56] N. I. Medvedev, V. I. Popov, J. J. Rodriguez Arellano et al., "The N -methyl-d-aspartate receptor antagonist CPP alters synapse and spine structure and impairs long-term potentiation and long-term depression induced morphological plasticity in dentate gyrus of the awake rat," *Neuroscience*, vol. 165, no. 4, pp. 1170–1181, 2010.
- [57] L. Ris and E. Godaux, "Synapse specificity of long-term potentiation breaks down with aging," *Learning & Memory*, vol. 14, no. 3, pp. 185–189, 2007.
- [58] F. L. Núñez-Santana, M. M. Oh, M. D. Antion, A. Lee, J. W. Hell, and J. F. Disterhoft, "Surface L-type Ca^{2+} channel expression levels are increased in aged hippocampus," *Aging Cell*, vol. 13, no. 1, pp. 111–120, 2014.
- [59] O. Thibault and P. W. Landfield, "Increase in single L-type calcium channels in hippocampal neurons during aging," *Science*, vol. 272, no. 5264, pp. 1017–1020, 1996.
- [60] L. M. Veng, M. H. Mesches, and M. D. Browning, "Age-related working memory impairment is correlated with increases in the L-type calcium channel protein α 1D (Cav1.3) in area CA1 of the hippocampus and both are ameliorated by chronic nimodipine treatment," *Brain Research Molecular Brain Research*, vol. 110, no. 2, pp. 193–202, 2003.
- [61] P. Hajieva, C. Kuhlmann, H. J. Luhmann, and C. Behl, "Impaired calcium homeostasis in aged hippocampal neurons," *Neuroscience Letters*, vol. 451, no. 2, pp. 119–123, 2009.
- [62] S. Shankar, T. J. Teyler, and N. Robbins, "Aging differentially alters forms of long-term potentiation in rat hippocampal area CA1," *Journal of Neurophysiology*, vol. 79, no. 1, pp. 334–341, 1998.
- [63] R. L. Doty, P. Shaman, S. L. Applebaum, R. Giberson, L. Siksorski, and L. Rosenberg, "Smell identification ability: changes with age," *Science*, vol. 226, no. 4681, pp. 1441–1443, 1984.
- [64] G. M. Shepherd, W. R. Chen, and C. A. Greer, "Olfactory bulb," in *The Synaptic Organization of the Brain*, G. M. Shepherd, Ed., pp. 165–216, Oxford University Press, New York, NY, USA, 2004.
- [65] R. Batista-Brito, J. Close, R. Machold, and G. Fishell, "The distinct temporal origins of olfactory bulb interneuron subtypes," *The Journal of Neuroscience*, vol. 28, no. 15, pp. 3966–3975, 2008.
- [66] S. Kikuta, M. L. Fletcher, R. Homma, T. Yamasoba, and S. Nagayama, "Odorant response properties of individual neurons in an olfactory glomerular module," *Neuron*, vol. 77, no. 6, pp. 1122–1135, 2013.
- [67] H. K. Kato, S. N. Gillet, A. J. Peters, J. S. Isaacson, and T. Komiyama, "Parvalbumin-expressing interneurons linearly control olfactory bulb output," *Neuron*, vol. 80, no. 5, pp. 1218–1231, 2013.
- [68] A. Hasenstaub, Y. Shu, B. Haider, U. Kraushaar, A. Duque, and D. A. McCormick, "Inhibitory postsynaptic potentials carry synchronized frequency information in active cortical networks," *Neuron*, vol. 47, no. 3, pp. 423–435, 2005.
- [69] J. A. Cardin, M. Carlén, K. Meletis et al., "Driving fast-spiking cells induces gamma rhythm and controls sensory responses," *Nature*, vol. 459, no. 7247, pp. 663–667, 2009.

- [70] J. Csicsvari, B. Jamieson, K. D. Wise, and G. Buzsáki, "Mechanisms of gamma oscillations in the hippocampus of the behaving rat," *Neuron*, vol. 37, no. 2, pp. 311–322, 2003.
- [71] M. N. Economo and J. A. White, "Membrane properties and the balance between excitation and inhibition control gamma-frequency oscillations arising from feedback inhibition," *PLoS Computational Biology*, vol. 8, no. 1, article e1002354, 2012.
- [72] X. J. Wang, "Neurophysiological and computational principles of cortical rhythms in cognition," *Physiological Reviews*, vol. 90, no. 3, pp. 1195–1268, 2010.
- [73] M. A. Whittington, R. D. Traub, N. Kopell, B. Ermentrout, and E. H. Buhl, "Inhibition-based rhythms: experimental and mathematical observations on network dynamics," *International Journal of Psychophysiology*, vol. 38, no. 3, pp. 315–336, 2000.
- [74] C. L. LaSarge, K. S. Montgomery, C. Tucker et al., "Deficits across multiple cognitive domains in a subset of aged Fischer 344 rats," *Neurobiology of Aging*, vol. 28, no. 6, pp. 928–936, 2007.
- [75] R. D. Prediger, L. C. Batista, and R. N. Takahashi, "Caffeine reverses age-related deficits in olfactory discrimination and social recognition memory in rats. Involvement of adenosine A1 and A2A receptors," *Neurobiology of Aging*, vol. 26, no. 6, pp. 957–964, 2005.
- [76] G. Schoenbaum, S. Nugent, M. P. Saddoris, and M. Gallagher, "Teaching old rats new tricks: age-related impairments in olfactory reversal learning," *Neurobiology of Aging*, vol. 23, no. 4, pp. 555–564, 2002.
- [77] J. H. Choi, C. H. Lee, K. Y. Yoo et al., "Age-related changes in calbindin-D28k, parvalbumin, and calretinin immunoreactivity in the dog main olfactory bulb," *Cellular and Molecular Neurobiology*, vol. 30, no. 1, pp. 1–12, 2010.
- [78] I. K. Hwang, D. S. Kim, H. Y. Lee et al., "Age-related changes of parvalbumin immunoreactive neurons in the rat main olfactory bulb," *Molecules and Cells*, vol. 16, no. 3, pp. 302–306, 2003.
- [79] S. B. Jessen, C. Mathiesen, B. L. Lind, and M. Lauritzen, "Interneuron deficit associates attenuated network synchronization to mismatch of energy supply and demand in aging mouse brains," *Cerebral Cortex*, vol. 27, no. 1, pp. 646–659, 2017.
- [80] Y. Abe and K. Toyosawa, "Age-related changes in rat hippocampal theta rhythms: a difference between type 1 and type 2 theta," *The Journal of Veterinary Medical Science*, vol. 61, no. 5, pp. 543–548, 1999.
- [81] J. Shen, C. A. Barnes, B. L. McNaughton, W. E. Skaggs, and K. L. Weaver, "The effect of aging on experience-dependent plasticity of hippocampal place cells," *The Journal of Neuroscience*, vol. 17, no. 17, pp. 6769–6782, 1997.
- [82] S. D. Berry and R. F. Thompson, "Prediction of learning rate from the hippocampal electroencephalogram," *Science*, vol. 200, no. 4347, pp. 1298–1300, 1978.
- [83] A. J. McDonald, F. Mascagni, and L. Guo, "Projections of the medial and lateral prefrontal cortices to the amygdala: a *Phaseolus vulgaris* leucoagglutinin study in the rat," *Neuroscience*, vol. 71, no. 1, pp. 55–75, 1996.
- [84] G. D. Petrovich, P. Y. Risold, and L. W. Swanson, "Organization of projections from the basomedial nucleus of the amygdala: a PHAL study in the rat," *The Journal of Comparative Neurology*, vol. 374, no. 3, pp. 387–420, 1996.
- [85] T. Kishi, T. Tsumori, S. Yokota, and Y. Yasui, "Topographical projection from the hippocampal formation to the amygdala: a combined anterograde and retrograde tracing study in the rat," *The Journal of Comparative Neurology*, vol. 496, no. 3, pp. 349–368, 2006.
- [86] M. Müller, H. Faber-Zuschratter, Y. Yanagawa, O. Stork, H. Schwegler, and R. Linke, "Synaptology of ventral CA1 and subiculum projections to the basomedial nucleus of the amygdala in the mouse: relation to GABAergic interneurons," *Brain Structure & Function*, vol. 217, no. 1, pp. 5–17, 2012.
- [87] D. Paré, D. R. Collins, and J. G. Pelletier, "Amygdala oscillations and the consolidation of emotional memories," *Trends in Cognitive Sciences*, vol. 6, no. 7, pp. 306–314, 2002.
- [88] T. Seidenbecher, T. R. Laxmi, O. Stork, and H. C. Pape, "Amygdalar and hippocampal theta rhythm synchronization during fear memory retrieval," *Science*, vol. 301, no. 5634, pp. 846–850, 2003.
- [89] D. Popa, S. Duvarci, A. T. Popescu, C. Léna, and D. Paré, "Coherent amygdalocortical theta promotes fear memory consolidation during paradoxical sleep," *Proceedings of the National Academy of Sciences of the United States of America*, vol. 107, no. 14, pp. 6516–6519, 2010.
- [90] G. G. Murphy, N. B. Fedorov, K. P. Giese et al., "Increased neuronal excitability, synaptic plasticity, and learning in aged Kvbeta1.1 knockout mice," *Current Biology*, vol. 14, no. 21, pp. 1907–1915, 2004.
- [91] M. Peters, M. Bletsch, J. Stanley, D. Wheeler, R. Scott, and T. Tully, "The PDE4 inhibitor HT-0712 improves hippocampus-dependent memory in aged mice," *Neuropsychopharmacology*, vol. 39, no. 13, pp. 2938–2948, 2014.
- [92] J. Y. Li, T. B. Kuo, and C. C. Yang, "Aged rats show dominant modulation of lower frequency hippocampal theta rhythm during running," *Experimental Gerontology*, vol. 83, pp. 63–70, 2016.
- [93] S. C. I. Pavarini, A. G. Brigola, B. M. Luchesi et al., "On the use of the P300 as a tool for cognitive processing assessment in healthy aging: a review," *Dementia & Neuropsychologia*, vol. 12, no. 1, pp. 1–11, 2018.
- [94] L. Penke, S. Muñoz Maniega, C. Murray et al., "A general factor of brain white matter integrity predicts information processing speed in healthy older people," *The Journal of Neuroscience*, vol. 30, no. 22, pp. 7569–7574, 2010.
- [95] N. E. Rawson, G. Gomez, B. J. Cowart, A. Kriete, E. Pribitkin, and D. Restrepo, "Age-associated loss of selectivity in human olfactory sensory neurons," *Neurobiology of Aging*, vol. 33, no. 9, pp. 1913–1919, 2012.
- [96] M. Serby, J. Corwin, P. Conrad, and J. Rotrosen, "Olfactory dysfunction in Alzheimer's disease and Parkinson's disease," *The American Journal of Psychiatry*, vol. 142, no. 6, pp. 781–782, 1985.
- [97] J. P. Kesslak, C. W. Cotman, H. C. Chui et al., "Olfactory tests as possible probes for detecting and monitoring Alzheimer's disease," *Neurobiology of Aging*, vol. 9, no. 4, pp. 399–403, 1988.
- [98] A. Masurkar and D. Devanand, "Olfactory dysfunction in the elderly: basic circuitry and alterations with normal aging and Alzheimer's disease," *Current Geriatrics Reports*, vol. 3, no. 2, pp. 91–100, 2014.
- [99] R. O. Roberts, T. J. H. Christianson, W. K. Kremers et al., "Association between olfactory dysfunction and amnesic

- mild cognitive impairment and Alzheimer disease dementia,” *JAMA Neurology*, vol. 73, no. 1, pp. 93–101, 2016.
- [100] A. Bahar-Fuchs, S. Moss, C. Rowe, and G. Savage, “Awareness of olfactory deficits in healthy aging, amnesic mild cognitive impairment and Alzheimer’s disease,” *International Psychogeriatrics*, vol. 23, no. 7, pp. 1097–1106, 2011.
- [101] C. D. Morgan, M. W. Geisler, J. W. Covington, J. Polich, and C. Murphy, “Olfactory P3 in young and older adults,” *Psychophysiology*, vol. 36, no. 3, pp. 281–287, 1999.
- [102] D. M. Yousem, J. A. Maldjian, T. Hummel et al., “The effect of age on odor-stimulated functional MR imaging,” *AJNR American Journal of Neuroradiology*, vol. 20, no. 4, pp. 600–608, 1999.
- [103] D. A. Kareken, D. M. Mosnik, R. L. Doty, M. Dzemidzic, and G. D. Hutchins, “Functional anatomy of human odor sensation, discrimination, and identification in health and aging,” *Neuropsychology*, vol. 17, no. 3, pp. 482–495, 2003.
- [104] B. Cerf-Ducastel and C. Murphy, “fMRI brain activation in response to odors is reduced in primary olfactory areas of elderly subjects,” *Brain Research*, vol. 986, no. 1–2, pp. 39–53, 2003.
- [105] F. S. Roman, B. Alescio-Lautier, and B. Soumireu-Mourat, “Age-related learning and memory deficits in odor-reward association in rats,” *Neurobiology of Aging*, vol. 17, no. 1, pp. 31–40, 1996.
- [106] E. Meisami, “A proposed relationship between increases in the number of olfactory receptor neurons, convergence ratio and sensitivity in the developing rat,” *Brain Research. Developmental Brain Research*, vol. 46, no. 1, pp. 9–19, 1989.
- [107] J. W. Hinds and N. A. McNelly, “Aging in the rat olfactory system: correlation of changes in the olfactory epithelium and olfactory bulb,” *The Journal of Comparative Neurology*, vol. 203, no. 3, pp. 441–453, 1981.
- [108] D. E. Frederick, A. Brown, E. Brim, N. Mehta, M. Vujovic, and L. M. Kay, “Gamma and beta oscillations define a sequence of neurocognitive modes present in odor processing,” *Journal of Neuroscience*, vol. 36, no. 29, pp. 7750–7767, 2016.
- [109] D. Rojas-Libano and L. M. Kay, “Olfactory system gamma oscillations: the physiological dissection of a cognitive neural system,” *Cognitive Neurodynamics*, vol. 2, no. 3, pp. 179–194, 2008.
- [110] M. Stopfer, S. Bhagavan, B. H. Smith, and G. Laurent, “Impaired odour discrimination on desynchronization of odour-encoding neural assemblies,” *Nature*, vol. 390, no. 6655, pp. 70–74, 1997.
- [111] J. Beshel, N. Kopell, and L. M. Kay, “Olfactory bulb gamma oscillations are enhanced with task demands,” *Journal of Neuroscience*, vol. 27, no. 31, pp. 8358–8365, 2007.
- [112] J. Taillard, P. Sagaspe, C. Berthomier et al., “Non-REM sleep characteristics predict early cognitive impairment in an aging population,” *Frontiers in Neurology*, vol. 10, p. 1, 2019.

Review Article

Memory and Cognition-Related Neuroplasticity Enhancement by Transcranial Direct Current Stimulation in Rodents: A Systematic Review

Carla Cavaleiro,^{1,2,3} João Martins,^{1,2,3,4} Joana Gonçalves ,^{1,2}
and Miguel Castelo-Branco ,^{1,2,3,4}

¹Coimbra Institute for Biomedical Imaging and Translational Research (CIBIT), University of Coimbra, Coimbra, Portugal

²Institute of Nuclear Sciences Applied to Health (ICNAS), University of Coimbra, Coimbra, Portugal

³CNC.IBILI Consortium, University of Coimbra, Coimbra, Portugal

⁴Coimbra Institute for Clinical and Biomedical Research (iCBR), Faculty of Medicine, University of Coimbra, Coimbra, Portugal

Correspondence should be addressed to Joana Gonçalves; jgoncalves@fmed.uc.pt
and Miguel Castelo-Branco; mbranco@fmed.uc.pt

Received 6 December 2019; Revised 27 January 2020; Accepted 6 February 2020; Published 26 February 2020

Guest Editor: Luca Marsili

Copyright © 2020 Carla Cavaleiro et al. This is an open access article distributed under the Creative Commons Attribution License, which permits unrestricted use, distribution, and reproduction in any medium, provided the original work is properly cited.

Brain stimulation techniques, including transcranial direct current stimulation (tDCS), were identified as promising therapeutic tools to modulate synaptic plasticity abnormalities and minimize memory and learning deficits in many neuropsychiatric diseases. Here, we revised the effect of tDCS on the modulation of neuroplasticity and cognition in several animal disease models of brain diseases affecting plasticity and cognition. Studies included in this review were searched following the terms (“transcranial direct current stimulation”) AND (mice OR mouse OR animal) and according to the PRISMA statement requirements. Overall, the studies collected suggest that tDCS was able to modulate brain plasticity due to synaptic modifications within the stimulated area. Changes in plasticity-related mechanisms were achieved through induction of long-term potentiation (LTP) and upregulation of neuroplasticity-related proteins, such as *c-fos*, brain-derived neurotrophic factor (BDNF), or N-methyl-D-aspartate receptors (NMDARs). Taken into account all revised studies, tDCS is a safe, easy, and noninvasive brain stimulation technique, therapeutically reliable, and with promising potential to promote cognitive enhancement and neuroplasticity. Since the use of tDCS has increased as a novel therapeutic approach in humans, animal studies are important to better understand its mechanisms as well as to help improve the stimulation protocols and their potential role in different neuropathologies.

1. Introduction

Transcranial direct current stimulation (tDCS) is a noninvasive brain stimulation technique that promotes transient polarity-dependent changes in spontaneous neuronal activity. This effect is mediated by the application of constant low-amplitude electrical currents using epicranially positioned electrodes above a specific brain region of interest [1–4]. The therapeutic use of low-amplitude electrical currents has a long historical track. Accordingly, both Greeks and Romans used electric torpedo fishes for migraine treatment, and in the 11th century, a similar therapeutic procedure was attempted to handle epilepsy [5]. In the 19th

century, the application of galvanic currents was attempted to heal melancholia [6]. Over the years, the scientific community interest in brain stimulation grew, and several noninvasive brain stimulation techniques were developed such as tDCS, deep brain stimulation, or transcranial magnetic stimulation. The epicranial application of direct currents promotes a weak electric field force and produces neuronal membrane potential changes [7, 8]. These alterations occur through sodium and calcium currents [1] modulating spontaneous neuronal activity [2]. The consequent regional neuronal inhibition or excitation depends on the applied current polarity [9, 10]. So, it was overall observed that cathodal currents produce inhibitory effects, and thus hyperpolarization,

whereas anodal currents increase excitability in the form of depolarization [2, 11] (Figure 1).

There is nowadays an ongoing discussion regarding the factors that interfere with tDCS outcomes. The initial brain resting state of each subject [12], his/her baseline performance [13], specific individual variations in brain tissue morphology [14], or even more particular details from the experimental design or stimulation protocol used [15] influence these outcomes. *In vivo* and *in vitro* studies are consensual to demonstrate that tDCS-modulated cortical excitability depends on several stimulation parameters, such as duration and frequency of stimulation [16]; polarity, intensity, and density of the applied current [17, 18]; and electrode size and position in the scalp [18–20]. Despite that, beneficial effects of tDCS in several brain disorders, such as PD [21, 22], depression [23], stroke [24, 25], or autism [26, 27], have been documented, and there is growing evidence proposing tDCS application in multiple other disease conditions affecting cognition and neuroplasticity mechanisms.

Both preclinical and clinical studies have demonstrated therapeutic effects of tDCS. Indeed, in human studies, anodal tDCS applied intermittently in the prefrontal cortex (PFC) during slow-wave sleep period, improved recall of declarative memories (word pairs). The authors correlated these findings with enhancement of slow oscillatory electroencephalogram (EEG) activity (<3 Hz, delta (δ) waves), responsible for neuronal plasticity facilitation [28]. Also, anodal tDCS over dorsolateral prefrontal cortex (DLPFC) improved working memory in PD patients and in major depression patients by boosting cortical excitability [21, 23]. Accordingly, preclinical animal studies reported that cortical anodal tDCS improved spatial memory in both wild type (WT) [29] and the AD rat model [30]. Beneficial effects were also found during the early stage of traumatic brain injury (TBI) [31] and following a pilocarpine-induced *status epilepticus* in normal rats [32]. Moreover, improvements were also reported concerning short-term memory in an animal model of attention deficit hyperactivity disorder (ADHD) [33].

The molecular mechanisms underlying the tDCS-mediated cognitive improvements and neuroplasticity processes have become the focus of recent interest. Accordingly, tDCS modulation over several cognition-related plasticity genes and their signaling pathways has been studied. In this review, we provide a state of the art on the application of different protocols of tDCS in animal models highlighting its effectiveness on neuroplasticity mechanisms and, consequently, their related learning and memory processes. Since the published systematic reviews focused on human application of tDCS, here, we provide a comprehensive revision of the effect of tDCS in *in vivo* rodent models of normal and pathological brain functioning.

2. Methods

2.1. Data Sources and Search. Studies included in this review were identified by searching PubMed. The search was run until 31 October 2019. The search terms were (“transcranial direct current stimulation”) AND (mice OR mouse OR animal). Articles were firstly assessed based on their abstracts

and titles, aiming to include studies that reported applying tDCS to cognitive impairment in animal models. Simultaneously, the following exclusion criteria were adopted to reject studies: (1) not written in English; (2) performing reviews; (3) in human subjects; (4) *in vitro* models; (5) employing other brain stimulation techniques (e.g., transcranial magnetic stimulation (TMS), deep brain stimulation (DBS), or transcranial alternating current stimulation (tACS)); and (6) not explicitly describing the tDCS protocol (stimulation area, number of sessions, frequency, intensity, and pattern).

2.2. Data Extraction. A data extraction sheet was developed seeking to retrieve relevant information from each study, namely, study design, sample size, animal model, whether additional therapy was performed, details of the tDCS protocol, outcome measures, and behavioral results.

2.3. Study Selection. The database search was elaborated according to the PRISMA statement requirements [34]. 404 records were found, which underwent a preliminary screening (of titles and abstracts), with 314 records being excluded because they did not meet the eligibility criteria. After the full-text analysis of each of the 90 individual articles, 44 rodent studies focusing on tDCS effects over cognition and neuroplasticity in both healthy and neuropathological animal models were selected (Figure 2).

3. Results

3.1. Role of Anodal tDCS in Cognition Processing in Healthy Animals. In healthy animals, studies demonstrated memory improvement in association with induction of synaptic plasticity mechanisms. In fact, tDCS to prefrontal cortex improved monkey’s performance on an associative learning task by altering low-frequency oscillations and functional connectivity, both locally and between distant brain areas [35]. Regarding rodent models, data are controversial regarding fear condition. Right frontal anodal tDCS administered 24 h before behavioral task did not alter contextual and auditory learning and memory [36]. Additionally, another study described that while the anodal stimulation did not affect fear retrieval, posttraining cathodal stimulation improved fear memory retrieval [37, 38]. However, left prefrontal anodal and cathodal tDCS impaired the acquisition of both contextual and cued fear memory, which could be explained by activity modulation of deep structures such as the amygdala and hippocampus [39].

Concerning learning and memory, de Souza Custódio and colleagues [29] reported better spatial working memory performance following administration of anodal currents to the medial prefrontal cortex (mPFC). In agreement, it was described that administration of hippocampal anodal tDCS improves learning and memory in the Morris water maze and novel object recognition tests [40]. Moreover, memory performance in the passive avoidance learning task was enhanced by anodal stimulation [41]. Also, cortical cathodal stimulation together with visuospatial memory training led to cognitive improvement [42].

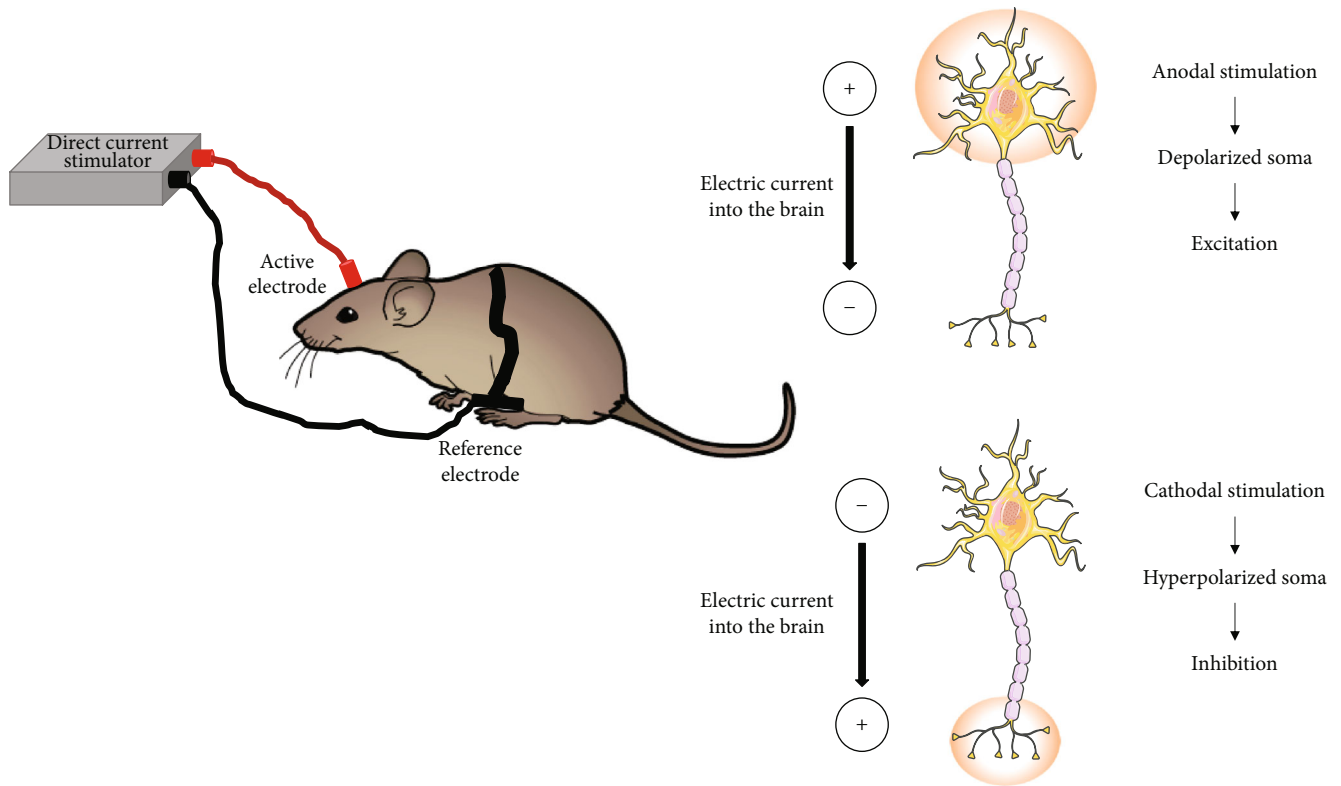


FIGURE 1: Illustration of transcranial direct current stimulation in the mice. Anodal stimulation depolarizes the neuronal membrane and enhances excitability. On the other hand, cathodal stimulation hyperpolarizes the neuronal membrane and decreases excitability.

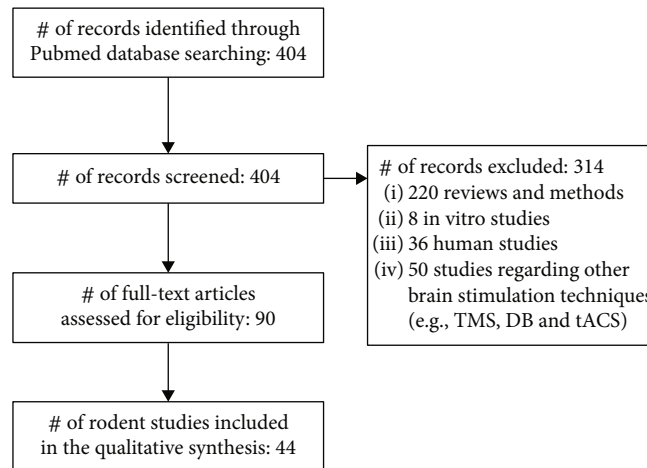


FIGURE 2: Search flow diagram (in accordance with PRISMA statement). Abbreviations: DB: deep brain stimulation; tACS: transcranial alternating current stimulation; TMS: transcranial magnetic stimulation.

The revised *in vivo* animal model studies regarding tDCS effects in memory and cognition of healthy animals are listed below in Table 1.

3.2. Beneficial Role of tDCS in Brain Diseases. Overall, reports using animal models of brain diseases described a beneficial role of tDCS in the mitigation of memory symptoms of neurologic conditions such as Alzheimer’s disease (AD) or traumatic brain injury (TBI). More recent studies demonstrated

that tDCS rescued AD-related cognitive symptoms, namely, spatial memory and motor skills [30, 43, 44]. The repetitive stimulation with anodal tDCS in the AD-like dementia rat model reduced the time interval animals needed to reach a food pellet and also decreased the number of errors in the attempt [43]. The same research group showed later that the abovementioned protocol rescued spatial learning and memory in a $A\beta_{1-40}$ -lesioned AD rat model [30]. Moreover, the impact of tDCS on cognitive performance

TABLE 1: Effect of transcranial direct current stimulation on memory and learning of healthy animals.

Author	Year	Animal model	Specimen; gender	N	Polarity	Position	Stimulation parameters			Main findings					
							Stimulation intensity (mA)	Stimulation size (m ²)	Stimulation duration (min)						
Dockery et al. [42]	2011	NDM	Long-Evans rats; males	41	a-tDCS vs. c-tDCS	Frontal cortex (left or right hemisphere)	0.2	0.035	30	57.1	Back	10.5	N	Y (3 days)	↑ Visuospatial working memory (c-tDCS)
					a-tDCS	Left mPFC	0.4	0.25	11	N/A	Neck	1	N	Y (5 days)	↑ Spatial working memory (1 h, 4 h, and 10 h poststimulation)
Faraji et al. [96]	2013	NDM	Long-Evans rats; males	24	a-tDCS vs. c-tDCS	Somatosensory cortex (bilateral)	0.065	N/A	10	N/A	Back of skull	N/A	N	Y	↑ Cortical neural density ↑ Motor learning (a-tDCS applied bilaterally or into paw preferred to reaching contralateral hemisphere)
					a-tDCS	Left parietal cortex (dorsal to hippocampal formation)	0.35	0.06	20	N/A	Ventral thorax	5.2	N	N (single session)	↑ BDNF expressions in the <i>hippocampus</i> CREB/CBP pathway activation
Podda et al. [40]	2016	NDM	C57BL/6 mice; males	16	a-tDCS vs. c-tDCS	Right frontal cortex	0.2	0.04	20	N/A	Chest	9.5	N/A	N	↓ Freezing time % and ↑ latency to the freezing (tDCS following 0.1 mg/kg ACPA injection)
					a-tDCS	Right frontal cortex	0.2	0.04	20	N/A	Ventral thorax	9.5	N	Y (2 sessions)	↑ Fear memory retrieval/freezing time (a-tDCS and propranolol injection before conditioning)
Nasehi et al. [37]	2017	NDM	NMRI mice; males	128	a-tDCS vs. c-tDCS	Left frontal cortex	0.2	0.04	20	N/A	Ventral thorax	9.5	N	Y (2 sessions)	↑ Contextual fear memory acquisition (a-tDCS before pre- or posttraining)
					a-tDCS	Left PFC	0.2	0.04	20 or 30	N/A	Chest	9.5	N	N (single session)	↓ Contextual and cued fear memory
Manteghi et al. [36]	2017	NDM	NMRI mice; males	64	a-tDCS vs. c-tDCS	Right frontal cortex	0.2	0.04	20	N/A	Chest	9.5	N/A	N	↓ Freezing time % and ↑ latency to the freezing (tDCS following 0.1 mg/kg ACPA injection)
					a-tDCS	Right PFC	0.2	0.04	20 or 30	N/A	Chest	9.5	N	N (single session)	↓ Contextual and cued fear memory
Nasehi et al. [38]	2017	NDM	NMRI mice; males	128	a-tDCS vs. c-tDCS	Left frontal cortex	0.2	0.04	20	N/A	Ventral thorax	9.5	N	Y (2 sessions)	↑ Contextual fear memory acquisition (a-tDCS before pre- or posttraining)
					a-tDCS	Left PFC	0.2	0.04	20 or 30	N/A	Chest	9.5	N	N (single session)	↓ Contextual and cued fear memory
Abbasi et al. [39]	2017	NDM	NMRI mice; males	41	a-tDCS vs. c-tDCS	Left PFC	0.2	0.04	20 or 30	N/A	Chest	9.5	N	N (single session)	↓ Contextual and cued fear memory
					a-tDCS	Left PFC	0.2	0.04	20 or 30	N/A	Chest	9.5	N	N (single session)	↓ Contextual and cued fear memory

TABLE 1: Continued.

Author	Year	Animal model	Specimen; gender	N	Stimulation electrode				Stimulation parameters				Reference electrode		Main findings	
					Polarity	Position	Stimulation intensity (mA)	Size (m ²)	Stimulation duration (min)	Current density (A/m ²)	Position	Area (cm ²)	Anesthesia	rtDCS		
Martins et al. [97]	2019	NDM	Male Wistar rats; males	50	a-tDCS	Left mPFC	0.4	N/A	13	N/A	N/A	N/A	N/A	N/A	Y (5 days)	↑ Spatial working memory ↑ GAP-43 (extinct by AMPAR antagonist PRP)
Yu et al. [41]	2019	NDM	Sprague Dawley rats; males	224	a-tDCS	SC, dorsal to the hippocampus	0.25	0.25	30	N/A	N/A	Anterior chest	N/A (EEG electrode)	Y	N (single session)	↑ Memory (passive avoidance memory retention) ↑ LTP in CA1 <i>hippocampus</i> (blocked by TrkB antagonist) ↑ BDNF in CA1 <i>hippocampus</i>

Abbreviations: rtDCS: repetitive transcranial direct current stimulation; a-tDCS: anodal transcranial direct current stimulation; c-tDCS: cathodal transcranial direct current stimulation; SC: stereotaxic coordinates; C57BL/6: mouse strain; NMR1: Naval Medical Research Institute outbred mice; NBM: no disease model; SHR: spontaneous hypertensive rats; WKY: Wistar Kyoto rats; PFC: prefrontal cortex; mPFC: medial prefrontal cortex; ITC: inferotemporal cortex; CA1: cornu ammonis 1 region in the hippocampus; PRP: perampanel; ACPA: anticitullinated protein antibody (selective cannabinoid CBI receptor agonist); AMPAR: α -amino-3-hydroxy-5-methyl-4-isoxazolepropionic acid receptor; Trk: tropomyosin receptor kinase receptor; CREB/CBP: cAMP response element binding protein; BDNF: brain-derived neurotrophic factor; GAP-43: growth-associated protein 43; LTP: long-term potentiation; EEG: electroencephalography; A/m²: ampere per square meter; mA: milliamper; cm²: square centimeter; mm: millimeter; h: hour; min: minute; vs.: versus; Y: yes; N: no; N/A: not available.

of streptozotocin-induced diabetic rats has been evaluated. Both anodal and cathodal stimulations in the prefrontal cortex restored memory impairment [45, 46] together with restoration of LTP [45]. Other authors evaluated the potential therapeutic effects of tDCS in memory impairment in an animal model of ADHD. It was found that this neuromodulation technique was able to improve short- and long-term memory deficits in the spontaneous hypertensive rats (SHR) but not in their control, Wistar Kyoto rats [33, 47]. In addition, no changes were detected in working memory of these control rats following administration of tDCS [47].

Anodal tDCS also ameliorated behavioral and spatial memory function in the early phase after TBI when it was delivered two weeks postinjury. However, earlier stimulation only improved spatial memory [31]. In a later phase of TBI, it was possible to observe motor recovery as well as spatial memory improvement following repeated anodal tDCS [48]. A growing number of studies has been reporting promising effects of neurostimulation in models of addictive disorders, by reducing craving and maladaptive pervasive learning [49]. In fact, repeated anodal stimulation in mouse frontal cortex decreased nicotine-induced conditioned place preference and further improved working memory [50]. Same polarity currents also could prevent cocaine-induced locomotor hyperactivity and place preference conditioning [51]. In addition, it has been reported that cathodal stimulation has an anticonvulsive effect [16, 32, 52–54]. Indeed, the administration of hippocampal tDCS rescued cognitive impairment by reducing hippocampal neural death and supragranular and CA3 mossy fiber sprouting in a *lithium-pilocarpine-induced status epilepticus* rat [32]. Other neuroplastic effects were evidenced in the reversion of motor symptoms in PD by tDCS administration. The application of anodal currents enhanced graft survival and dopaminergic re-innervation of the surrounding striatal tissue and pronounced behavioral recovery [55].

Despite the fact that many studies reported recovery from memory deficits following tDCS stimulation, there are some opposing reports in animal models of disease affecting cognition. In a recent study from Gondard and collaborators using a triple transgenic (3xTg) mouse model of AD, it was evidenced that a neurostimulation was not able to ameliorate memory symptoms [56]. To reconcile this discrepancy, previous authors have suggested the importance of choosing an optimal current intensity in order to modulate cortical excitability since LTP alterations were dependent on current intensity [57].

The reports regarding tDCS effects in cognition and memory in animal models of brain disease are listed in Tables 2 and 3.

3.3. Effect of tDCS on Cellular and Molecular Neuroplasticity Mechanisms. Neuronal network reorganization underlies neuroplasticity processes like developmental synaptogenesis, or neurogenesis and synaptic turnover later on, which ultimately contributes to optimal brain development and aging, as well as functional recovery upon trauma [58]. Interestingly, several reports using genetic engineered animals, phar-

macologically induced animal models of disease, or *in vitro* techniques enlightened the potential of direct current stimulation (DCS) to interact with a myriad of neuroplasticity-related processes such as neuroinflammation [59, 60], neural stem cell migration [59], neurite growth [61], or neurogenesis [62]. Moreover, both human and *in vivo* animal studies evidenced a tDCS-induced effect on memory and learning [28, 35, 63]. However, the underlying cellular and molecular mechanisms remain to be elucidated.

3.3.1. Modulation of the Excitatory/Inhibitory Network. To date, animal experimental evidence highlighted tDCS influences on synaptic plasticity, through alterations in the functional connectivity of cognition-related areas [35] and by modulation of excitatory/inhibitory network *tonus* [64], which may involve both the GABAergic and glutamatergic systems. Accordingly, a study conducted with older adults remarked an anodal stimulation effect in gamma-aminobutyric acid (GABA) levels [65]. Similarly, in human healthy volunteers, an anodal tDCS effect in motor learning was correlated with a decrease in GABA levels, an outcome known to be a determinant factor in the promotion of long-term potentiation- (LTP-) dependent plasticity and therefore learning [66, 67].

Several preclinical studies probed LTP enhancement following direct current stimulation. Anodal DCS enhanced LTP in both mouse cortex [68] and rat hippocampal slices [69, 70]. Further, this neurostimulation method increased local field potential (LFPs) amplitudes in primary somatosensory cortex of rabbits [63]. Also, other works demonstrated that neurostimulation-enhanced hippocampal LTP was associated with better spatial memory performance along with an increase in brain-derived neurotrophic factor (BDNF) expression levels [40]. An opposite effect on LTP and LFPs was obtained with administration of cathodal currents. In agreement, a report from Sun et al. [71] evidenced that cathodal currents applied in mouse neocortical slices induced field excitatory postsynaptic potential depression. This type of LTD was smothered by application of an mGluR5 negative allosteric modulator [72]. These findings support a possible modulatory effect of tDCS on mGluR5-mTOR signaling [72]; these molecular pathways are recognized to disturb cognition-related synaptic plasticity.

Further evidence supporting tDCS effect on LTP-like mechanisms was recently brought to light by Stafford et al. [73]. These authors observed that a single anodal tDCS increased both the phosphorylation at the S831 of GluA1 subunit and the translocation of α -amino-3-hydroxy-5-methyl-4-isoxazole propionic acid receptors (AMPA) from cytosolic to synaptic fractions in the hippocampus. These data could be favoring learning enhancement, as this translocation has been associated with hippocampal LTP induction [72]. Accordingly, others reported a spatial working memory enhancement after anodal stimulation over left medial PFC that was lost with the administration of the AMPAR antagonist perampanel (PRP). In contrast to cathodal currents, anodal currents enhanced intracellular calcium (Ca^{2+}) intake in cell cultures including astrocytes [74–76], a process associated with AMPAR phosphorylation

TABLE 2: Continued.

Author	Year	Animal model	Specimen; gender	N	Polarity	Stimulation electrode			Stimulation parameters			Reference electrode		Main findings		
						Position	Stimulation intensity (mA)	Size (cm ²)	Stimulation duration (min)	Current density (A/m ²)	Position	Area (cm ²)				
Leffa et al. [33]	2016	SHR	SHR rats and WKT rats; males	48	a-tDCS	Frontal cortex	0.5	1.5	20	33.4	Between ears	1.5	N	Y (8 consecutive days)	rtDCS	↑ DA levels in STR in both rat strains and in the hippocampus following tDCS treatment in WKY ↑ BDNF levels in WKY rats Short-term memory improvement
Wu et al. [45]	2017	STZ-induced diabetic rats	Sprague Dawley rats; males	130	a-tDCS	dPFC	0.2	0.0314	30	N/A	Anterior chest	0.25	Y	Y		↑ Spatial working memory and mPFC LTP restoring
Pedron et al. [50]	2017	Cocaine injections	Swiss mice; females	165	a-tDCS	Left frontal cortex	0.2	0.035	2 × 20	N/A	Ventral thorax	9.5	N	Y (5 days stimulation, twice a day; 5 h intersimulation interval)		↓ Cocaine-induced locomotor activity No cocaine-induced place preference (5 mg/kg and 25 mg/kg) ↑ Zif268 basal expression under the electrode area, in the STR and cortex
Leffa et al. [55]	2018	ADHD	SHR and WKY rats; males	30	a-tDCS (bicephalic)	Frontal cortex (supraorbital area)	0.5	1.5 (ECG electrode)	20	33.3	Neck	1.5 (ECG electrode)	N/A	Y (8 days)		↓ Inflammatory cytokines and reversion of long-term memory deficits in SHR rats
Bragina et al. [47]	2018	CCI	Mice; N/A	40	a-tDCS	Parietal somatosensory cortex	0.1	N/A	15	N/A	Ventral thorax	N/A	N/A	Y (daily for 4 days, over 4 weeks and 3 days interval)		Motor coordination recovery Spatial memory and learning performance improvement ↑ CBF bilaterally (regional arteriolar dilatation and hypoxia reduction)
Roostaei et al. [44]	2019	STZ-induced diabetic rats	Wistar rats; males	64	a-tDCS vs. c-tDCS	Left frontal cortex	0.2	3.5	20	N/A	Ventral thorax	9.5	N	Y (twice a day over 2 days)		Restoration of STZ-induced amnesia (both polarities)

TABLE 2: Continued.

Author	Year	Animal model	Specimen; gender	N	Polarity	Position	Stimulation electrode			Stimulation parameters			Reference electrode	Anesthesia	rtDCS	Main findings
							Stimulation intensity (mA)	Size (cm ²)	Stimulation duration (min)	Current density (A/m ²)	Position	Area (cm ²)				
Gondard et al. [55]	2019	Animal model of AD-triple transgenic (3xTg) mice	Triple transgenic (3xTg) mice; males	27	c-tDCS and a-tDCS	Secondary motor cortex (M2) (c-tDCS) and dorsal temporal <i>hippocampus</i> (a-tDCS)	0.05	0.0325	20	N/A	N/A	0.0325	N/A	N/A	Y (5 days/week for 3 weeks)	No treatment effect on memory outcome or AD neuropathological biomarkers

Abbreviations: rtDCS: repetitive transcranial direct current stimulation; a-tDCS: anodal transcranial direct current stimulation; c-tDCS: cathodal transcranial direct current stimulation; TBI: traumatic brain injury; ADHD: attention deficit hyperactivity disorder; SHR: spontaneous hypertensive rats; WKY: Wistar Kyoto rats; CBF: cerebral blood flow; PFC: prefrontal cortex; mPFC: medial prefrontal cortex; dPFC: dorsolateral prefrontal cortex; DG: dentate gyrus; STR: striatum; M2: secondary motor cortex; ITC: inferotemporal cortex; CA3: cornu ammonis 3 region in the *hippocampus*; STZ: streptozotocin; AD: Alzheimer's disease; Aβ₁₋₄₀: amyloid beta peptide 1–40; ACh: acetylcholine; BDNF: brain-derived neurotrophic factor; DA: dopamine; GFAP: glial fibrillary acidic protein; Zlf268: zinc finger transcription factor 268; LTP: long-term potentiation; IP: intraperitoneal; SC: subcutaneous; SE: *status epilepticus*; ECG: electrocardiography; mg: milligram; kg: kilogram; A/m²: ampere per square meter; mA: milliampere; cm²: square centimeter; mm: millimeter; h: hour; min: minute; vs.: versus; Y: yes; N: no; N/A: not available.

TABLE 3: Role of transcranial direct current stimulation on neuroplasticity with a focus on animal models of neurotrauma.

Author	Year	Animal model	Specimen; gender	N	Stimulation parameters						Main findings					
					Polarity	Position	Stimulation intensity (mA)	Stimulation electrode Size (cm ²)	Stimulation duration (min)	Current density (A/m ²)		Reference electrode Position	Area (cm ²)	Anesthesia	rtDCS	
Nekhendzy et al. [97]	2004	Inflammatory nociception model	Sprague Dawley rats; males	31	c-tDCS	Frontal cortex	2.25	N/A	45	N/A	N/A	Bimastoid	N/A	Y	Y (8 days)	↓ Nociceptive response (effects lasted up to 50 min poststimulation)
Taib et al. [98]	2009	Left hemispherectomy	Wistar rats; males	9	a-tDCS	Right or left motor cortex	0.4	0.071	20	56.3	0.0064	Supraorbital region	N/A	Y	Y	↑ T corticomuscular response amplitudes
Kim et al. [99]	2010	MCAO	Sprague Dawley rats; both genders	61	c-tDCS vs. a-tDCS	Left primary motor cortex (M1)	0.1	0.785	30	N/A	9	Trunk	9	Y	Y (2 weeks)	Neuroprotection over white matter and ischemic size ↓ (a-tDCS) ↑ Motor function
Jiang et al. [95]	2012	MCAO	Sprague Dawley rats; both genders	90	a-tDCS and c-tDCS	Motor cortex	0.1	0.785	30	1.27	9	Trunk	9	Y	Y (daily, for 3, 7, or 14 days postlesion)	↑ Motor function (7 and 14 days poststroke) ↑ Dendritic spine density ↓ PXI expression (7th and 14h day poststroke)
Yoon et al. [56]	2012	MCAO	Sprague Dawley rats; males	30	a-tDCS	Left primary motor cortex (M1)	0.2	N/A	20	28.2	48.0	Anterior chest	48.0	Y	Y (5 days stimulation 1 week vs. 1 day postischemia)	↑ Motor function and Barnes maze performance (a-tDCS applied 1 week after ischemic injury) ↑ MAP-2 and GAP-43 expression around the perilesional area (a-tDCS applied 1 week postischemic injury)
Laste et al. [100]	2012	CFA injection/chronic inflammation induction	Wistar rats; males	18	a-tDCS	Parietal cortex	0.5	1.5 (ECG electrode)	20	33.4	1.5 (ECG electrode)	Supraorbital area	1.5 (ECG electrode)	N	Y (8 days)	Significant differences in nociceptive response (immediately after and 24 h poststimulation)
Adachi et al. [101]	2012	CRS	Wistar rats; males	48	a-tDCS	Parietal cortex	0.5	1.5 (ECG electrode)	20	3.3	1.5 (ECG electrode)	Supraorbital area	1.5 (ECG electrode)	N	Y (8 days)	↓ Nociceptive response in chronic stress condition ↓ TNF expression in the hippocampus

TABLE 3: Continued.

Author	Year	Animal model	Specimen; gender	N	Polarity	Position	Stimulation electrode			Stimulation parameters			Reference electrode	Anesthesia	rtDCS	Main findings
							Stimulation intensity (mA)	Size (cm ²)	Stimulation duration (min)	Current density (A/m ²)	Position	Area (cm ²)				
Peruzzotti-Jametti et al. [60]	2013	MCAO	C57BL/6 mice; males	137	c-tDCS vs. a-tDCS	Left parietal cortex	0.25	0.0144	40	55	Ventral thorax	5.2	N/A	N (single session)	↑ Infarct volume and ↑ BBB leakage (a-tDCS ipsilesional hemisphere) Cortical Glu activity ↓, functional ↑ and ischemic damage ↓ (c-tDCS ipsilesional hemisphere)	
Notturmo et al. [102]	2014	MCAO	Sprague Dawley rats; both genders	53	c-tDCS	Left motor cortex	0.2	0.07	120	28.6	Ventral thorax	10.5	Y	N (single session)	Ischemia volume ↓	
Lu et al. [103]	2015	MPTP injection	C57bl mice; males	36	a-tDCS	Left frontal cortex	0.2	0.035	10	57	Between shoulders	9	N/A	Y (daily for 3 weeks)	↑ Motor coordination (until 21 days poststimulation) ↑ TH and DA expression ↓ Oxidative stress	
Spezia Adachi et al. [104]	2015	Restraint stress model	Wistar rats; males	78	a-tDCS	Parietal cortex (midline)	0.5	1.5 (ECG electrode)	20	N/A	Supraorbital area	1.5 (ECG electrode)	N	Y (daily for 8 days)	↓ Stress-induced nociceptive response ↑ Pain threshold ↓ BDNF levels (spinal cord and brainstem) in unstressed animals	
Yoon et al. [31]	2016	Lateral fluid percussion method	Sprague Dawley rats; males	36	a-tDCS	Hippocampus	0.2	0.0225	20	28.2	Chest	48 (corset)	Y	Y (daily for 5 days)	↑ Perilesional area BDNF expression (tDCS 2 weeks post-TBI) ↑ Choline/creatinine ratios (tDCS 1 week post-TBI) Motor performance recovery (2 weeks of tDCS)	
Leffa et al. [33]	2016	SHR	SHR rats and WKT rats; males	48	a-tDCS	Frontal cortex	0.5	1.5	20	33.4	Between ears	1.5	N	Y (8 consecutive days)	↑ DA levels in STR in both rat strains and in the hippocampus following tDCS treatment in WKY rats ↑ BDNF levels in WKY rats	

TABLE 3: Continued.

Author	Year	Animal model	Specimen; gender	N	Stimulation parameters				Main findings						
					Polarity	Position	Stimulation intensity (mA)	Stimulation electrode Size (cm ²)		Stimulation duration (min)	Current density (A/m ²)	Reference electrode Position	Area (cm ²)	Anesthesia	rtDCS
Liu et al. [105]	2016	PTI	Sprague Dawley rats; N/A	58	c-tDCS	Right S1FL	2	N/A	20	20.37	Venter	N/A	N/A	N (single session)	Ischemia expansion inhibition (c-tDCS immediately posts ischemia induction) ↓ NeuN expression (c-tDCS+PSS group)
Braun et al. [106]	2016	MCAO	Wistar rats; males	41	c-tDCS vs. a-tDCS	Left primary motor cortex (M1)	0.5	0.035	15	N/A	Ventral thorax	N/A	Y	Y (10-day stimulation; 5 days with 2-day interval)	Gait recovery at day 16 poststroke (both polarities) Faster recovery of limb strength (fully recovered strength at day 10 and gait at day 14 with c-tDCS) ↑ Microglia and neuroblasts in lesion ipsilateral cortex
Cioato et al. [107]	2016	Sciatic nerve chronic constriction	Wistar rats; males	84	a-tDCS and c-tDCS	Parietal cortex (bicephalic)	0.5	1.5 (ECG electrode)	20	N/A	Supraorbital area	1.5 (ECG electrode)	N	Y (8 days)	Nociceptive relieve (for up to 7 days poststimulation) Reversion of T IL-1 β levels (48 h and 7 days poststimulation)
Filho et al. [108]	2016	Partial sciatic nerve compression	Wistar rats; males	144	a-tDCS	Parietal cortex	0.5	1.5 (ECG electrode)	20	N/A	Supraorbital area	1.5 (ECG electrode)	N	Y (8 days)	↓ BDNF expression (48 h poststimulation) Reversion of behavioral alterations (analgesic and anxiolytic) associated with neuropathic pain
Moreira et al. [109]	2016	Pain and menopause (ovariectomised animals)	Wistar rats; females	45	C-tDCS	Parietal cortex	0.5	1.5 (ECG electrode)	20	N/A	Supraorbital area	1.5 (ECG electrode)	N	Y (8 days)	↓ Hypothalamic BDNF levels and T serum BDNF in ovariectomised animals
Dimov et al. [87]	2016	N/A	Wistar rats; males	25	c-tDCS	Left primary motor cortex (M1)	0.25	0.0227	15	N/A	Ventral thorax	N/A	N	N (single session)	Bilateral ↓ Egr-1 expression in the PAG Spinal ENK immunoreactivity ↓ in the DHSC

TABLE 3: Continued.

Author	Year	Animal model	Specimen; gender	N	Stimulation parameters			Main findings
					Stimulation intensity (mA)	Stimulation duration (min)	Current density (A/m ²)	
Liu et al. [110]	2017	PTI	Sprague Dawley rats; males	58	2	20	N/A	Prevention of ischemia injury expansion during hyperacute phase of ischemia (c-tDCS+PSS)
Kim & Han [111]	2017	Modified Tang's method [128]	Sprague Dawley rats; N/A	31	0.2	30	0.26	Early recovery of consciousness and MEP and SEP prolonged latency (tDCS applied right after TBI) ↓ Astroglial GFAP immunoreactivity
Winkler et al. [112]	2017	Striatal 6-OHDA injection	Sprague Dawley rats; females	24	N/A	20	8	Graft survival, striatal dopaminergic reinnervation and motor recovery (a-tDCS)
de Souza et al. [113]	2017	PSNL	Swiss mice; males	N/A	0.5	5; 10; 15; 20	N/A	Antiallodynamic effect (seen 4 h poststimulation of 15 min and 20 min)
Leffa et al. [46]	2018	ADHD	SHR and WKY rats; males	30	0.5	20	33.3	↓ Inflammatory cytokines and reversal of long-term memory deficits in SHR rats
Paciello et al. [114]	2018	NIHL	Wistar rats; males	124	0.35	20	56	↑ Dendritic spines density (layer 2/3 pyramidal neurons of the auditory cortex) ↑ BDNF and synaptophysin expression in auditory cortex (24 h poststimulation)
Fregni et al. [115]	2018	N/A	Wistar rats; males	32	N/A	20	N/A	tDCS prior to stress exposure prevented thermal hyperalgesia

TABLE 3: Continued.

Author	Year	Animal model	Specimen; gender	N	Polarity	Position	Stimulation electrode		Stimulation parameters			Reference electrode Position	Reference electrode Area (cm ²)	Anesthesia	rtDCS	Main findings
							Stimulation intensity (mA)	Size (cm ²)	Stimulation duration (min)	Current density (A/m ²)						
Lee et al. [116]	2019	MPTP injection	C57bl mice; male	60	a-tDCS	Primary motor cortex (M1)	N/A	N/A	30	N/A	Between shoulders	N/A	N/A	Y (daily for 5 days)	↑ Motor coordination Rescue of MPTP-induced mitochondrial dysfunction (C, ATP and GDH and \$ Drp1 levels)	
Callai et al. [117]	2019	CCI-ION	Wistar rats, males	151	a-tDCS	Parietal cortex (bicephalic)	0.5	1.5 (ECG electrode)	20	N/A	Supraorbital area	1.5 (ECG electrode)	N	Y (8 days)	↓ Mechanical hyperalgesia ↓ TNF-α expression (7 days poststimulation) ↓ IL-10 (7 days poststimulation) ↓ LDH serum levels	
Scarabelot et al. [118]	2019	CFA injection/chronic inflammation induction	Sprague Dawley rats; males	104	a-tDCS	Parietal cortex (bicephalic)	0.5	1.5 (ECG electrode)	20	N/A	Supraorbital area	1.5 (ECG electrode)	N/A	Y (8 days)	↓ Thermal and mechanical hyperalgesia ↑ IL-6 (in brainstem 24 h poststimulation) ↓ IL-10 (7 days poststimulation) Normalization of BDNF levels (24 h poststimulation)	

Abbreviations: rtDCS: repetitive transcranial direct current stimulation; a-tDCS: anodal transcranial direct current stimulation; c-tDCS: cathodal transcranial direct current stimulation; C57BL/6: mouse strain; SHR: spontaneous hypertensive rats; WKY: Wistar Kyoto rats; ADHD: attention deficit hyperactivity disorder; 6-OHDA: 6-hydroxydopamine; MPTP: 1-methyl-4-phenyl-1,2,3,6-tetrahydropyridine; TBI: traumatic brain injury; PTI: photothrombotic ischemia; MCAO: middle cerebral artery occlusion; PSS: peripheral sensory stimulation; NIH1: noise-induced hearing loss; CC-ION: chronic constriction of the infraorbital nerve (pain model); PSNL: partial sciatic nerve ligation (pain model); CRS: chronic restraint stress (pain model); CFA: complete Freund's adjuvant (pain model); BBB: blood-brain barrier; SJFL: forelimb region of the primary somatosensory cortex; M1: primary motor area; PAG: periaqueductal grey; DHSC: dorsal horn of the spinal cord; MEP: motor-evoked potentials; SEP: somatosensory evoked potentials; GFAP: glial fibrillary acidic protein; BDNF: brain-derived neurotrophic factor; Glu: glutamate NeuN: neuronal marker; PX1: pannexin 1; TH: thyroxine hydroxylase; Egr-1: early growth response protein 1; TNF: tumor necrosis factor; IL-1β: interleukin 1 beta; IL-6: interleukin 6; IL-10: interleukin 10; LDH: lactate dehydrogenase enzyme; ATP: adenosine triphosphate; GDH: glutamate dehydrogenase; Drp1: dynamin-related protein; MAP-2: microtubule associated protein 2; GAP-43: growth associated protein 43; ENK: early embryo specific NK; DA: dopamine; ECG: electrocardiography; EEG: electroencephalogram; A/m²: ampere per square meter; mA: milliampere; vs.: versus; min: minute; cm²: square centimeter; mm: millimeter; Y: yes; N: no; N/A: not available.

and trafficking to postsynaptic density [77] and ultimately, allowing LTP facilitation, a cellular correlate of learning and memory.

3.3.2. Activation of Neuroplasticity-Associated Gene Expression. Neurostimulation could have long-lasting effects in memory as data from different studies evidenced [40]. Authors have been argued that tDCS cognition modulation is associated with neuroplasticity-associated gene expression alterations [78]. One of the neuroplasticity-associated genes, known to be essential for hippocampal LTP, is BDNF [79]. Several studies elucidated the role of BDNF in memory modulation by tDCS. In fact, it was reported that anodal currents could increase BDNF expression [68], and its activation *via* tropomyosin receptor kinase (Trk) receptors [80], triggering NMDAR opening, and inducing a later phase LTP (L-LTP) facilitation [81]. Accordingly, Yu et al. [41] found that the administration the Trk inhibitor ANA-12 prevented the anodal tDCS-induced hippocampal CA1 LTP increase. Other studies, using the same polarity currents, revealed a link between the upregulation of BDNF and cAMP response element binding protein/CREB-binding protein (CREB/CBP) [40] involved in LTP and memory formation [82]. Also, the application of cortical anodal currents in frontal cortex was able to upregulate BDNF together with striatal dopamine [33]. The upregulation of BDNF following neurostimulation was associated with the augmentation of expression levels of immediate early genes (IEGs), such as *c-fos* and *zif268* [69]. Moreover, Kim et al. [78] confirmed that repetitive anodal tDCS in right sensorimotor cortex of healthy rats promoted a significant increase of mRNA levels of plasticity-associated genes, namely, BDNF, cAMP response element binding protein (CREB), synapsin I, Ca²⁺/calmodulin-dependent protein kinase II (CaMKII), activity-regulated cytoskeleton-associated protein (Arc), and *c-fos*. It was also demonstrated that sensory evoked cortical responses were boosted after tDCS *via* alpha-1 adrenergic receptor-mediated astrocytic Ca²⁺/IP3 signaling, thus involving also glia and the adrenergic system [75]. Anodal tDCS actions in glia were further confirmed by Mishima et al. [76]. Using a mouse model lacking Ca²⁺ uptake in astrocytes, the inositol trisphosphate receptor type 2 (IP3R2) knockout (KO) mouse and also an adrenergic receptor antagonist, they confirmed decreased microglia motility along with soma enlargement in tDCS stimulated animals [76].

In poststroke recovery, it was found that anodal currents significantly increased the GAP-43 and the microtubule-associated protein 2 (MAP-2) expression around the infarct area [56]. These neuronal growth-promoting proteins are overexpressed during dendritic remodeling and axonal regrowth throughout the acute phase of stroke [83, 84]. Anodal stimulation also modulated pannexin-1 (PX1) hemichannel levels [85, 86] and, following an ischemic insult, neurostimulation decreased rat PX1 mRNA and, consequently, augmented dendritic spine density in the surrounding areas of cerebral infarction; these cellular outcomes were associated with the improvement of motor function [85]. Some authors proposed that tDCS-induced improvement of stroke/TBI symptoms might be due to increase of BDNF expres-

sion and associated with choline/creatine ratios in the perilesional cortex [31].

Overall, tDCS methodology was able to modulate molecular pathways involved in the regulation of cognition-related synaptic plasticity mechanisms (Figure 3). The revised *in vivo* animal studies regarding tDCS-induced effects in the cellular and molecular mechanisms of memory and learning are listed in Table 4.

4. Discussion

This systematic review collected several studies that confirm the potential effects of tDCS on neuronal activity and synaptic plasticity. Here, we documented a variable combination of stimulation protocols, stimulation areas, and healthy and disease animal models. Most of the existent literature is focused on human application of tDCS. The comprehensive revision of the effect of tDCS on rodent models of normal and pathological brain functioning does therefore provide a novel contribution to the field. Overall, the revised studies indicated that tDCS was able to modulate synaptic plasticity and, consequently, learning and memory processes [87, 88].

Memory formation and consolidation are recognized to rely on activity-dependent modifications, such as LTD and LTP [89], both dependent on the activation of calcium-dependent kinases (e.g., CaMKs), which in turn control the trafficking of NMDARs and AMPARs [90]. Despite the wide set of stimulation protocols, tDCS-induced modulation of NMDAR signaling and synaptic protein upregulation resulting in LTP and cognitive enhancement have been consistently reported in animal studies. Anodal tDCS increased AMPAR synapse translocation [73, 89] and induced spatial memory improvement by involving both CREB and BDNF expression alterations [53]. Also, an increase in hippocampal and cortical mRNA levels of *c-fos*, synapsin, CaMKII, and Arc was observed poststimulation [78].

Similar results highlighting tDCS effects in neuroplasticity were obtained with *in vitro* studies. Accordingly, Ranieri and coworkers [69] probed that anodal currents increased NMDAR-dependent LTP in hippocampal CA3-CA1 synapses [69], in part, due to production of BDNF [68]. In addition, it was demonstrated that tDCS-induced hippocampal BDNF release is dependent on histone acetylation of BDNF gene promoters [40]. Overall, the abovementioned works provide positive evidence for the effect of tDCS on cognitive function enhancement.

Although tDCS impaired the acquisition of both contextual and cued fear memory [39], there are no studies on possible cascades/proteins involved in tDCS-induced neuroplasticity alterations following fear memory changes. Nevertheless, a very recent paper demonstrated chronic repetitive TMS of the ventromedial prefrontal cortex reversed stress-induced behavior impairments with an increase of *c-fos* activity [91].

Cortical anodal currents have been shown to be mostly excitatory and support memory enhancement and neuroplasticity. The literature is also consistent with the notion that the stimulation over the cortical region functionally involved in a certain cognitive task increases performance in that specific task. Marshall et al. demonstrated that anodal

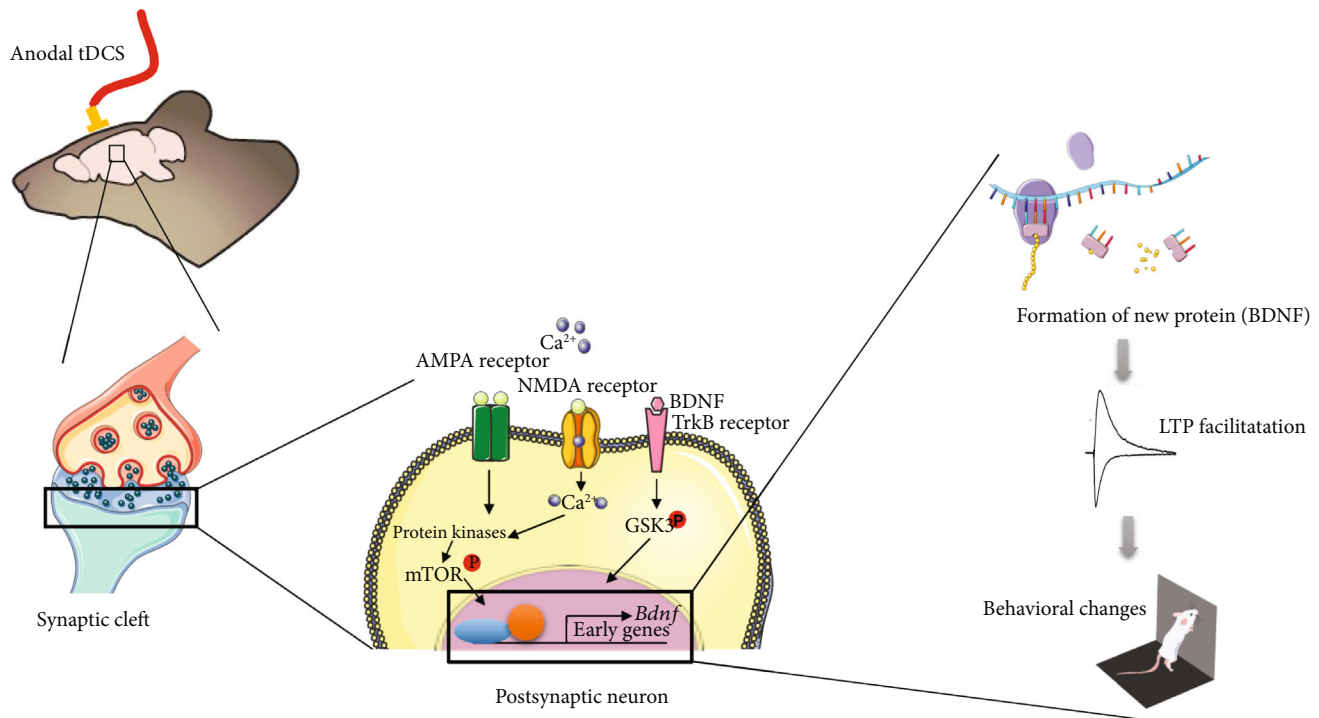


FIGURE 3: Schematic illustration of molecular mechanisms underlying the effect of anodal transcranial direct current stimulation (tDCS) on neuronal physiology. The neurostimulation in the target cortical area depolarizes neuronal membrane and glutamate released in presynaptic neuron and binds in NMDA and AMPA receptors (see book chapter Rozisky et al., 2015). Consequently, there is intracellular Ca^{2+} upregulation in the postsynaptic neuron, which can activate protein kinases that in turn modulate numerous neuronal signaling pathways (such as the mTOR pathway) leading to transcriptional changes. The tDCS also activates molecular cascades to promote BDNF production. As a long-term mechanism, gene transcription is modulated leading to the formation of new proteins that in turn lead to facilitation of LTP and improvement of cognition. Abbreviations: AMPA: α -amino-3-hydroxy-5-methyl-4-isoxazolepropionic acid; BDNF: brain-derived neurotrophic factor; CBP: CREB-binding protein; CREB: cAMP response element binding protein; GSK3: glycogen synthase kinase 3; LTP: long-term potentiation; mTOR: mammalian target of rapamycin; NMDA: N-methyl-D-aspartate; TrkB: tropomyosin receptor kinase B.

currents over the PFC, a region involved in memory encoding, during slow wave sleep improved declarative memory [28]. However, it was described that cortical cathodal stimulation simultaneously with training task was able to increase visuospatial working memory, in spite of the fact that it was associated with decreased excitability [42]. This suggests that modulatory effects of tDCS were influenced by the polarity-dependent electrical dynamics established between the stimulated area and its related neuronal networks. In agreement, a recent report observed an inhibitory effect in motor learning tasks following anodal currents in the cerebellum; the anodal excitatory effect over the Purkinje cell activity led to an overall inhibition of downstream structures, reducing as a result the vestibulo-ocular reflex gain [90]. Similar paradoxical results have been observed in humans. Recently, Moliadze and collaborators [92] reported that tDCS-induced neural modulation depended on several parameters, namely, the age. In fact, an excitatory effect was seen in young subjects, but not in the older participants.

Nowadays, TMS, another important noninvasive brain stimulation technique, is useful for evaluating excitability in the primary motor cortex (M1) and conductivity along the cortical-spinal tract. This technique has been amply used in rehabilitation of stroke patients [93] and in neuropsychiatric

disorders, namely, depression [94]. tDCS and TMS are undergoing the most active investigation and share a capacity to modulate regional cortical excitability, and both are well-tolerated by children and adults [95]. However, TMS has been already approved for clinical use and tDCS is still undergoing investigation as a plausible therapy for a range of neuropsychiatric disorders [95]. The rationale, in part, for this is because data on the efficacy and safety of tDCS are sparse and employ heterogeneous stimulation protocols. Indeed, there is a paucity of strictly conducted randomized, sham controlled clinical trials, and case considerable follow-up periods, which makes it difficult to use these results to inform clinical practice concerning the putative beneficial role of tDCS. Moreover, tDCS effects seem to be clearly dependent on structure, connectivity, and function of the target brain region. Importantly, these outcomes were intrinsically correlated with GABAergic neurotransmission which raises the issue that one has to take into account that during development GABA can act as an excitatory neurotransmitter [96].

5. Conclusions

There is growing evidence that tDCS modulates brain activity and, consequently, enhances synaptic plasticity and cognitive

TABLE 4: Cellular and molecular mechanisms underlying transcranial direct current stimulation effect in the brain.

Author	Year	Animal model	Specimen; gender	N	Stimulation electrode			Stimulation parameters			Reference electrode		Main findings	
					Polarity	Position	Stimulation intensity (mA)	Size (cm ²)	Stimulation duration (min)	Current density (A/m ²)	Position	Area (cm ²)		rtDCS
Márquez-Ruiz et al. [63]	2012	NDM	New Zealand White albino rabbits; N/A	13	a-tDCS and c-tDCS	Somatosensory cortex (S1)	0.5; 1; 1.5 and 2	0.7857	10	3.7	Ear	35	N (single session)	↑ LFP in S1 (a-tDCS) and ↓ LFP S1 (c-tDCS)
Rohan et al. [57]	2015	NDM	Sprague Dawley rats; male	34	a-tDCS	SC dorsal to the hippocampus	0.1 or 0.25	0.25	30	N/A	Between shoulders	8.04	N (single session)	# LTP and PPF in the hippocampus
Yoon et al. [31]	2016	Lateral fluid percussion method	Sprague Dawley rats; males	36	a-tDCS	Hippocampus	0.2	0.0225	20	28.2	Chest	48 (corset)	Y (daily for 5 days)	# perilesional area BDNF expression (tDCS 2 weeks post-TBI) # choline/creatinine ratios (tDCS 1 week post-TBI) Motor performance recovery (2 weeks of tDCS)
Leffa et al. [33]	2016	SHR	SHR rats and WKT rats; males	48	a-tDCS	Frontal cortex	0.5	1.5	20	33.4	Between ears	1.5	Y (8 consecutive days)	# DA levels in STR in both rat strains and in the hippocampus following tDCS treatment in WKY rats # BDNF levels in WKY rats Short-term memory improvement
Podda et al. [40]	2016	NDM	C57BL/6 mice; males	16	a-tDCS vs. c-tDCS	Left parietal cortex (dorsal to hippocampal formation)	0.35	0.06	20	N/A	Ventral thorax	5.2	N (single session)	# spatial learning and memory (a-tDCS); benefits observable one week after # BDNF expression in the hippocampus CREB/CBP pathway activation

TABLE 4: Continued.

Author	Year	Animal model	Specimen; gender	N	Polarity	Position	Stimulation electrode			Stimulation parameters			Reference electrode		Main findings
							Stimulation intensity (mA)	Size (cm ²)	Stimulation duration (min)	Current density (A/m ²)	Position	Area (cm ²)	Anesthesia	rtDCS	
Monai et al. [75]	2016	NDM	G7NG817 mice; N/A	10	a-tDCS	Primary visual cortex (V1)	0.1	0.02	10	N/A	Neck	N/A	N	N (single session)	Up to 50% expansion of visual evoke active area (up to 2 h poststimulation effect) tDCS-induced plasticity depends on the activity of IP, R2, and A1AR
Kim et al. [78]	2017	NDM	Sprague Dawley rats; males	90	a-tDCS	Right sensorimotor cortex	0.25	0.071	20	N/A	Right anterior chest	0.5	N	Y (7 days)	# BDNF, CREB, synapsin, and CaMKII mRNA expression levels (ipsilateral cortex) and c-fos (<i>hippocampus</i>)
Stafford et al. [73]	2018	NDM	Sprague Dawley rats; males	16	a-tDCS	Caudal to bregma	0.25	0.25	30	N/A	Ventral thorax	N/A	N	N (single session)	↑ AMPAR translocation to the synapse in the hippocampus and ↑ phosphorylation of the S831 site on GluA1
Martins et al. [97]	2019	NDM	Male Wistar rats; males	50	a-tDCS	Left mPFC	0.4	N/A	13	N/A	N/A	N/A	N/A	Y (5 days)	↑ Spatial working memory ↑ GAP-43 (extinct by AMPAR antagonist PRP)
Yu et al. [41]	2019	NDM	Sprague Dawley rats; males	224	a-tDCS	SC dorsal to the <i>hippocampus</i>	0.25	0.25	30	N/A	Anterior chest	N/A (EEG electrode)	Y	N (single session)	↑ Memory (passive avoidance memory retention) ↑ LTP in CA1 <i>hippocampus</i> (blocked by <i>TrkB antagonist</i>) ↑ BDNF in CA1 <i>hippocampus</i>

Abbreviations: rtDCS: repetitive transcranial direct current stimulation; a-tDCS: anodal transcranial direct current stimulation; c-tDCS: cathodal transcranial direct current stimulation; C57BL/6: mouse strain; SC: stereotaxic coordinates; NDM: no disease model; SHR: spontaneous hypertensive rats; WKY: Wistar Kyoto rats; PFC: prefrontal cortex; mPFC: medial prefrontal cortex; dPFC: dorsolateral prefrontal cortex; DG: dentate gyrus; STR: *striatum*; S1: somatosensory cortex; V1: primary visual cortex; ITC: inferotemporal cortex; CA1: cornu ammonis 1 region in the hippocampus; TBI: traumatic brain injury; PRP: perampanel; CREB: cAMP response element-binding protein (transcription factor); CREB/CBP: cAMP response element binding protein; BDNF: brain-derived neurotrophic factor; DA: dopamine; GAP-43: growth associate protein 43; CaMKII: Ca²⁺/calmodulin-dependent protein kinase; mRNA: messenger ribonucleic acid; IP3R2: inositol triphosphate type 2 receptor; A1AR: adenosine A2A receptor; AMPAR: α-amino-3-hydroxy-5-methyl-4-isoxazolepropionic acid receptor; GluA1: AMPA receptor subunit A1; LFP: local field potential; LTP: long-term potentiation; PPF: paired pulse facilitation; EEG: electroencephalography; A/m²: ampere per square meter; mA: milliampere; cm²: square centimeter; mm: millimeter; h: hour; min: minute; vs.: versus; Y: yes; N: no; N/A: not available.

performance. Overall, reports from laboratory animal research present tDCS as a promising noninvasive brain stimulation technique. The presented evidence is therefore consistent with human studies suggesting that this technique is useful to mitigate neurologic symptoms of several brain disorders, thus improving learning and memory. Further research is needed so that this technique can be fully translated into optimal therapeutic strategies.

Conflicts of Interest

The authors declare that there is no conflict of interest regarding the publication of this paper.

Authors' Contributions

Joana Gonçalves and Miguel Castelo-Branco share senior authorship.

Acknowledgments

This work was supported by grants POCI-01-0145-FEDER-016428 and CENTRO-01-0145-FEDER-000016 financed by Centro 2020 FEDER, COMPETE, FLAD Life Sciences Ed 2 2016, FCT/UID 4950 COMPETE, POCI-01-0145-FEDER-007440, FCT, and European Grant H2020 STIPED.

References

- [1] G. Ruffini, F. Wendling, I. Merlet et al., "Transcranial current brain stimulation (tCS): models and technologies," *IEEE Transactions on Neural Systems and Rehabilitation Engineering*, vol. 21, no. 3, pp. 333–345, 2013.
- [2] M. A. Nitsche and W. Paulus, "Excitability changes induced in the human motor cortex by weak transcranial direct current stimulation," *The Journal of Physiology*, vol. 527, no. 3, pp. 633–639, 2000.
- [3] T. Wagner, A. Valero-Cabre, and A. Pascual-Leone, "Noninvasive human brain stimulation," *Annual Review of Biomedical Engineering*, vol. 9, no. 1, pp. 527–565, 2007.
- [4] M. Nitsche, D. Liebetanz, A. Antal, N. Lang, F. Tergau, and W. Paulus, "Modulation of cortical excitability by weak direct current stimulation—technical, safety and functional aspects," *Supplements to Clinical Neurophysiology*, vol. 56, pp. 255–276, 2003.
- [5] P. Kellaway, "The part played by electrical fish in the early history of bioelectricity and electrotherapy," *Bulletin of the History of Medicine*, vol. 20, no. 2, pp. 130–134, 1946.
- [6] A. Parent, "Giovanni Aldini: from animal electricity to human brain stimulation," *The Canadian Journal of Neurological Sciences*, vol. 31, no. 4, pp. 576–584, 2004.
- [7] T. Bullock and C. Terzuolo, "Diverse forms of activity in the somata of spontaneous and integrating ganglion cells," *The Journal of Physiology*, vol. 138, no. 3, pp. 341–364, 1957.
- [8] C. Poreisz, K. Boros, A. Antal, and W. Paulus, "Safety aspects of transcranial direct current stimulation concerning healthy subjects and patients," *Brain Research Bulletin*, vol. 72, no. 4–6, pp. 208–214, 2007.
- [9] L. Bindman, O. Lippold, and J. Redfearn, "The action of brief polarizing currents on the cerebral cortex of the rat (1) during current flow and (2) in the production of long-lasting after-effects," *The Journal of Physiology*, vol. 172, pp. 369–382, 1964.
- [10] C. A. Terzuolo and T. H. Bullock, "Measurement of imposed voltage gradient adequate to modulate neuronal firing," *Proceedings of the National Academy of Sciences of the United States of America*, vol. 42, no. 9, pp. 687–694, 1956.
- [11] M. A. Nitsche and W. Paulus, "Sustained excitability elevations induced by transcranial DC motor cortex stimulation in humans," *Neurology*, vol. 57, no. 10, pp. 1899–1901, 2001.
- [12] A. Antal, D. Terney, C. Poreisz, and W. Paulus, "Towards unravelling task-related modulations of neuroplastic changes induced in the human motor cortex," *The European Journal of Neuroscience*, vol. 26, no. 9, pp. 2687–2691, 2007.
- [13] B. Krause and R. Cohen Kadosh, "Not all brains are created equal: the relevance of individual differences in responsiveness to transcranial electrical stimulation," *Frontiers in Systems Neuroscience*, vol. 8, 2014.
- [14] M. Bikson, A. Rahman, and A. Datta, "Computational models of transcranial direct current stimulation," *Clinical EEG and Neuroscience*, vol. 43, no. 3, pp. 176–183, 2012.
- [15] A. Fertonani and C. Miniussi, "Transcranial electrical stimulation: what we know and do not know about mechanisms," *The Neuroscientist*, vol. 23, no. 2, pp. 109–123, 2017.
- [16] D. Liebetanz, F. Klinker, D. Hering et al., "Anticonvulsant effects of transcranial direct-current stimulation (tDCS) in the rat cortical ramp model of focal epilepsy," *Epilepsia*, vol. 47, no. 7, pp. 1216–1224, 2006.
- [17] D. Liebetanz, R. Koch, S. Mayenfels, F. König, W. Paulus, and M. A. Nitsche, "Safety limits of cathodal transcranial direct current stimulation in rats," *Clinical Neurophysiology*, vol. 120, no. 6, pp. 1161–1167, 2009.
- [18] M. Jackson, D. Truong, M. Brownlow et al., "Safety parameter considerations of anodal transcranial direct current stimulation in rats," *Brain, Behavior, and Immunity*, vol. 64, pp. 152–161, 2017.
- [19] M. Nitsche, L. Cohen, E. Wassermann et al., "Transcranial direct current stimulation: state of the art 2008," *Brain Stimulation*, vol. 1, no. 3, pp. 206–223, 2008.
- [20] K. Monte-Silva, M. Kuo, D. Liebetanz, W. Paulus, and M. A. Nitsche, "Shaping the optimal repetition interval for cathodal transcranial direct current stimulation (tDCS)," *Journal of Neurophysiology*, vol. 103, no. 4, pp. 1735–1740, 2010.
- [21] P. S. Boggio, R. Ferrucci, S. P. Rigonatti et al., "Effects of transcranial direct current stimulation on working memory in patients with Parkinson's disease," *Journal of the Neurological Sciences*, vol. 249, no. 1, pp. 31–38, 2006.
- [22] M. Horiba, Y. Ueki, I. Nojima et al., "Impaired motor skill acquisition using mirror visual feedback improved by transcranial direct current stimulation (tDCS) in patients with Parkinson's disease," *Frontiers in Neuroscience*, vol. 13, p. 602, 2019.
- [23] F. Fregni, P. S. Boggio, M. A. Nitsche, S. P. Rigonatti, and A. Pascual-Leone, "Cognitive effects of repeated sessions of transcranial direct current stimulation in patients with depression," *Depression and Anxiety*, vol. 23, no. 8, pp. 482–484, 2006.
- [24] F. Fregni, P. Boggio, C. Mansur et al., "Transcranial direct current stimulation of the unaffected hemisphere in stroke patients," *Neuroreport*, vol. 16, no. 14, pp. 1551–1555, 2005.

- [25] F. Hummel, P. Celnik, P. Giraux et al., "Effects of non-invasive cortical stimulation on skilled motor function in chronic stroke," *Brain*, vol. 128, no. 3, pp. 490–499, 2005.
- [26] M. C. W. English, E. S. Kitching, M. T. Maybery, and T. A. W. Visser, "Modulating attentional biases of adults with autistic traits using transcranial direct current stimulation: a pilot study," *Autism Research*, vol. 11, no. 2, pp. 385–390, 2018.
- [27] J. Kang, E. Cai, J. Han et al., "Transcranial direct current stimulation (tDCS) can modulate EEG complexity of children with autism spectrum disorder," *Frontiers in Neuroscience*, vol. 12, p. 201, 2018.
- [28] L. Marshall, M. Mölle, M. Hallschmid, and J. Born, "Transcranial direct current stimulation during sleep improves declarative memory," *Journal of Neuroscience*, vol. 24, no. 44, pp. 9985–9992, 2004.
- [29] J. C. de Souza Custódio, C. W. Martins, M. D. M. V. Lugon, F. Fregni, and E. M. Nakamura-Palacios, "Epidural direct current stimulation over the left medial prefrontal cortex facilitates spatial working memory performance in rats," *Brain Stimulation*, vol. 6, no. 3, pp. 261–269, 2013.
- [30] X. Yu, Y. Li, H. Wen, Y. Zhang, and X. Tian, "Intensity-dependent effects of repetitive anodal transcranial direct current stimulation on learning and memory in a rat model of Alzheimer's disease," *Neurobiology of Learning and Memory*, vol. 123, pp. 168–178, 2015.
- [31] K. J. Yoon, Y. T. Lee, S. W. Chae, C. R. Park, and D. Y. Kim, "Effects of anodal transcranial direct current stimulation (tDCS) on behavioral and spatial memory during the early stage of traumatic brain injury in the rats," *Journal of the Neurological Sciences*, vol. 362, pp. 314–320, 2016.
- [32] T. Kamida, S. Kong, N. Eshima, T. Abe, M. Fujiki, and H. Kobayashi, "Transcranial direct current stimulation decreases convulsions and spatial memory deficits following pilocarpine-induced status epilepticus in immature rats," *Behavioural Brain Research*, vol. 217, no. 1, pp. 99–103, 2011.
- [33] D. T. Leffa, A. de Souza, V. L. Scarabelot et al., "Transcranial direct current stimulation improves short-term memory in an animal model of attention-deficit/hyperactivity disorder," *European Neuropsychopharmacology*, vol. 26, no. 2, pp. 368–377, 2016.
- [34] D. Moher, A. Liberati, J. Tetzlaff, D. G. Altman, and The PRISMA Group, "Preferred reporting items for systematic reviews and meta-analyses: the PRISMA statement," *PLoS Medicine*, vol. 6, no. 7, article e1000097, 2009.
- [35] M. R. Krause, T. P. Zanos, B. A. Csorba et al., "Transcranial direct current stimulation facilitates associative learning and alters functional connectivity in the primate brain," *Current Biology*, vol. 27, no. 20, pp. 3086–3096.e3, 2017.
- [36] F. Manteghi, M. Nasehi, and M. Zarrindast, "Precondition of right frontal region with anodal tDCS can restore the fear memory impairment induced by ACPA in male mice," *EXCLI Journal*, vol. 16, pp. 1–13, 2017.
- [37] M. Nasehi, R. Soltanpour, M. Ebrahimi-Ghiri, S. Zarrabian, and M. R. Zarrindast, "Interference effects of transcranial direct current stimulation over the right frontal cortex and adrenergic system on conditioned fear," *Psychopharmacology*, vol. 234, no. 22, pp. 3407–3416, 2017.
- [38] M. Nasehi, M. Khani-Abyaneh, M. Ebrahimi-Ghiri, and M. R. Zarrindast, "The effect of left frontal transcranial direct-current stimulation on propranolol-induced fear memory acquisition and consolidation deficits," *Behavioural Brain Research*, vol. 331, pp. 76–83, 2017.
- [39] S. Abbasi, M. Nasehi, H. R. S. Lichaei, and M. R. Zarrindast, "Effects of left prefrontal transcranial direct current stimulation on the acquisition of contextual and cued fear memory," *Iranian Journal of Basic Medical Sciences*, vol. 20, no. 6, pp. 623–630, 2017.
- [40] M. Podda, S. Cocco, A. Mastrodonato et al., "Anodal transcranial direct current stimulation boosts synaptic plasticity and memory in mice via epigenetic regulation of Bdnf expression," *Scientific Reports*, vol. 6, p. 22180, 2016.
- [41] T. H. Yu, Y. J. Wu, M. E. Chien, and K. S. Hsu, "Transcranial direct current stimulation induces hippocampal metaplasticity mediated by brain-derived neurotrophic factor," *Neuropharmacology*, vol. 144, no. 1, pp. 358–367, 2019.
- [42] C. Dockery, D. Liebetanz, N. Birbaumer, M. Malinowska, and M. J. Wesierska, "Cumulative benefits of frontal transcranial direct current stimulation on visuospatial working memory training and skill learning in rats," *Neurobiology of Learning and Memory*, vol. 96, no. 3, pp. 452–460, 2011.
- [43] S. Yu, S. Park, and K. Sim, "The effect of tDCS on cognition and neurologic recovery of rats with Alzheimer's disease," *Journal of Physical Therapy Science*, vol. 26, no. 2, pp. 247–249, 2014.
- [44] C. H. Chang, H. Y. Lane, and C. H. Lin, "Brain stimulation in Alzheimer's disease," *Frontiers in Psychiatry*, vol. 9, 2018.
- [45] A. Roostaei, G. Vaezi, M. Nasehi, A. Haeri-Rohani, and M. R. Zarrindast, "The involvement of D1 and D2 dopamine receptors in the restoration effect of left frontal anodal, but not cathodal, tDCS on streptozocin-induced amnesia," *Archives of Iranian Medicine*, vol. 22, no. 3, pp. 144–154, 2019.
- [46] Y. Wu, C. Lin, C. Yeh et al., "Repeated transcranial direct current stimulation improves cognitive dysfunction and synaptic plasticity deficit in the prefrontal cortex of streptozotocin-induced diabetic rats," *Brain Stimulation*, vol. 10, no. 6, pp. 1079–1087, 2017.
- [47] D. T. Leffa, B. Bellaver, A. A. Salvi et al., "Transcranial direct current stimulation improves long-term memory deficits in an animal model of attention-deficit/hyperactivity disorder and modulates oxidative and inflammatory parameters," *Brain Stimulation*, vol. 11, no. 4, pp. 743–751, 2018.
- [48] O. Bragina, D. Lara, E. Nemoto, C. W. Shuttleworth, O. V. Semyachkina-Glushkovskaya, and D. E. Bragin, "Increases in microvascular perfusion and tissue oxygenation via vasodilatation after anodal transcranial direct current stimulation in the healthy and traumatized mouse brain," *Advances in Experimental Medicine and Biology*, vol. 1072, pp. 27–31, 2018.
- [49] P. Spagnolo and D. Goldman, "Neuromodulation interventions for addictive disorders: challenges, promise and roadmap for future research," *Brain*, vol. 140, no. 5, pp. 1183–1203, 2017.
- [50] S. Pedron, J. Monnin, E. Haffen, D. Sechter, and V. van Waes, "Repeated transcranial direct current stimulation prevents abnormal behaviors associated with abstinence from chronic nicotine consumption," *Neuropsychopharmacology*, vol. 39, no. 4, pp. 981–988, 2014.
- [51] S. Pedron, J. Beverley, E. Haffen, P. Andrieu, H. Steiner, and V. van Waes, "Transcranial direct current stimulation produces long-lasting attenuation of cocaine-induced behavioral responses and gene regulation in corticostriatal circuits," *Addiction Biology*, vol. 22, no. 5, pp. 1267–1278, 2017.
- [52] T. Kamida, S. Kong, N. Eshima, and M. Fujiki, "Cathodal transcranial direct current stimulation affects seizures and

- cognition in fully amygdala-kindled rats,” *Neurological Research*, vol. 35, no. 6, pp. 602–607, 2013.
- [53] M. Zobeiri and G. van Luijckelaar, “Noninvasive transcranial direct current stimulation in a genetic absence model,” *Epilepsy & Behavior*, vol. 26, no. 1, pp. 42–50, 2013.
- [54] S. C. Dhamne, D. Ekstein, Z. Zhuo et al., “Acute seizure suppression by transcranial direct current stimulation in rats,” *Annals of Clinical and Translational Neurology*, vol. 2, no. 8, pp. 843–856, 2015.
- [55] J. G. Rohan, K. A. Carhuatanta, S. M. McInturf, M. K. Miklasevich, and R. Jankord, “Modulating hippocampal plasticity with in vivo brain stimulation,” *The Journal of Neuroscience*, vol. 35, no. 37, pp. 12824–12832, 2015.
- [56] E. Gondard, M. Soto-Montenegro, A. Cassol, A. M. Lozano, and C. Hamani, “Transcranial direct current stimulation does not improve memory deficits or alter pathological hallmarks in a rodent model of Alzheimer’s disease,” *Journal of Psychiatric Research*, vol. 114, pp. 93–98, 2019.
- [57] K. J. Yoon, B. M. Oh, and D. Y. Kim, “Functional improvement and neuroplastic effects of anodal transcranial direct current stimulation (tDCS) delivered 1 day vs. 1 week after cerebral ischemia in rats,” *Brain Research*, vol. 1452, pp. 61–72, 2012.
- [58] D. Hebb, *The Organization of Behavior*, Wiley, New York, 1949.
- [59] M. Rueger, M. Keuters, M. Walberer et al., “Multi-session transcranial direct current stimulation (tDCS) elicits inflammatory and regenerative processes in the rat brain,” *PLoS One*, vol. 7, no. 8, article e43776, 2012.
- [60] L. Peruzzotti-Jametti, M. Cambiaghi, M. Bacigaluppi et al., “Safety and efficacy of transcranial direct current stimulation in acute experimental ischemic stroke,” *Stroke*, vol. 44, no. 11, pp. 3166–3174, 2013.
- [61] C. McCaig, L. Sangster, and R. Stewart, “Neurotrophins enhance electric field-directed growth cone guidance and directed nerve branching,” *Developmental Dynamics*, vol. 217, no. 3, pp. 299–308, 2000.
- [62] A. Pikhovych, N. P. Stolberg, L. Jessica Flitsch et al., “Transcranial direct current stimulation modulates neurogenesis and microglia activation in the mouse brain,” *Stem Cells International*, vol. 2016, 9 pages, 2016.
- [63] J. Márquez-Ruiz, R. Leal-Campanario, R. Sánchez-Campusano et al., “Transcranial direct-current stimulation modulates synaptic mechanisms involved in associative learning in behaving rabbits,” *Proceedings of the National Academy of Sciences of the United States of America*, vol. 109, no. 17, pp. 6710–6715, 2012.
- [64] B. Krause, J. Márquez-Ruiz, and R. C. Kadosh, “The effect of transcranial direct current stimulation: a role for cortical excitation/inhibition balance?,” *Frontiers in Human Neuroscience*, vol. 7, no. 602, 2013.
- [65] D. Antonenko, F. Schubert, F. Bohm et al., “tDCS-induced modulation of GABA levels and resting-state functional connectivity in older adults,” *The Journal of Neuroscience*, vol. 37, no. 15, pp. 4065–4073, 2017.
- [66] C. Stagg and M. Nitsche, “Physiological basis of transcranial direct current stimulation,” *The Neuroscientist*, vol. 17, no. 1, pp. 37–53, 2011.
- [67] C. J. Stagg, V. Bachtiar, U. Amadi et al., “Local GABA concentration is related to network-level resting functional connectivity,” *eLife*, vol. 3, no. 3, pp. 1–9, 2014.
- [68] B. Fritsch, J. Reis, K. Martinowich et al., “Direct current stimulation promotes BDNF-dependent synaptic plasticity: potential implications for motor learning,” *Neuron*, vol. 66, no. 2, pp. 198–204, 2010.
- [69] F. Ranieri, M. Podda, E. Riccardi et al., “Modulation of LTP at rat hippocampal CA3-CA1 synapses by direct current stimulation,” *Journal of Neurophysiology*, vol. 107, no. 7, pp. 1868–1880, 2012.
- [70] G. Kronberg, M. Bridi, T. Abel, M. Bikson, and L. C. Parra, “Direct current stimulation modulates LTP and LTD: activity dependence and dendritic effects,” *Brain Stimulation*, vol. 10, no. 1, pp. 51–58, 2017.
- [71] Y. Sun, J. Lipton, L. Boyle et al., “Direct current stimulation induces mGluR5-dependent neocortical plasticity,” *Annals of Neurology*, vol. 80, no. 2, pp. 233–246, 2016.
- [72] C. Lüscher and R. Malenka, “NMDA receptor-dependent long-term potentiation and long-term depression (LTP/LTD),” *Cold Spring Harbor Perspectives in Biology*, vol. 4, no. 6, p. a005710, 2012.
- [73] J. Stafford, M. Brownlow, A. Qualley, and R. Jankord, “AMPA receptor translocation and phosphorylation are induced by transcranial direct current stimulation in rats,” *Neurobiology of Learning and Memory*, vol. 150, pp. 36–41, 2018.
- [74] S. Perret, A. Cantereau, J. Audin, B. Dufy, and D. Georgescauld, “Interplay between Ca^{2+} release and Ca^{2+} influx underlies localized hyperpolarization-induced $[\text{Ca}^{2+}]_i$ waves in prostatic cells,” *Cell Calcium*, vol. 25, no. 4, pp. 297–311, 1999.
- [75] H. Monai, M. Ohkura, M. Tanaka et al., “Calcium imaging reveals glial involvement in transcranial direct current stimulation-induced plasticity in mouse brain,” *Nature Communications*, vol. 7, p. 11100, 2016.
- [76] T. Mishima, T. Nagai, K. Yahagi et al., “Transcranial direct current stimulation (tDCS) induces adrenergic receptor-dependent microglial morphological changes in mice,” *eNeuro*, vol. 6, no. 5, pp. 1–12, 2019.
- [77] P. Opazo, S. Labrecque, C. Tigaret et al., “CaMKII triggers the diffusional trapping of surface AMPARs through phosphorylation of stargazin,” *Neuron*, vol. 67, no. 2, pp. 239–252, 2010.
- [78] M. S. Kim, H. Koo, S. W. Han et al., “Repeated anodal transcranial direct current stimulation induces neural plasticity-associated gene expression in the rat cortex and hippocampus,” *Restorative Neurology and Neuroscience*, vol. 35, no. 2, pp. 137–146, 2017.
- [79] G. Leal, C. Bramham, and C. Duarte, “BDNF and hippocampal synaptic plasticity,” *Vitamins and Hormones*, vol. 104, pp. 153–195, 2017.
- [80] C. McCaig, A. Rajnecik, B. Song, and M. Zhao, “Controlling cell behavior electrically: current views and future potential,” *Physiological Reviews*, vol. 85, no. 3, pp. 943–978, 2005.
- [81] L. Minichiello, “TrkB signalling pathways in LTP and learning,” *Nature Reviews Neuroscience*, vol. 10, no. 12, pp. 850–860, 2009.
- [82] C. M. Alberini, “Transcription factors in long-term memory and synaptic plasticity,” *Physiological Reviews*, vol. 89, no. 1, pp. 121–145, 2009.
- [83] S. T. Carmichael, I. Archibeque, L. Luke, T. Nolan, J. Momiy, and S. Li, “Growth-associated gene expression after stroke: evidence for a growth-promoting region in peri-infarct

- cortex," *Experimental Neurology*, vol. 193, no. 2, pp. 291–311, 2005.
- [84] Y. Li, N. Jiang, C. Powers, and M. Chopp, "Neuronal damage and plasticity identified by microtubule-associated protein 2, growth-associated protein 43, and cyclin D1 immunoreactivity after focal cerebral ischemia in rats," *Stroke*, vol. 29, no. 9, pp. 1972–1981, 1998.
- [85] T. Jiang, R. X. Xu, A. W. Zhang et al., "Effects of transcranial direct current stimulation on hemichannel pannexin-1 and neural plasticity in rat model of cerebral infarction," *Neurosciences*, vol. 226, pp. 421–426, 2012.
- [86] P. Bargiotas, H. Monyer, and M. Schwaninger, "Hemichannels in cerebral ischemia," *Current Molecular Medicine*, vol. 9, no. 2, pp. 186–194, 2009.
- [87] L. Dimov, A. Franciosi, A. Campos, A. R. Brunoni, and R. L. Pagano, "Top-down effect of direct current stimulation on the nociceptive response of rats," *PLoS One*, vol. 11, no. 4, article e0153506, 2016.
- [88] M. Rioult-Pedotti, D. Friedman, and J. Donoghue, "Learning-induced LTP in neocortex," *Science*, vol. 290, no. 5491, pp. 533–536, 2000.
- [89] R. Malenka and M. Bear, "LTP and LTD: an embarrassment of riches," *Neuron*, vol. 44, no. 1, pp. 5–21, 2004.
- [90] J. Lisman, K. Cooper, M. Sehgal, and A. J. Silva, "Memory formation depends on both synapse-specific modifications of synaptic strength and cell-specific increases in excitability," *Nature Neuroscience*, vol. 21, no. 3, pp. 309–314, 2018.
- [91] M. Legrand, R. Troubat, B. Brizard, A. M. le Guisquet, C. Belzung, and W. el-Hage, "Prefrontal cortex rTMS reverses behavioral impairments and differentially activates c-Fos in a mouse model of post-traumatic stress disorder," *Brain Stimulation*, vol. 12, no. 1, pp. 87–95, 2019.
- [92] V. Moliadze, E. Lyzhko, T. Schmanke, S. Andreas, C. M. Freitag, and M. Siniatchkin, "1 mA cathodal tDCS shows excitatory effects in children and adolescents: insights from TMS evoked N100 potential," *Brain Research Bulletin*, vol. 140, pp. 43–51, 2018.
- [93] F. Fisicaro, G. Lanza, A. A. Grasso et al., "Repetitive transcranial magnetic stimulation in stroke rehabilitation: review of the current evidence and pitfalls," *Therapeutic Advances in Neurological Disorders*, vol. 12, p. 1756286419878317, 2019.
- [94] M. Cantone, A. Bramanti, G. Lanza et al., "Cortical plasticity in depression," *ASN Neuro*, vol. 9, no. 3, 2017.
- [95] U. Palm, F. M. Segmiller, A. N. Epple et al., "Transcranial direct current stimulation in children and adolescents: a comprehensive review," *Journal of Neural Transmission (Vienna)*, vol. 123, no. 10, pp. 1219–1234, 2016.
- [96] X. Leinekugel, I. Khalilov, H. McLean et al., "GABA is the principal fast-acting excitatory transmitter in the neonatal brain," *Advances in Neurology*, vol. 79, pp. 189–201, 1999.
- [97] C. W. Martins, L. C. de Melo Rodrigues, M. A. Nitsche, and E. M. Nakamura-Palacios, "AMPA receptors are involved in prefrontal direct current stimulation effects on long-term working memory and GAP-43 expression," *Behavioural Brain Research*, vol. 362, pp. 208–212, 2019.
- [98] V. Nekhendzy, C. Fender, M. Davies et al., "The antinociceptive effect of transcranial electrostimulation with combined direct and alternating current in freely moving rats," *Anesthesia and Analgesia*, vol. 98, no. 3, pp. 730–7, table of contents, 2004.
- [99] N. O. B. Taib and M. Manto, "Trains of transcranial direct current stimulation antagonize motor cortex hypoexcitability induced by acute hemispherectomy," *Journal of Neurosurgery*, vol. 111, no. 4, pp. 796–806, 2009.
- [100] S. Kim, B. Kim, Y. Ko, M. S. Bang, M. H. Kim, and T. R. Han, "Functional and histologic changes after repeated transcranial direct current stimulation in rat stroke model," *Journal of Korean Medical Science*, vol. 25, no. 10, pp. 1499–1505, 2010.
- [101] G. Laste, W. Caumo, L. Adachi et al., "After-effects of consecutive sessions of transcranial direct current stimulation (tDCS) in a rat model of chronic inflammation," *Experimental Brain Research*, vol. 221, no. 1, pp. 75–83, 2012.
- [102] L. N. S. Adachi, W. Caumo, G. Laste et al., "Reversal of chronic stress-induced pain by transcranial direct current stimulation (tDCS) in an animal model," *Brain Research*, vol. 1489, pp. 17–26, 2012.
- [103] F. Notturmo, M. Pace, F. Zappasodi, E. Cam, C. L. Bassetti, and A. Uncini, "Neuroprotective effect of cathodal transcranial direct current stimulation in a rat stroke model," *Journal of the Neurological Sciences*, vol. 342, no. 1-2, pp. 146–151, 2014.
- [104] C. Lu, Y. Wei, R. Hu, Y. Wang, K. Li, and X. Li, "Transcranial Direct Current Stimulation Ameliorates Behavioral Deficits and Reduces Oxidative Stress in 1-Methyl-4-Phenyl-1,2,3,6-Tetrahydropyridine-Induced Mouse Model of Parkinson's Disease," *Neuromodulation*, vol. 18, no. 6, pp. 442–447, 2015.
- [105] L. N. S. Adachi, A. S. Quevedo, A. de Souza et al., "Exogenously induced brain activation regulates neuronal activity by top-down modulation: conceptualized model for electrical brain stimulation," *Experimental Brain Research*, vol. 233, no. 5, pp. 1377–1389, 2015.
- [106] Y.-H. Liu, L.-D. Liao, S. J. Chan, A. Bandla, and N. V. Thakor, "An integrated neuroprotective intervention for brain ischemia validated by ECoG-fPAM," in *2016 38th Annual International Conference of the IEEE Engineering in Medicine and Biology Society (EMBC)*, pp. 4009–4012, Orlando, FL, USA, Aug. 2016.
- [107] R. Braun, R. Klein, H. Walter et al., "Transcranial direct current stimulation accelerates recovery of function, induces neurogenesis and recruits oligodendrocyte precursors in a rat model of stroke," *Experimental Neurology*, vol. 279, pp. 127–136, 2016.
- [108] S. G. Cioato, L. F. Medeiros, P. R. M. Filho et al., "Long-lasting effect of transcranial direct current stimulation in the reversal of hyperalgesia and cytokine alterations induced by the neuropathic pain model," *Brain Stimulation*, vol. 9, no. 2, pp. 209–217, 2016.
- [109] P. R. M. Filho, R. Vercelino, S. G. Cioato et al., "Transcranial direct current stimulation (tDCS) reverts behavioral alterations and brainstem BDNF level increase induced by neuropathic pain model: Long-lasting effect," *Progress in Neuro-Psychopharmacology & Biological Psychiatry*, vol. 64, pp. 44–51, 2016.
- [110] S. F. da Silva Moreira, L. F. Medeiros, A. de Souza et al., "Transcranial direct current stimulation (tDCS) neuromodulatory effects on mechanical hyperalgesia and cortical BDNF levels in ovariectomized rats," *Life Sciences*, vol. 145, pp. 233–239, 2016.
- [111] Y. Liu, S. Chan, H. Pan et al., "Integrated treatment modality of cathodal-transcranial direct current stimulation with

- peripheral sensory stimulation affords neuroprotection in a rat stroke model,” *Neurophotonic*, vol. 4, no. 4, article 045002, 2017.
- [112] C. Winkler, J. Reis, N. Hoffmann et al., “Anodal transcranial direct current stimulation enhances survival and integration of dopaminergic cell transplants in a rat Parkinson model,” *eNeuro*, vol. 4, no. 5, pp. 1–11, 2017.
- [113] A. Souza, D. F. Martins, L. F. Medeiros et al., “Neurobiological mechanisms of antiallodynic effect of transcranial direct current stimulation (tDCS) in a mice model of neuropathic pain,” *Brain Research*, vol. 1682, pp. 14–23, 2018.
- [114] F. Paciello, M. V. Podda, R. Rolesi et al., “Anodal transcranial direct current stimulation affects auditory cortex plasticity in normal-hearing and noise-exposed rats,” *Brain Stimulation*, vol. 11, no. 5, pp. 1008–1023, 2018.
- [115] F. Fregni, I. Macedo, L. Spezia-Adachi et al., “Transcranial direct current stimulation (tDCS) prevents chronic stress-induced hyperalgesia in rats,” *Brain Stimulation*, vol. 11, no. 2, pp. 299–301, 2018.
- [116] S. Lee, J. Youn, W. Jang, and H. O. Yang, “Neuroprotective effect of anodal transcranial direct current stimulation on 1-methyl-4-phenyl-1,2,3,6-tetrahydropyridine (MPTP)-induced neurotoxicity in mice through modulating mitochondrial dynamics,” *Neurochemistry International*, vol. 129, p. 104491, 2019.
- [117] E. M. M. Callai, V. L. Scarabelot, L. Fernandes Medeiros et al., “Transcranial direct current stimulation (tDCS) and trigeminal pain: a preclinical study,” *Oral Diseases*, vol. 25, no. 3, pp. 888–897, 2019.
- [118] V. Scarabelot, C. de Oliveira, L. Medeiros et al., “Transcranial direct-current stimulation reduces nociceptive behaviour in an orofacial pain model,” *Journal of Oral Rehabilitation*, vol. 46, no. 1, pp. 40–50, 2019.

Research Article

Electroacupuncture Improved Chronic Cerebral Hypoperfusion-Induced Anxiety-Like Behavior and Memory Impairments in Spontaneously Hypertensive Rats by Downregulating the ACE/Ang II/AT1R Axis and Upregulating the ACE2/Ang-(1-7)/MasR Axis

Peipei Feng,¹ Zemin Wu,² Hao Liu,¹ Yafang Shen ¹, Xu Yao,¹ Xinwei Li ¹, and Zui Shen ²

¹Department of Acupuncture and Moxibustion, Tongde Hospital of Zhejiang Province, Hangzhou, China

²Department of Neurobiology and Acupuncture Research, The Third Clinical Medical College, Zhejiang Chinese Medical University, Key Laboratory of Acupuncture and Neurology of Zhejiang Province, Hangzhou, China

Correspondence should be addressed to Xinwei Li; 29183545@qq.com and Zui Shen; shenzui1228@163.com

Received 21 October 2019; Revised 5 January 2020; Accepted 28 January 2020; Published 26 February 2020

Guest Editor: Luca Marsili

Copyright © 2020 Peipei Feng et al. This is an open access article distributed under the Creative Commons Attribution License, which permits unrestricted use, distribution, and reproduction in any medium, provided the original work is properly cited.

Electroacupuncture (EA) can effectively alleviate anxiety disorders and memory impairments caused by various neurodegenerative diseases; however, the molecular mechanisms underlying its neuroprotective effects are unclear. Previous studies have shown that the renin-angiotensin system (RAS) comprises of two axes with mutual antagonism: the classical angiotensin converting enzyme/angiotensin II/angiotensin II type 1 receptor (ACE/Ang II/AT1R) axis and the protective angiotensin converting enzyme 2/angiotensin-(1-7)/Mas receptor (ACE2/Ang-(1-7)/MasR) axis. In this study, we observed that chronic cerebral hypoperfusion (CCH) mediated anxiety-like behavior and memory impairments in spontaneously hypertensive rats (SHR) via upregulation of the hippocampal classical axis (ACE/Ang II/AT1R) and the partial hippocampal protective axis (ACE2/Ang-(1-7)). However, Ang II levels were much higher than those of Ang-(1-7), indicating that the ACE/Ang II/AT1R axis plays a dominant role in the comorbidity of CCH and hypertension. Moreover, candesartan cilexetil (Canc) and perindopril (Peril) were used as positive control drugs. We found that EA, Canc, and Peril attenuated CCH-induced anxiety-like behavior and memory impairments in SHR, potentially via downregulation of the hippocampal classical axis (ACE/Ang II/AT1R) and upregulation of the whole hippocampal protective axis (ACE2/Ang-(1-7)/MasR). These results suggest that EA therapy for CCH with hypertension may be mediated by two hippocampal RAS axes.

1. Introduction

Chronic cerebral hypoperfusion (CCH) is a common pathophysiological state of the central nervous system [1, 2]. Long-term CCH can trigger neurodegeneration and eventually lead to progressive cognitive dysfunction [3–5]. Clinical research has shown that CCH is the common pathological foundation of Alzheimer's disease, vascular dementia, vascular cognitive impairment, and other neurodegenerative diseases [6–8]. Therefore, understanding the mechanisms underlying CCH will facilitate the development of therapeutic strategies for

the prevention and treatment of CCH-induced neurodegeneration [6].

The pathological and neuroprotective mechanisms of CCH are complicated. The function and structural integrity of the brain depend on a blood supply consistent with changes in its energy needs; therefore, adequate cerebral blood flow is a key factor in maintaining normal brain function [9]. In humans, CCH is not an isolated pathophysiological phenomenon, but rather occurs alongside other vascular risk factors, including hypertension [10]. Therefore, in order to better replicate the pathophysiology of human diseases,

CCH should be studied alongside other vascular risk factors, for example hypertension. In addition, accumulating evidence suggests that cerebral hypoperfusion and hypertension have an interdependent relationship and promote the development of memory impairment [10–13]. CCH [14, 15] and hypertension [16] are risk factors for anxiety, but the effect of their comorbidity on anxiety is unclear. Therefore, the role of CCH with hypertension in the development of anxiety and memory impairment requires elucidation.

The renin-angiotensin system (RAS) comprises of two axes with mutual antagonism: the classical angiotensin converting enzyme/angiotensin II/angiotensin II type 1 receptor (ACE/Ang II/AT1R) axis and the alternative angiotensin converting enzyme 2/angiotensin-(1-7)/Mas receptor (ACE2/Ang-(1-7)/MasR) axis. Studies have confirmed that these two axes in the brain tissue can exert neuronal damage and neuroprotection, respectively. Studies have confirmed that the brain RAS plays an important role in the pathogenesis of CCH [17]. The RAS is also a key system in the regulation of blood pressure [18] and in the process of vascular aging [19]. Furthermore, the over-activation of the RAS protective axis can reduce anxiety-like behavior [20]. Increasing evidence has shown that the brain RAS is related to memory impairments in many neurodegenerative diseases [21]. However, it is unclear how the brain RAS, especially the interaction of the two axes, is involved in CCH with hypertension and the regulation of emotion and memory-related behaviors.

Our previous studies have shown that electroacupuncture (EA) could alleviate cognitive impairment in rats with chronic cerebral ischemia [22] and aged rats [23]. Furthermore, accumulating evidence has demonstrated that EA can effectively alleviate anxiety disorders [24] and memory impairments caused by Alzheimer's disease [25, 26] and vascular dementia [27]. However, whether EA regulates CCH with hypertension and whether this is related to the RAS remain unclear. In this study, we investigated the anxiolytic and memory-ameliorating effects of EA in spontaneously hypertensive rats (SHR) with CCH and the potential role of the brain RAS in the neuroprotective effects of EA.

2. Materials and Methods

2.1. Animals and Groups. Male SHR (12 weeks old, weighing 250–300 g) were purchased from Vital River Laboratory Animal Technology Co., Ltd., Beijing, China. The rats were housed in groups of four in plastic cages with soft bedding at the University Animal Care Facility under an artificial 12/12 h light-dark cycle. Animals received food and water ad libitum, and a constant room temperature of 23–25°C and relative humidity of 40–70% were maintained. All animal procedures performed in this work were in accordance with the Regulations for the Administration of Affairs Concerning Experimental Animals and were approved by the Animal Care and Welfare Committee of Zhejiang Chinese Medical University, Zhejiang, China.

SHR were randomly divided into sham (sham), CCH model (model), CCH+candesartan cilexetil (Canc),

CCH+perindopril (Peril), and CCH+electroacupuncture (EA) groups.

2.2. CCH Model. The modified two-vessel occlusion (2VO) method of Cechetti et al. was used to prepare the CCH model [28]. Briefly, after inhalation of isoflurane for anesthesia, a 1 cm incision was made in the middle of the neck of the rat, and the vagus nerve was dissected to expose the common carotid artery. The right common carotid artery was ligated with a 5-0 surgical suture. The wound was sutured layer by layer. The left common carotid artery was ligated in the same manner one week later. The sham group underwent surgery to dissect the vagus nerve without common carotid artery ligation. Strict aseptic conditions were maintained during and after surgery to prevent infection.

2.3. EA and Drug Treatment. EA was performed on the rats at the acupoints of Baihui (GV 20) and Dazhui (GV 14) each day during the experimental procedure. Sterilized disposable stainless steel acupuncture needles (Huatuotuo, Suzhou Medical Co. Ltd., Jiangsu, China) with a 0.35 mm diameter were inserted as deep as 5 mm. The GV 20 acupoint is located above the apex auriculate in the midline of the head. The GV 14 acupoint is located on the posterior midline and in the depression below the spinous process of the 7th cervical vertebra in the prone position. The ends of the needles were attached to a pair of electrodes from an electrical stimulator (HANS 200E, Huawei Co. Ltd., Beijing, China). The EA parameters were set as follows: a constant square wave current output (15 Hz), with the intensities remaining at 1 mA (causing slight vibration of the muscles around the acupoints) for 30 min once a day starting from day 1 postoperatively. In the whole procedure, all rats remained calm without any struggling or vocalizing. Rats in the drug groups received drugs dissolved in physiological saline via intragastric administration at a dose of 1 mg/kg/day for 4 weeks.

2.4. Regional Cerebral Blood Flow (rCBF) Monitoring. rCBF was monitored using laser Doppler flowmetry (Probe 403 connected to PeriFlux 5000; Perimed AB, Sweden) following the method of Farkas et al. [29]. After anesthesia was induced using 5% isoflurane, the rats were given a breathing mask and anesthesia was maintained with 2% isoflurane until the end of modeling. The operating table was heated to maintain a body temperature of 37°C. After iodine disinfection followed by alcohol deiodination, a 1 cm long transverse incision was made between the right eye of the rat and the external auditory canal. The subcutaneous tissue was bluntly separated to expose the temporal bone, and the surface tissue was removed using 3% hydrogen peroxide. When the surface of the temporal bone was dry, the probe base was fixed on the smooth surface of the temporal bone using Loctite 4161 instant adhesive (Loctite, Hartford, CT, USA). rCBF was monitored by inserting the probe into the pedestal. After monitoring was completed, the skin was sutured using a 5-0 surgical suture, and iodine and penicillin sodium were used to disinfect the local skin. The rats were kept in cages after awakening.

2.5. Open-Field Test (OFT). The OFT is widely used to assess anxiety-like behavior in rodents [30]. A square black box (100 cm wide and 50 cm high) with a camera above the center was used to perform this test. The bottom of the box was virtually divided into 16 squares (25 cm × 25 cm), and the four squares in the middle were termed the center area. The rats were gently placed in the center area at the start of the experiment. The activity of each rat in a 5 min period was then recorded and analyzed using an automatic image tracking system (SMART3.0, Panlab, Spanish). The parameters recorded included time spent in the center area, number of entries into the center area, and total distance traveled. After each rat was tested, the bottom and sides of the box were thoroughly scrubbed with 70% alcohol to remove feces and other odors, preventing these from affecting the behavior of other rats.

2.6. Novel-Object Recognition Test (NORT). The NORT is a test of learning and memory based on the principle that animals innately explore new objects. It is a method commonly employed to assess hippocampal-dependent memory in experimental animals [31]. In the NORT, rats are allowed to perform learning and memory tests in a freely active state, which more closely simulates human learning and memory behavior. A square PVC plastic box with no lid (70 cm × 70 cm × 50 cm) and three objects were used to perform this test. The three objects comprised two identical cuboids, 8 cm in length, 8 cm in width, and 6 cm in height (object A), and a cylinder with a diameter of 7 cm and height of 10 cm (object B). The objects could not be moved by the rats. The experiment consisted of three phases, namely, adaptation, familiarity, and detection phases [32, 33]. The rats were stroked daily before starting the test to avoid stress responses during the test. In the adaptation phase, rats were gently placed in the box and allowed to move around freely for 10 min. In the familiar phase, two identical objects were placed in the same corner of the box, 10 cm away from the side. The rat was then gently placed next to the inner wall of the box away from the object and allowed to move freely for 5 min. The detection phase was carried out after 24 h. In the detection phase, one object A was replaced by the novel object B, and a camera recorded the exploration of the rat for 5 min. This test was initiated on the 20th day after 2VO. A rat was considered to be exploring an object when its head was within 2 cm of the object. Object A was termed the familiar object, and object B was termed the novel object. Analysis was performed using SMART3.0 (Panlab, Spanish). The discrimination index ($d1 = TN - TF$) and the discrimination ratio [$d2 = (TN - TF)/(TN + TF)$] were calculated, where TN is the amount of time the rat spent exploring the novel object and TF is the amount of time the rat explored the familiar object. After each rat was tested, the box and objects were thoroughly scrubbed with 70% alcohol to remove feces and other odors, preventing these from affecting the behavior of other rats.

2.7. Morris Water Maze (MWM) Test. The MWM is a test of hippocampal-dependent spatial learning and memory in rodents [34]. The test was initiated on the 23rd day after

2VO and lasted for 6 consecutive days. The first phase was a 5-day continuous navigation test which evaluated the learning ability of the rats. Rats need to find a platform (diameter, 10 cm) hidden 2 cm underwater within 1 min. After the rats climbed onto the platform, they needed to remain on the platform for at least 10 s. If rats did not find the hidden platform within 1 min, the experimenter would guide the rats to the platform and maintain it there for 30 s. The escape latency is the time taken for a rat to find the platform. Rats underwent four trials per day for 5 days and were excluded if they failed to find the platform on the 5th day. The second phase, named the spatial probe test, on the 6th day, was performed to test the memory ability of the rats by observing the time spent in the quadrant that previously contained the platform. The activity of the rats was recorded and analyzed using SMART3.0 software (Panlab, Spanish).

2.8. Enzyme-Linked Immunosorbent Assay (ELISA). Rats were sacrificed after urethane anesthesia (1.2 g/kg i.p., Sigma-Aldrich). Animals were perfused with 4°C saline, and hippocampal tissues were quickly removed and placed in freeze storage at -70°C. Thawed hippocampal samples were homogenized in lysis buffer containing a protease inhibitor cocktail (Applygen, Beijing, China). The levels of ACE, ACE2, Ang I, Ang II, and Ang-(1-7) were measured in the supernatants using a Parameter™ ACE (Nanjing Jiancheng Bioengineering Institute, China), ACE2 (Anaspec, USA), Ang I (R&D Systems, USA), Ang II (R&D Systems, USA), or Ang-(1-7) (R&D Systems, USA) immunoassay kit, respectively, according to the manufacturer's instructions. The absorbance at 405 nm was read using a SpectraMax M4 microplate reader (Molecular Devices, USA), and the concentration was determined by fitting curves using SoftMax Pro software (version 5.0, Molecular Devices, USA). Five rats from each group were randomly selected for ELISA.

2.9. Western Blotting. The unfrozen hippocampal samples were homogenized with lysis buffer containing a cocktail of phosphatase and proteinase inhibitors and PMSF (Beyotime, Shanghai, China). After denaturation, the lysates were separated on a 10% SDS-PAGE gel and transferred to polyvinylidene difluoride (PVDF) membranes (Bio-Rad, USA). The membranes were blocked with 5% non-fat powdered milk in TBST (containing 0.1% Tween 20) for 1 h at 25°C and incubated for 15–18 h at 4°C with a monoclonal rabbit anti-MasR (1:2000, Proteintech Group), anti-AT1R (1:500, Proteintech Group), or anti-GAPDH (1:5000, Proteintech Group) primary antibody. After TBST cleaning, the membrane was incubated for 1 h at 25°C with a horseradish peroxidase- (HRP-) conjugated goat anti-rabbit antibody (1:5000, Jackson ImmunoResearch Laboratories, USA) and the protein bands were visualized using an ECL system (Immun-Star™ HRP Chemiluminescence Kit, Bio-Rad). The band images were recorded using the ImageQuant LAS 4000 system (GE Healthcare, Japan), and the band intensities were quantified using ImageQuant TL software (version 7.0, GE Healthcare, Japan). Five rats from each group were randomly selected for western blotting.

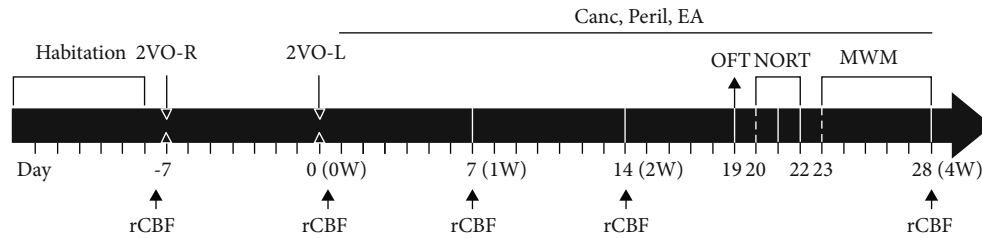


FIGURE 1: The basic experimental procedure. Abbreviations: Canc = candesartan cilexetil; Peril = perindopril; EA = electroacupuncture; 2VO-R = right common carotid artery occlusion; 2VO-L = left common carotid artery occlusion; OFT = open-field test; NORT = novel object recognition test; MWM = Morris water maze; rCBF = regional cerebral blood flow; W = week.

2.10. Immunofluorescence. After the sacrificed animals were perfused with 4°C saline and 4°C paraformaldehyde (PFA), the brains were removed and placed in 4°C paraformaldehyde for 24 h. After 15% and 30% sucrose gradient dehydration, the brain tissues were stored at -70°C until they completely sank to the bottom. A cryostat microtome (Microm HM 550, Thermo Fisher Scientific Inc., Germany) was used to cut 20 μm thick coronal brain slices for immunofluorescence. Slices containing the hippocampal CA1, CA3, and DG region (-2.3 mm to -4.16 mm from the bregma) were chosen by the experimenters. Brain slices were blocked with 10% normal goat serum solution at 37°C for 2 h and then incubated for 18–20 h at 4°C with an anti-MasR antibody (rabbit polyclonal, 1:500, Alomone, Israel) or an anti-AT1R antibody (rabbit polyclonal, 1:500, Alomone, Israel). After washing with PBS, the slices were incubated with an Alexa Fluor 647-conjugated goat anti-rabbit secondary antibody (1:1000, Jackson ImmunoResearch Laboratories, USA) at 37°C for 1.5 h. Finally, the slices were visualized using a Nikon Eclipse Ti confocal microscope (Nikon, Japan) and images in the hippocampal CA1, CA3, and DG region were captured using NIS-Elements software (Nikon, Japan).

2.11. Statistical Analysis. All data were expressed as mean ± standard error (mean ± S.E.). Data from rCBF monitoring and the MWM positioning navigation test were analyzed using repeated measures analysis of variance (RM ANOVA). The remaining data were analyzed using a one-way ANOVA. If the variance was uniform, the Bonferroni test was used. If the variance was not uniform, Dunnett's T3 test was used. $P < 0.05$ was considered statistically significant.

3. Results

As shown in Figure 1, after each group of SHR was acclimated for 1 week, the 2VO model induction was initiated. On day 7, the right common carotid artery (2VO-R) was occluded; 1 week later, the left common carotid artery (2VO-L) was occluded using the same method. Following this preparation of the CCH model, the EA, Canc, and Peril interventions were initiated for 28 days (4 weeks).

The rCBF in each group was measured before 2VO-R (baseline), immediately after 2VO-L, and 1, 2, and 4 weeks after 2VO-L. The OFT was performed on day 19, the NORT was performed on days 20–22, and the MWM test was performed on days 23–28. After the end of the MWM test on

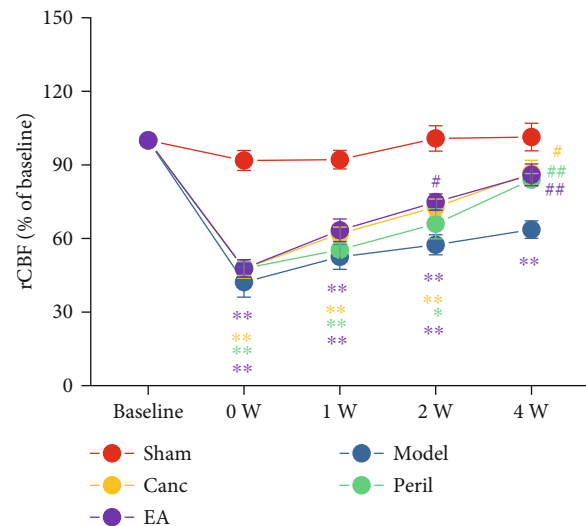


FIGURE 2: Changes in regional cerebral blood flow (rCBF) in each group before (baseline) and after two-vessel occlusion (2VO). Abbreviations: Canc = candesartan cilexetil; Peril = perindopril; EA = electroacupuncture; rCBF = regional cerebral blood flow; W = week. * $P < 0.05$ and ** $P < 0.01$ compared to the sham group; # $P < 0.05$ and ## $P < 0.01$ compared to the model group.

day 28, the rats were anesthetized and sacrificed, and ELISA, immunofluorescence, and immunoblotting were conducted.

3.1. EA Enhanced CCH-Induced Low rCBF in SHR. In this experiment, we used laser Doppler flowmetry to monitor rCBF in rats before 2VO-R, immediately after 2VO-L, and 1, 2, and 4 weeks after 2VO-L. Pre-2VO rCBF (baseline) showed no significant difference between the groups ($P > 0.05$, one-way ANOVA).

The results of the spherical test showed that rCBF was correlated with both the group and time after the intervention. Therefore, the data from this experiment were statistically processed using two-way repeated measures ANOVA. The results showed that compared to the sham group, the rCBF of the model group was significantly lower at each time point after 2VO (one-way RM ANOVA; all $P < 0.01$, Bonferroni test; Figure 2). Furthermore, compared to the sham group, the Canc, Peril, and EA groups exhibited significantly lower rCBF immediately after 2VO (one-way RM ANOVA; all $P < 0.01$, Bonferroni test; Figure 2), 1 week

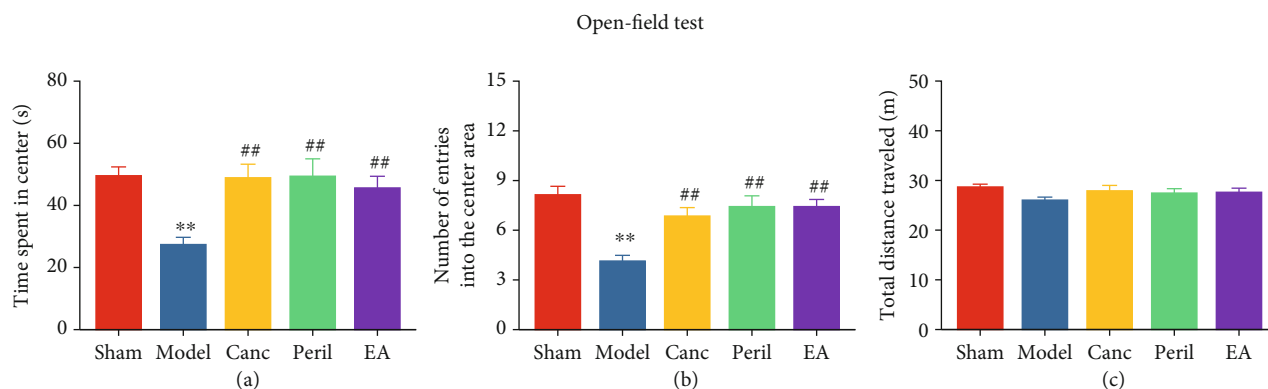


FIGURE 3: Changes in anxiety-like behavior in each group. Abbreviations: Canc = candesartan cilexetil; Peril = perindopril; EA = electroacupuncture. ** $P < 0.01$ compared to the sham group; # $P < 0.05$ and ## $P < 0.01$ compared to the model group.

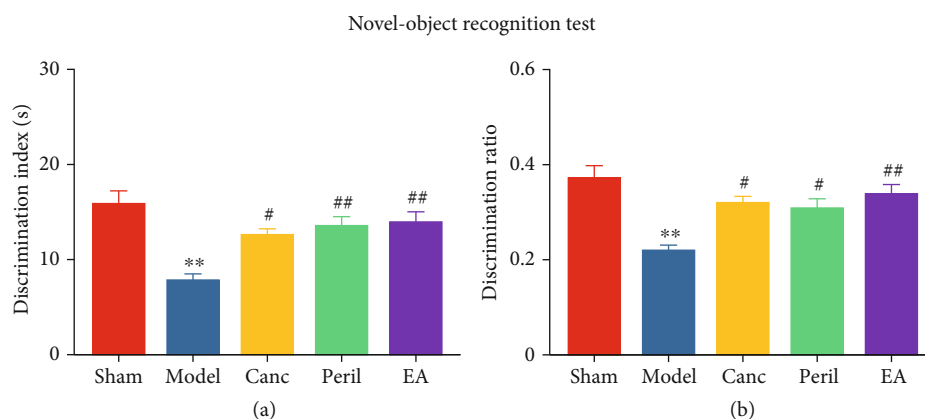


FIGURE 4: Changes in object recognition memory in each group. Abbreviations: Canc = candesartan cilexetil; Peril = perindopril; EA = electroacupuncture. ** $P < 0.01$ compared to the sham group; # $P < 0.05$ and ## $P < 0.01$ compared to the model group.

after 2VO (one-way RM ANOVA; all $P < 0.01$, Bonferroni test; Figure 2), and 2 weeks after 2VO (one-way RM ANOVA; $P < 0.05$ or $P < 0.01$, Bonferroni test; Figure 2). However, the Canc, Peril, and EA groups did not exhibit significantly different rCBF compared to that of the sham group 4 weeks after 2VO (one-way RM ANOVA; $P > 0.05$, Bonferroni test; Figure 2).

Compared to the model group, the rCBF of the Canc and Peril groups was not significantly different immediately after, 1 week, or 2 weeks after 2VO (one-way RM ANOVA; all $P > 0.05$, Bonferroni test; Figure 2). However, these groups exhibited significantly higher rCBF compared to the model group 4 weeks after 2VO (one-way RM ANOVA; $P < 0.01$, Bonferroni test; Figure 2). Compared to the model group, the rCBF of the EA group was not significantly different immediately or 1 week after 2VO (one-way RM ANOVA; both $P > 0.05$, Bonferroni test; Figure 2) but was significantly higher 2 and 4 weeks after 2VO (one-way RM ANOVA; $P < 0.05$ or $P < 0.01$, Bonferroni test; Figure 2). There were no significant differences in rCBF between the Canc, Peril, and EA groups at any of the recorded time points (one-way RM ANOVA; all $P > 0.05$, Bonferroni test; Figure 2).

3.2. EA Attenuated CCH-Induced Anxiety-Like Behavior in SHR. The results of the OFT showed that compared to the sham group, the time spent in the central area (Figure 3(a)) and number of entries into the central area (Figure 3(b)) were significantly reduced in the model group (one-way ANOVA; all $P < 0.01$, Bonferroni test). Compared to the model group, the time spent in the central area (Figure 3(a)) and the number of entries into the central area (Figure 3(b)) were significantly lower in the Canc, Peril, and EA groups (one-way ANOVA; $P < 0.05$ or $P < 0.01$, Bonferroni test). There were no significant differences in the total distance traveled between five groups ($P > 0.05$, one-way ANOVA; Figure 3(c)).

3.3. EA Attenuated CCH-Induced Object Recognition Memory Impairments in SHR. In the NORT, compared to the sham group, the discrimination index (d1, Figure 4(a)) and discrimination ratio (d2, Figure 4(b)) of the model group were significantly lower (one-way ANOVA; both $P < 0.01$, Bonferroni test; Figures 4(a) and 4(b)). Compared to the model group, the d1 and d2 of the Canc, Peril, and EA groups were significantly higher (one-way ANOVA; $P < 0.05$ or

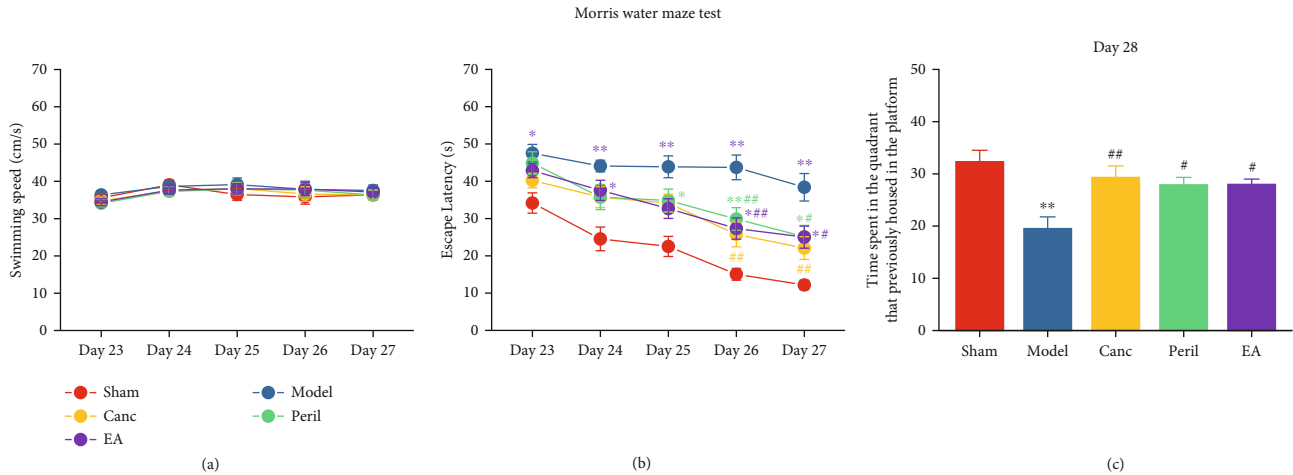


FIGURE 5: Changes in spatial learning (a, b) and memory (c) in each group. Abbreviations: Canc = candesartan cilexetil; Peril = perindopril; EA = electroacupuncture. * $P < 0.05$ and ** $P < 0.01$ compared to the sham group; # $P < 0.05$ and ## $P < 0.01$ compared to the model group.

$P < 0.01$, Bonferroni test; Figure 4(a) and 4(b)). There were no significant differences in d1 or d2 between the Canc, Peril, and EA groups (one-way ANOVA; both $P > 0.05$, Bonferroni test).

3.4. EA Attenuated CCH-Induced Spatial Learning and Memory Impairments in SHR. The spatial learning performance of the rats was observed during 5 days of MWM training. There was no significant difference in the swimming speed of the SHR treated with different interventions ($P > 0.05$, two-way RM ANOVA; Figure 5(a)). This eliminated the possible impact of the 2VO model itself on the free movement of rats. Compared to the sham group, the escape latency of the model (days 23-27), Peril (days 25-27), and EA (day 24, days 26-27) groups was significantly higher (one-way RM ANOVA; $P < 0.05$ or $P < 0.01$, Bonferroni test; Figure 5(b)). Compared to the model group, the escape latency of the Canc (days 26-27), Peril (days 26-27), and EA (days 26-27) groups was significantly lower (one-way RM ANOVA; $P < 0.05$ or $P < 0.01$, Bonferroni test; Figure 5(b)).

After 5 days of training, on day 28, the platform was removed to test the spatial memory performance of the rats. Relative to the sham group, the time spent in the quadrant that previously contained the platform was significantly decreased in the model group (one-way ANOVA; $P < 0.01$, Bonferroni test; Figure 5(c)). Relative to the model group, the time spent in the quadrant that previously contained the platform was significantly increased in the Canc, Peril, and EA groups (one-way ANOVA; $P < 0.05$ or $P < 0.01$, Bonferroni test; Figure 5(c)).

3.5. EA Attenuated CCH-Induced Increased Hippocampal ACE Activity, ACE2 Activity, and Ang I Level in SHR. Relative to the sham group, hippocampal ACE activity was significantly higher in the model group (one-way ANOVA; $P < 0.01$, Bonferroni test; Figure 6(a)). Relative to the model group, hippocampal ACE activity was significantly lower in the Canc, Peril, and EA groups (one-way ANOVA; all $P < 0.01$, Bonferroni test; Figure 6(a)). There

was no significant difference in ACE activity between the Canc, Peril, and EA groups (one-way ANOVA; $P > 0.05$, Bonferroni test).

Relative to the sham group, hippocampal ACE2 activity was significantly higher in the model, Canc, Peril, and EA groups (one-way ANOVA; all $P < 0.01$, Bonferroni test; Figure 6(b)). Relative to the model group, hippocampal ACE2 activity was significantly lower in the Canc, Peril, and EA groups (one-way ANOVA; $P < 0.05$ or $P < 0.01$, Bonferroni test; Figure 6(b)). There was no significant difference in hippocampal ACE2 activity between the Canc, Peril, and EA groups (one-way ANOVA; $P > 0.05$, Bonferroni test).

Relative to the sham group, the hippocampal Ang I level was significantly higher in the model group (one-way ANOVA; $P < 0.01$, Bonferroni test; Figure 6(c)). Relative to the model group, the hippocampal Ang I level was significantly lower in the Canc, Peril, and EA groups (one-way ANOVA; $P < 0.05$ or $P < 0.01$, Bonferroni test; Figure 6(c)). There was no significant difference in the hippocampal Ang I level between the Canc, Peril, and EA groups (one-way ANOVA; $P > 0.05$, Bonferroni test).

3.6. EA Attenuated CCH-Induced Increased Hippocampal Ang II Level and Ang III/Ang-(1-7) Ratio in SHR. Relative to the sham group, the hippocampal Ang II level was significantly higher in the model, Canc, Peril, and EA groups (one-way ANOVA; all $P < 0.01$, Bonferroni test; Figure 7(a)). Relative to the model group, the hippocampal Ang II level was significantly lower in the Canc, Peril, and EA groups (one-way ANOVA; all $P < 0.01$, Bonferroni test; Figure 7(a)). There was no significant difference in the hippocampal Ang II level between the Canc, Peril, and EA groups (one-way ANOVA; all $P > 0.05$, Bonferroni test).

Relative to the sham group, the Ang-(1-7) level was significantly higher in the model, Canc, Peril, and EA groups (one-way ANOVA; all $P < 0.01$, Bonferroni test; Figure 7(b)). There was no significant difference in the hippocampal Ang-(1-7) level between the Canc, Peril, and EA groups (one-way ANOVA; all $P > 0.05$, Bonferroni test).

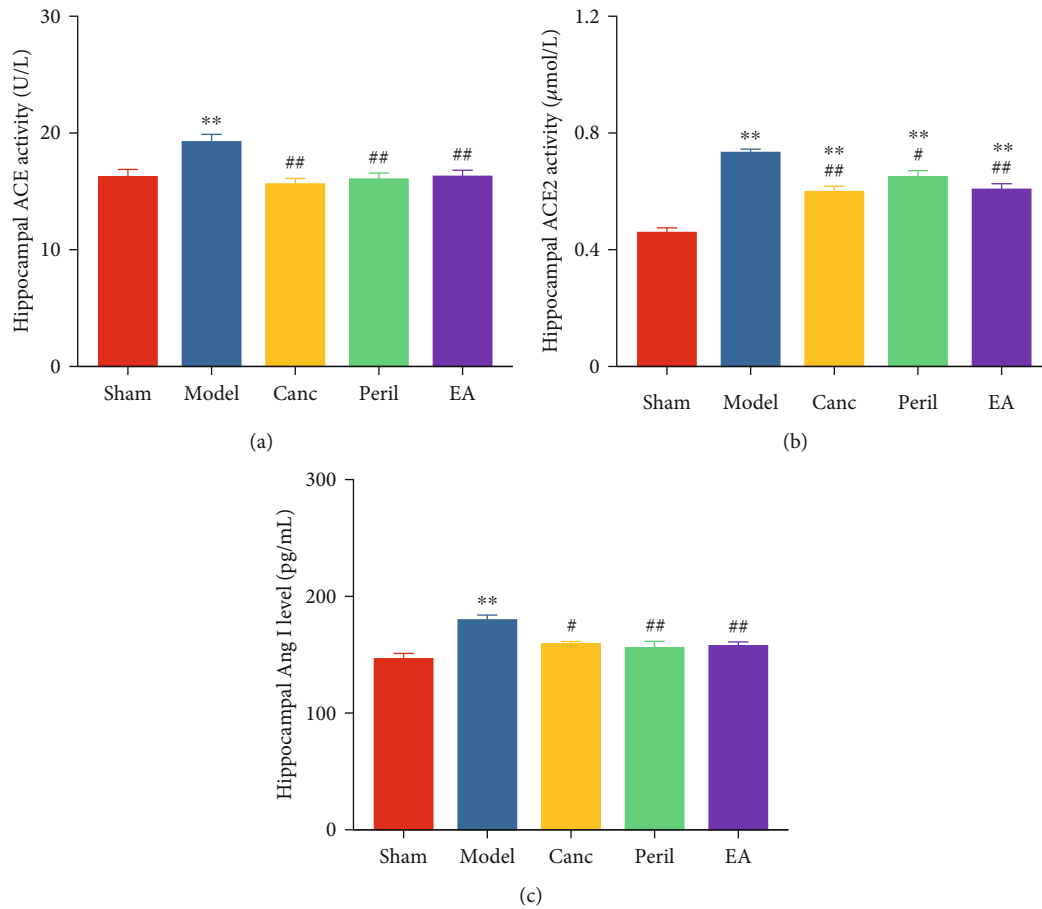


FIGURE 6: Changes in hippocampal ACE activity (a), ACE2 activity (b), and Ang I level (c) in each group. Abbreviations: ACE = angiotensin converting enzyme; ACE2 = angiotensin I converting enzyme 2; Ang I = angiotensin I; Canc = candesartan cilexetil; Peril = perindopril; EA = electroacupuncture. ** $P < 0.01$ compared to the sham group; # $P < 0.05$ and ## $P < 0.01$ compared to the model group.

Furthermore, relative to the sham group, the Ang II/Ang-(1-7) ratio was significantly higher in the model group (one-way ANOVA; $P < 0.01$, Bonferroni test; Figure 7(c)) and significantly lower in the Canc, Peril, and EA groups (one-way ANOVA; $P < 0.05$ or $P < 0.01$, Bonferroni test; Figure 7(c)). Relative to the model group, the Ang II/Ang-(1-7) ratio was significantly lower in the Canc, Peril, and EA groups (one-way ANOVA; all $P < 0.01$, Bonferroni test; Figure 7(c)). There was no significant difference in the hippocampal Ang II/Ang-(1-7) ratio between the Canc, Peril, and EA groups (one-way ANOVA; all $P > 0.05$, Bonferroni test).

3.7. EA Attenuated CCH-Induced Increased Hippocampal AT1R Expression and Strengthened CCH-Induced Reduced Hippocampal MasR Expression in SHR. The results of AT1R immunofluorescence (Figure 8(a)) showed that AT1R (red) was expressed in the CA1, CA3, and DG area of the hippocampus, and AT1R-positive cells were costained with the nuclear stain DAPI (blue).

When AT1R expression was quantified relative to that of GAPDH (internal reference protein) (Figure 8(b)), relative to the sham group, the expression of AT1R was significantly higher in the model group (one-way ANOVA; $P < 0.01$, Bonferroni test; Figure 8(b)). Relative to the model group,

the expression of AT1R was significantly lower in the Canc, Peril, and EA groups (one-way ANOVA; $P < 0.05$ or $P < 0.01$, Bonferroni test; Figure 8(b)). There was no significant difference in AT1R expression between the Canc, Peril, and EA groups (one-way ANOVA; all $P > 0.05$, Bonferroni test).

The results of MasR immunofluorescence (Figure 8(c)) showed that MasR (red) was expressed in the CA1, CA3, and DG area of the hippocampus and MasR-positive cells were costained with the nuclear stain DAPI (blue).

The expression of MasR was quantified relative to that of GAPDH using western blotting (Figure 8(d)). Relative to the sham group, MasR protein expression was significantly lower in the model group (one-way ANOVA; $P < 0.01$, Bonferroni test; Figure 8(d)). Relative to the model group, the expression of MasR was significantly higher in the Canc, Peril, and EA groups (one-way ANOVA; $P < 0.05$ or $P < 0.01$, Bonferroni test; Figure 8(d)). There was no significant difference in MasR expression between the Canc, Peril, and EA groups (one-way ANOVA; all $P > 0.05$, Bonferroni test).

4. Discussion

In this study, the OFT, NORT, and MWM test were used to observe the effects of CCH on anxiety, recognition memory,

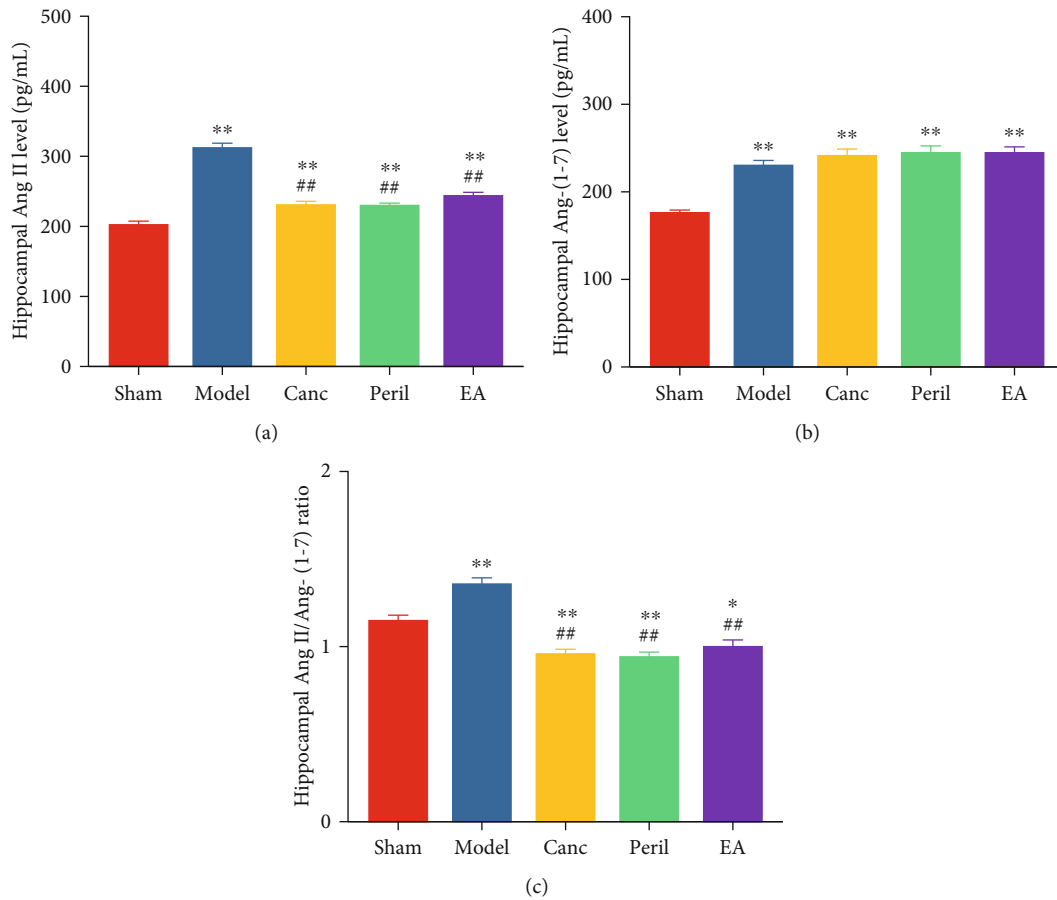


FIGURE 7: Changes in hippocampal Ang II level (a), Ang-(1-7) level (b), and Ang II/Ang-(1-7) ratio (c) in each group. Abbreviations: Ang II = angiotensin II; Ang-(1-7) = angiotensin 1-7; Canc = candesartan cilexetil; Peril = perindopril; EA = electroacupuncture. * $P < 0.05$ and ** $P < 0.01$ compared to the sham group; ## $P < 0.01$ compared to the model group.

and spatial learning and memory in SHR and to investigate how these were affected by EA. Previous studies have shown that CCH can cause anxiety [35] and memory impairment [36], but it is still unclear whether CCH combined with hypertension also has similar detrimental effects. Our results show that CCH induces memory impairments and anxiety in SHR and EA can effectively alleviate CCH-induced anxiety and memory impairment in SHR.

Accumulating evidence has proven that angiotensinogen (AGT) is the sole precursor protein that harbors Ang I at the N-terminus, which is specifically cleaved by renin [37]. Ang II is obtained by a strong vasoconstrictor (ACE) cleaving Ang I [38]. The combination of Ang II and AT1R could induce vascular remodeling, promote vascular inflammation and oxidative stress injury, and subsequently cause brain damage [39, 40]. The accepted view is that Ang II in the brain acts through a complex neural network to mediate hypertension [41, 42]. Ang II infusion in chronic hypertension induces learning and spatial memory impairment, as well as anxiety [43]. Furthermore, the activation of the ACE/Ang II/AT1R axis also causes no hypertensive disorders, such as cerebral hypoperfusion and ischemic injury [44–46]. Those disorders induced anxiety-like behavior and memory loss [14, 47]. In our study, relative to SHR, CCH in SHR induced

significantly activation of the ACE/Ang II/AT1R axis and exacerbated anxiety-like behavior and memory deficits. These indicate that the ACE/Ang II/AT1R axis is involved in the superposition effect of CCH and causes more serious functional damage.

In addition to binding to AT1R, a part of Ang II is hydrolyzed to Ang-(1-7) by ACE2, which plays a neuroprotective role by acting on the MasR, exerting anxiolytic effects [48] and ameliorating memory impairment [49]. Studies have shown that hypertension could induce decreased ACE2 levels and reduced generation of Ang-(1-7) [50]. Overexpression of ACE2 could decrease hypertension in SHR [51]. Emerging evidence suggests that the activation of the ACE2-Ang-(1-7)-MasR axis could attenuate the development of hypertension and pathologic progress of atherosclerosis [52]. However, in ischemic cerebrovascular diseases, ischemic stroke could induce the upregulation of ACE2, Ang-(1-7), and MasR in the brain [53, 54]. In our study, relative to SHR, CCH in SHR induced activation of hippocampal ACE2 and Ang-(1-7), but the Ang II level was much higher than that of Ang-(1-7), i.e., the Ang II/Ang-(1-7) ratio remained high. Those indicate that the CCH-induced increase of ACE2 and Ang-(1-7) could result in a partial and limited self-protective response and does

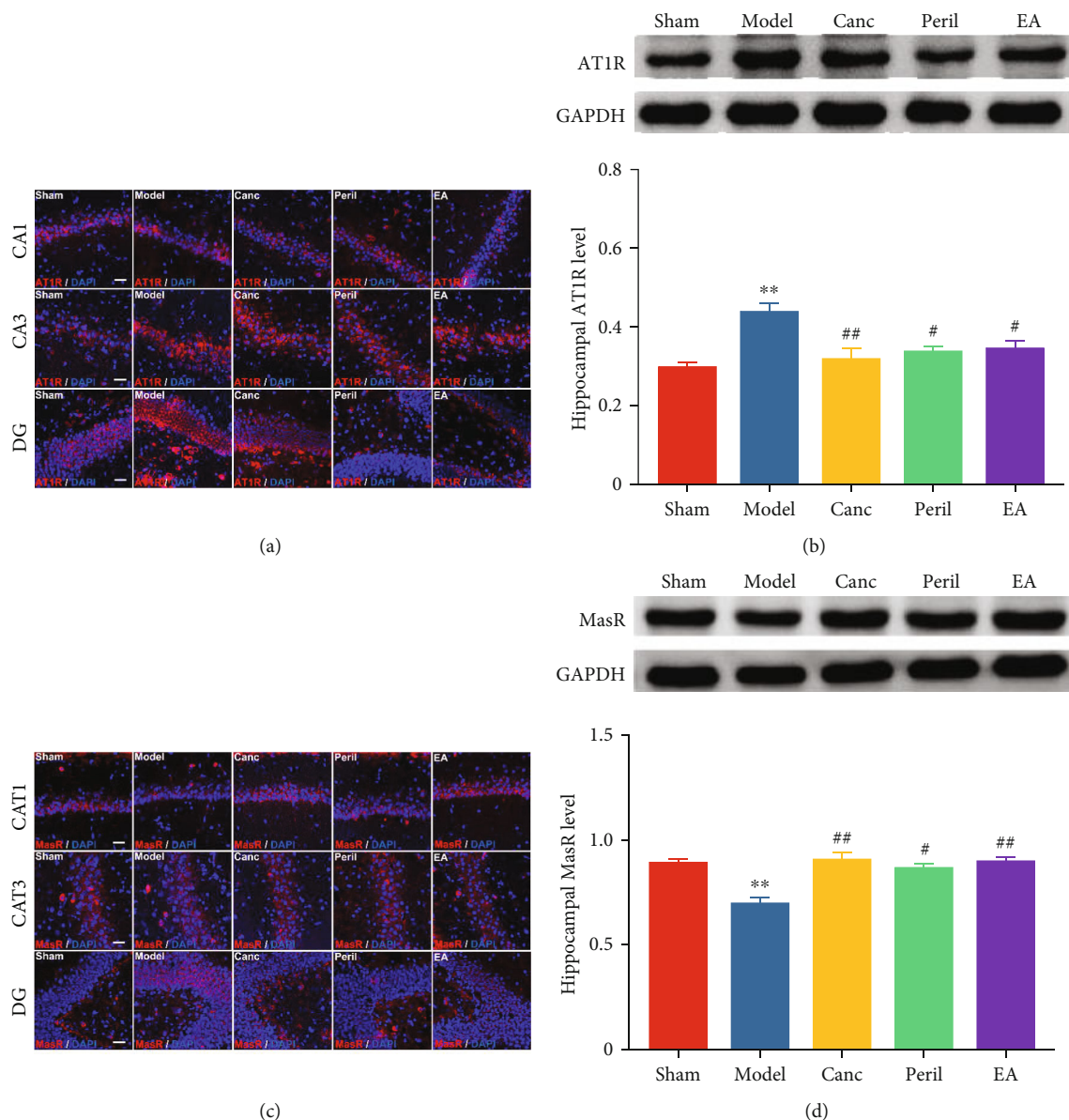


FIGURE 8: Changes in hippocampal AT1R (a, b) and MasR levels (c, d) in each group. Abbreviations: AT1R = angiotensin II type 1 receptor; MasR = Mas receptor; Canc = candesartan cilexetil; Peril = perindopril; EA = electroacupuncture. ** $P < 0.01$ compared to the sham group; # $P < 0.05$ and ## $P < 0.01$ compared to the model group.

not relieve memory impairment and anxiety-like behavior in SHR.

In this study, Canc and Peril were used as positive control drugs. Canc is an AT1R antagonist typically used for the treatment of hypertension. Studies showed that Canc inhibits the actions of Ang II by specifically binding with AT1R in the central nervous system, reducing oxidative stress, increasing cerebral blood flow, and protecting against CCH-induced memory damage [1, 55–57]. It is also documented that the anxiolytic effect of the Canc can be observed in the elevated plus maze [58]. Furthermore, Peril, a classical ACE inhibitor, is used to treat hypertension by blocking the conversion of Ang I to Ang II and decreasing the expression of Ang II. Peril could be useful for preventing CCH-induced complications,

such as memory deficits and dysphagia [59, 60], but the effect of Peril on CCH-induced anxiety-like behavior is not clear.

In our studies, EA and the two positive control drugs (Canc and Peril) generated similar relieving effects on CCH-induced memory loss and anxiety in SHR. After EA, ACE activity, Ang I level, Ang II level, AT1R expression, and the ratio of Ang II to Ang-(1-7) all decreased, and ACE2 activity, Ang-(1-7) level, and MasR expression all increased. We speculate that although EA is not as targeted as the two positive control drugs, the effect of EA may be multitargeted. EA may make the ACE/Ang II/AT1R axis and ACE2/Ang-(1-7)/MasR axis reach a new balance by downregulating the ACE/Ang II/AT1R pressor axis and upregulating the ACE2/Ang-(1-7)/MasR protective axis.

5. Conclusions

In summary, EA can improve CCH-induced anxiety-like behavior and memory impairments in SHR. EA therapy for CCH with hypertension may be mediated via downregulation of the hippocampal ACE/Ang II/AT1R axis and upregulation of the hippocampal ACE2/Ang-(1-7)/MasR axis.

Data Availability

The data used to support the findings of this study are available from the corresponding author upon request.

Conflicts of Interest

The authors have no conflicts of interest to declare.

Authors' Contributions

Peipei Feng and Zemin Wu contributed equally to this work as co-first authors.

Acknowledgments

This study was supported by the Zhejiang Provincial Natural Science Found of China (Y16H270024), the National Natural Science Foundation of China (81804183), the Special Financial Grant from the China Postdoctoral Science Foundation (2019T120532), the Class General Financial Grant from the China Postdoctoral Science Foundation (2018M642492), and the Zhejiang Post-Doctoral Preferential Fund Project (zj20180152).

References

- [1] S. Q. Du, X. R. Wang, L. Y. Xiao et al., "Molecular mechanisms of vascular dementia: what can be learned from animal models of chronic cerebral hypoperfusion?," *Molecular Neurobiology*, vol. 54, no. 5, pp. 3670–3682, 2017.
- [2] Y. Shu, H. Zhang, T. Kang et al., "PI3K/Akt signal pathway involved in the cognitive impairment caused by chronic cerebral hypoperfusion in rats," *PLoS One*, vol. 8, no. 12, article e81901, 2013.
- [3] H. Jian, W. Yi-Fang, L. Qi, H. Xiao-Song, and Z. Gui-Yun, "Cerebral blood flow and metabolic changes in hippocampal regions of a modified rat model with chronic cerebral hypoperfusion," *Acta Neurologica Belgica*, vol. 113, no. 3, pp. 313–317, 2013.
- [4] P. Luo, Y. Lu, C. Li et al., "Long-lasting spatial learning and memory impairments caused by chronic cerebral hypoperfusion associate with a dynamic change of HCN1/HCN2 expression in hippocampal CA1 region," *Neurobiology of Learning and Memory*, vol. 123, pp. 72–83, 2015.
- [5] Z. Jing, C. Shi, L. Zhu et al., "Chronic cerebral hypoperfusion induces vascular plasticity and hemodynamics but also neuronal degeneration and cognitive impairment," *Journal of Cerebral Blood Flow & Metabolism*, vol. 35, no. 8, pp. 1249–1259, 2015.
- [6] Y. Zhao and C. X. Gong, "From chronic cerebral hypoperfusion to Alzheimer-like brain pathology and neurodegeneration," *Cellular and Molecular Neurobiology*, vol. 35, no. 1, pp. 101–110, 2015.
- [7] Y. Hei, R. Chen, X. Yi, Q. Long, D. Gao, and W. Liu, "HMGB1 neutralization attenuates hippocampal neuronal death and cognitive impairment in rats with chronic cerebral hypoperfusion via suppressing inflammatory responses and oxidative stress," *Neuroscience*, vol. 383, pp. 150–159, 2018.
- [8] T. Yang, Y. Sun, Z. Lu, R. K. Leak, and F. Zhang, "The impact of cerebrovascular aging on vascular cognitive impairment and dementia," *Ageing Research Reviews*, vol. 34, pp. 15–29, 2017.
- [9] K. Kisler, A. R. Nelson, A. Montagne, and B. V. Zlokovic, "Cerebral blood flow regulation and neurovascular dysfunction in Alzheimer disease," *Nature Reviews Neuroscience*, vol. 18, no. 7, pp. 419–434, 2017.
- [10] J. Y. Choi, Y. Cui, and B. G. Kim, "Interaction between hypertension and cerebral hypoperfusion in the development of cognitive dysfunction and white matter pathology in rats," *Neuroscience*, vol. 303, pp. 115–125, 2015.
- [11] P. S. Chou, Y. H. Kao, M. N. Wu et al., "Effect of the interaction between hypertension and cerebral white matter changes on the progression of Alzheimer disease," *Current Alzheimer Research*, vol. 15, no. 14, pp. 1354–1360, 2018.
- [12] X. L. Yao, Z. H. Yao, L. Li, L. Nie, and S. F. Zhang, "Oxiracetam can improve cognitive impairment after chronic cerebral hypoperfusion in rats," *Psychiatry Research*, vol. 246, pp. 284–292, 2016.
- [13] H. Sekaran, C. Y. Gan, A. A. Latiff et al., "Changes in blood-brain barrier permeability and ultrastructure, and protein expression in a rat model of cerebral hypoperfusion," *Brain Research Bulletin*, vol. 152, pp. 63–73, 2019.
- [14] Y. Lu, C. J. Li, C. Chen et al., "Activation of GABA_{B2} subunits alleviates chronic cerebral hypoperfusion-induced anxiety-like behaviours: A role for BDNF signalling and Kir3 channels," *Neuropharmacology*, vol. 110, Part A, pp. 308–321, 2016.
- [15] P. Venkat, M. Chopp, and J. Chen, "Models and mechanisms of vascular dementia," *Experimental Neurology*, vol. 272, pp. 97–108, 2015.
- [16] Y. Pan, W. Cai, Q. Cheng, W. Dong, T. An, and J. Yan, "Association between anxiety and hypertension: a systematic review and meta-analysis of epidemiological studies," *Neuropsychiatric Disease and Treatment*, vol. 11, pp. 1121–1130, 2015.
- [17] Y. F. Dong, K. Kataoka, K. Toyama et al., "Attenuation of brain damage and cognitive impairment by direct renin inhibition in mice with chronic cerebral hypoperfusion," *Hypertension*, vol. 58, no. 4, pp. 635–642, 2011.
- [18] T. Yang and C. Xu, "Physiology and pathophysiology of the intrarenal renin-angiotensin system: an update," *Journal of the American Society of Nephrology*, vol. 28, no. 4, pp. 1040–1049, 2017.
- [19] E. N. Kim, M. Y. Kim, J. H. Lim et al., "The protective effect of resveratrol on vascular aging by modulation of the renin-angiotensin system," *Atherosclerosis*, vol. 270, pp. 123–131, 2018.
- [20] L. Wang, A. D. de Kloet, D. Pati et al., "Increasing brain angiotensin converting enzyme 2 activity decreases anxiety-like behavior in male mice by activating central Mas receptors," *Neuropharmacology*, vol. 105, pp. 114–123, 2016.
- [21] L. D. Jackson, W. Eldahshan, S. Fagan, and A. Ergul, "Within the brain: the renin angiotensin system," *International Journal of Molecular Sciences*, vol. 19, no. 3, p. 876, 2018.

- [22] D. Han, Z. Liu, G. Wang, Y. Zhang, and Z. Wu, "Electroacupuncture improves cognitive deficits through increasing regional cerebral blood flow and alleviating inflammation in CCI rats," *Evidence-Based Complementary and Alternative Medicine*, vol. 2017, Article ID 5173168, 8 pages, 2017.
- [23] P. P. Feng, P. Deng, L. H. Liu et al., "Electroacupuncture alleviates postoperative cognitive dysfunction in aged rats by inhibiting hippocampal neuroinflammation activated via microglia/TLRs pathway," *Evidence-Based Complementary and Alternative Medicine*, vol. 2017, Article ID 6421260, 10 pages, 2017.
- [24] D. Amorim, J. Amado, I. Brito et al., "Acupuncture and electroacupuncture for anxiety disorders: a systematic review of the clinical research," *Complementary Therapies in Clinical Practice*, vol. 31, pp. 31–37, 2018.
- [25] M. Zhang, G.-H. Xu, W.-X. Wang, D.-J. Meng, and Y. Ji, "Electroacupuncture improves cognitive deficits and activates Ppar- γ in a rat model of Alzheimer's disease," *Acupuncture in Medicine*, vol. 35, no. 1, pp. 44–51, 2018.
- [26] M. C. Leung, K. K. Yip, C. T. Lam et al., "Acupuncture improves cognitive function: a systematic review," *Neural Regeneration Research*, vol. 8, no. 18, pp. 1673–1684, 2013.
- [27] F. Li, C.-Q. Yan, L.-T. Lin et al., "Acupuncture attenuates cognitive deficits and increases pyramidal neuron number in hippocampal CA1 area of vascular dementia rats," *BMC Complementary and Alternative Medicine*, vol. 15, no. 1, p. 133, 2015.
- [28] F. Cechetti, P. V. Worm, L. O. Pereira, I. R. Siqueira, and C. A. Netto, "The modified 2VO ischemia protocol causes cognitive impairment similar to that induced by the standard method, but with a better survival rate," *Brazilian Journal of Medical and Biological Research*, vol. 43, no. 12, pp. 1178–1183, 2010.
- [29] E. Farkas, T. P. Obrenovitch, A. Institoris, and F. Bari, "Effects of early aging and cerebral hypoperfusion on spreading depression in rats," *Neurobiology of Aging*, vol. 32, no. 9, pp. 1707–1715, 2011.
- [30] L. Prut and C. Belzung, "The open field as a paradigm to measure the effects of drugs on anxiety-like behaviors: a review," *European Journal of Pharmacology*, vol. 463, no. 1-3, pp. 3–33, 2003.
- [31] J. S. Kim, H. J. Lee, J. C. Kim et al., "Transient impairment of hippocampus-dependent learning and memory in relatively low-dose of acute radiation syndrome is associated with inhibition of hippocampal neurogenesis," *Journal of Radiation Research*, vol. 49, no. 5, pp. 517–526, 2008.
- [32] M. Milic, T. Timic, S. Joksimovic et al., "PWZ-029, an inverse agonist selective for α_5 GABA_A receptors, improves object recognition, but not water-maze memory in normal and scopolamine-treated rats," *Behavioural Brain Research*, vol. 241, pp. 206–213, 2013.
- [33] J. Kim, M. Yang, S. H. Kim et al., "Possible role of the glycogen synthase kinase-3 signaling pathway in trimethyltin-induced hippocampal neurodegeneration in mice," *PLoS One*, vol. 8, no. 8, article e70356, 2013.
- [34] R. Morris, "Developments of a water-maze procedure for studying spatial learning in the rat," *Journal of Neuroscience Methods*, vol. 11, no. 1, pp. 47–60, 1984.
- [35] Y. Zhao, J. H. Gu, C. L. Dai et al., "Chronic cerebral hypoperfusion causes decrease of O-GlcNAcylation, hyperphosphorylation of tau and behavioral deficits in mice," *Frontiers in Aging Neuroscience*, vol. 6, p. 10, 2014.
- [36] Y. Yang, J. Ju, M. Deng et al., "Hypoxia inducible factor 1α promotes endogenous adaptive response in rat model of chronic cerebral hypoperfusion," *International Journal of Molecular Sciences*, vol. 18, no. 1, p. 3, 2017.
- [37] M. K. S. Wong, "Chapter 29 - renin-angiotensin system," in *Handbook of Hormones*, Y. Takei, H. Ando, and K. Tsutsui, Eds., pp. 253–254, Academic Press, 2016.
- [38] J. F. Riordan, "Angiotensin-I-converting enzyme and its relatives," *Genome Biology*, vol. 4, no. 8, p. 225, 2003.
- [39] J. M. Saavedra, "Angiotensin II AT₁ receptor blockers as treatments for inflammatory brain disorders," *Clinical Science*, vol. 123, no. 10, pp. 567–590, 2012.
- [40] Y. Wei, A. T. Whaley-Connell, K. Chen et al., "NADPH oxidase contributes to vascular inflammation, insulin resistance, and remodeling in the transgenic (mRen2) rat," *Hypertension*, vol. 50, no. 2, pp. 384–391, 2007.
- [41] C. N. Young and R. L. Davisson, "Angiotensin-II, the brain, and hypertension: an update," *Hypertension*, vol. 66, no. 5, pp. 920–926, 2015.
- [42] E. Farag, D. I. Sessler, Z. Ebrahim et al., "The renin angiotensin system and the brain: new developments," *Journal of Clinical Neuroscience*, vol. 46, pp. 1–8, 2017.
- [43] S. Duchemin, E. Belanger, R. Wu, G. Ferland, and H. Girouard, "Chronic perfusion of angiotensin II causes cognitive dysfunctions and anxiety in mice," *Physiology & Behavior*, vol. 109, pp. 63–68, 2013.
- [44] W. Wang, X. Ma, J. Han et al., "Neuroprotective effect of scutellarin on ischemic cerebral injury by down-regulating the expression of angiotensin-converting enzyme and AT₁ receptor," *PLoS One*, vol. 11, no. 1, article e0146197, 2016.
- [45] J. M. Saavedra and J. Benicky, "Brain and peripheral angiotensin II play a major role in stress," *Stress*, vol. 10, no. 2, pp. 185–193, 2007.
- [46] D. Kumaran, M. Udayabanu, M. Kumar, R. Aneja, and A. Kalyal, "Involvement of angiotensin converting enzyme in cerebral hypoperfusion induced anterograde memory impairment and cholinergic dysfunction in rats," *Neuroscience*, vol. 155, no. 3, pp. 626–639, 2008.
- [47] L. Wang, Y. Du, K. Wang, G. Xu, S. Luo, and G. He, "Chronic cerebral hypoperfusion induces memory deficits and facilitates A β generation in C57BL/6j mice," *Experimental Neurology*, vol. 283, pp. 353–364, 2016.
- [48] L. M. Kangussu, A. F. Almeida-Santos, F. A. Moreira et al., "Reduced anxiety-like behavior in transgenic rats with chronically overproduction of angiotensin-(1–7): role of the Mas receptor," *Behavioural Brain Research*, vol. 331, pp. 193–198, 2017.
- [49] A. S. Kamel, N. F. Abdelkader, S. S. Abd El-Rahman, M. Emara, H. F. Zaki, and M. M. Khatat, "Stimulation of ACE2/ANG(1–7)/Mas axis by diminazene ameliorates Alzheimer's disease in the D-galactose-ovariectomized rat model: role of PI3K/Akt pathway," *Molecular Neurobiology*, vol. 55, no. 10, pp. 8188–8202, 2018.
- [50] J. C. Zhong, D. Y. Huang, Y. M. Yang et al., "Upregulation of angiotensin-converting enzyme 2 by All-trans Retinoic acid in spontaneously hypertensive rats," *Hypertension*, vol. 44, no. 6, pp. 907–912, 2004.
- [51] M. Yamazato, Y. Yamazato, C. Sun, C. Diez-Freire, and M. K. Raizada, "Overexpression of angiotensin-converting enzyme 2 in the rostral ventrolateral medulla causes long-term decrease

- in blood pressure in the spontaneously hypertensive rats," *Hypertension*, vol. 49, no. 4, pp. 926–931, 2007.
- [52] T. Jiang, L. Gao, J. Lu, and Y. D. Zhang, "ACE2-Ang-(1-7)-Mas axis in brain: a potential target for prevention and treatment of ischemic stroke," *Current Neuropharmacology*, vol. 11, no. 2, pp. 209–217, 2013.
- [53] J. Lu, T. Jiang, L. Wu et al., "The expression of angiotensin-converting enzyme 2-angiotensin-(1-7)-Mas receptor axis are upregulated after acute cerebral ischemic stroke in rats," *Neuropeptides*, vol. 47, no. 5, pp. 289–295, 2013.
- [54] D. M. Bennion, E. A. Haltigan, A. J. Irwin et al., "Activation of the neuroprotective angiotensin-converting enzyme 2 in rat ischemic stroke," *Hypertension*, vol. 66, no. 1, pp. 141–148, 2015.
- [55] R. Cernes, M. Mashavi, and R. Zimlichman, "Differential clinical profile of candesartan compared to other angiotensin receptor blockers," *Vascular Health and Risk Management*, vol. 7, pp. 749–759, 2011.
- [56] V. H. Ozacmak, H. Sayan, A. Cetin, and A. Akyildiz-Igdem, "AT1 receptor blocker candesartan-induced attenuation of brain injury of rats subjected to chronic cerebral hypoperfusion," *Neurochemical Research*, vol. 32, no. 8, pp. 1314–1321, 2007.
- [57] X. Huang, G. Lu, G. Li et al., "Dynamic changes in the renin-angiotensin-aldosterone system and the beneficial effects of renin-angiotensin-aldosterone inhibitors on spatial learning and memory in a rat model of chronic cerebral ischemia," *Frontiers in Neuroscience*, vol. 11, p. 359, 2017.
- [58] J. M. Saavedra, H. Ando, I. Armando et al., "Anti-stress and anti-anxiety effects of centrally acting angiotensin II AT₁ receptor antagonists," *Regulatory Peptides*, vol. 128, no. 3, pp. 227–238, 2005.
- [59] R. Goel, S. A. Bhat, K. Hanif, C. Nath, and R. Shukla, "Perindopril attenuates lipopolysaccharide-induced amyloidogenesis and memory impairment by suppression of oxidative stress and RAGE activation," *ACS Chemical Neuroscience*, vol. 7, no. 2, pp. 206–217, 2016.
- [60] J. Ikeda, N. Kojima, K. Saeki, M. Ishihara, and M. Takayama, "Perindopril increases the swallowing reflex by inhibiting substance P degradation and tyrosine hydroxylase activation in a rat model of dysphagia," *European Journal of Pharmacology*, vol. 746, pp. 126–131, 2015.

Research Article

The Long-Term Effects of Acupuncture on Hippocampal Functional Connectivity in aMCI with Hippocampal Atrophy: A Randomized Longitudinal fMRI Study

Hui Li,^{1,2} Zhiqun Wang,³ Haikuo Yu,⁴ Ran Pang,¹ Hong Ni,¹ Chiang-shan R. Li,^{5,6,7} and Kuncheng Li^{1,2} 

¹Department of Radiology, Xuanwu Hospital, Capital Medical University, Beijing 10053, China

²Beijing Key Lab of MRI and Brain Informatics, Beijing 10053, China

³Department of Radiology, Aerospace Center Hospital, Beijing 100049, China

⁴Department of Rehabilitation Medicine, Xuanwu Hospital, Capital Medical University, Beijing 10053, China

⁵Department of Psychiatry, Yale University School of Medicine, New Haven, CT, USA

⁶Department of Neuroscience, Yale University School of Medicine, New Haven, CT, USA

⁷Beijing Huilongguan Hospital, Beijing, China

Correspondence should be addressed to Kuncheng Li; cjr.likuncheng@vip.163.com

Received 15 October 2019; Revised 23 December 2019; Accepted 21 January 2020; Published 10 February 2020

Guest Editor: Marco Canevelli

Copyright © 2020 Hui Li et al. This is an open access article distributed under the Creative Commons Attribution License, which permits unrestricted use, distribution, and reproduction in any medium, provided the original work is properly cited.

Background. Acupuncture has been used to treat amnesic mild cognitive impairment (aMCI) for many years in China. However, the long-term effects of continuous acupuncture treatment remained unclear. **Objective.** We aimed to explore the long-term effects of continuous acupuncture treatment on hippocampal functional connectivity (FC) in aMCI. **Methods.** Fifty healthy control (HC) participants and 28 aMCI patients were recruited for resting-state functional magnetic resonance imaging (fMRI) at baseline. The 28 aMCI patients were then divided into the aMCI acupuncture group, which received acupuncture treatment for 6 months, and the aMCI control group, which received no intervention. All aMCI patients completed the second resting-state fMRI scanning after 6 months of acupuncture treatment. Analysis based on the region of interest and two-way analysis of covariance were both used to explore the long-term effects of acupuncture on cognition change and hippocampal FC in aMCI. **Results.** Compared to HC, aMCI showed decreased right hippocampal FC with the right inferior/middle temporal gyrus (ITG/MTG), left amygdala, and the right fusiform and increased FC with bilateral caudates at baseline. After acupuncture treatment, the right hippocampal FC with right ITG/MTG enhanced significantly in the aMCI acupuncture group, but continued to decrease in the aMCI control group. Whole brain FC analysis showed enhanced right hippocampal FC with the right ITG and the left MTG in the aMCI acupuncture group relative to the aMCI control group. Furthermore, FC strength of the right hippocampus with right ITG at baseline was negatively correlated with the changes in memory scores of aMCI acupuncture patients. **Conclusion.** Acupuncture treatment could alleviate the progression of cognitive decline and could enhance hippocampal FC with ITG and MTG in aMCI that may be associated with resilience to resistant against neurodegeneration. The findings provided a better understanding of the long-term effects of acupuncture treatment and confirmed the therapeutic role of acupuncture in aMCI.

1. Introduction

Amnesic mild cognitive impairment (aMCI) is considered as the prodromal stage of Alzheimer's disease (AD) [1]. It is reported that about 11.1% of the population between 70 and 89 years is affected by aMCI and among them about

16-41% develop AD every year [2, 3]. As dementia can severely affect quality of life and is a leading cause of death in elderly people, once the disease occurs, there is no cure for it; early diagnosis and treatment of AD at the prodromal stage is of great significance. As an important component of traditional Chinese medicine, acupuncture has been used to

treat dementia in China for many years [4–6] and the potential mechanisms underlying its therapeutic efficacy have attracted increasing attention.

Functional magnetic resonance imaging (fMRI) provides a noninvasive means to investigate the neural mechanisms of the effects of acupuncture in different diseases, such as Parkinson's disease and insomnia disorder [7, 8]. Accumulating evidence has suggested acupuncture as a promising treatment for MCI by modulating cerebral functional connectivity (FC) [9–11] and intrinsic activity [12, 13]. Feng et al. reported that acupuncture enhanced functional correlations in memory-related brain regions, including the hippocampus (HP), thalamus, and fusiform gyrus [9] in MCI patients. In other studies, acupuncture could remediate the dysfunctional connections of the HP [10] and alleviate the loss of small world in MCI patients by enhancing the nodal centrality of the HP, postcentral cortex, and anterior cingulate cortex. [11] Further, as quantified by the amplitude of low-frequency fluctuation (ALFF), acupuncture modulated intrinsic activities of cognition-related brain regions, including the right superior temporal gyrus (STG) and HP, in MCI patients [12, 13].

In traditional Chinese medicine, a combination of several acupoints is often used in acupuncture as a treatment. In the theory of traditional Chinese medicine, the Si Guan (four gates) acupoints, composed of bilateral Hegu (LI4) and Tai-chong (Liv3), could harmonize yin and yang and regulate qi and blood to improve the cognitive capacity. With LI4 and Liv3 as the acupoints, previous studies have demonstrated increased or decreased activities of temporal and frontal brain regions in MCI and AD patients following acupuncture [14, 15]. Increased FC between the left HP and right middle frontal gyrus (MFG) and between the right HP and right inferior temporal gyrus (ITG) and STG have also been demonstrated in AD patients [5].

However, these earlier studies focused on the instantaneous effects of acupuncture, and the long-term effects of acupuncture were rarely reported. Tan et al. performed acupuncture on MCI subjects for 4 consecutive weeks and reported that acupuncture could regulate the cognitive-related brain networks and improve the cognitive ability [4]. In the present study, we performed acupuncture treatment on aMCI patients for six months to explore its long-term effects and the neural processes for the long-term treatment. Considering that the HP is one of the earliest pathological sites of aMCI and HP activity appeared to be modulated by the instantaneous effects of acupuncture, we defined bilateral hippocampi as the regions of interest (ROIs). We hypothesized that acupuncture at the Si Guan acupoints would modulate the HP connectivity and alleviate the progression of cognitive decline in aMCI patients.

2. Materials and Methods

We used a randomized single-blinded clinical trial, with a 2×2 flexible factorial design, to investigate the long-term effects of acupuncture treatment on aMCI. The research protocol for the study was approved by the Ethics Committee of the Xuanwu Hospital (Clinical Research Review 2016 004).

2.1. Participants. Healthy control (HC) participants were recruited from community while aMCI patients were recruited from Xuanwu Hospital of Capital Medical University in Beijing. The objectives and procedures were explained in detail to all participants and written informed consents were collected before participating in this study.

The criteria for aMCI were as follows: (1) compliance with the core clinical criteria stipulated by the National Institute on Aging and the Alzheimer's Association [16]; (2) a Clinical Dementia Rating (CDR) score of 0.5, with a score of at least 0.5 on the memory domain; (3) hippocampal atrophy on MRI; and (4) regular use of rivastigmine (12 mg/day).

The criteria for HC were as follows: (1) no complaints of cognitive changes, (2) no neurological deficiencies in physical examinations, (3) no any abnormal findings on brain MRI, and (4) CDR score = 0.

Subjects were excluded when the following conditions occurred: (1) current or previous diagnosis of any neurological or psychiatric disorders; (2) major medical illness, severe visual or hearing loss; (3) contraindications for MRI such as use of cardiac pacemakers and claustrophobia; and (4) aMCI patients who did not complete the whole acupuncture treatment.

In this study, we defined the pattern of HP-FC and neuropsychological measurement scales as our primary outcome measures. At baseline, all participants underwent MRI scans and neuropsychological evaluation with the Mini Mental State Examination (MMSE), Montreal Cognitive Assessment (MoCA), CDR, and Auditory Verb Learning Test (AVLT). Then, aMCI patients were randomly divided into two subgroups, namely the aMCI acupuncture group and the aMCI control group. The aMCI acupuncture group received acupuncture treatment for 6 months while the aMCI control group received no intervention. After acupuncture treatments were completed, all the aMCI patients completed a follow-up fMRI scan and neuropsychological evaluation that were identical to the baseline examination. The neuropsychological scale test was performed by a designated experienced neurologist, and the clinic was closed and quiet.

2.2. Acupuncture Intervention. The Si Guan acupoints were targeted in the study (Figure 1). The subjects laid down in the supine position and the skins over Si Guan acupoints were disinfected with 70% alcohol. Each needle (silver needle with a diameter of 0.30 mm and length of 25 mm) was inserted vertically at a depth of approximately 20 mm and manually twirled using mild reinforcing-reducing method to bring about the needling sensation. The needles would be retained for 20 minutes and be rotated 5 times. Needling sensation, known as “de qi” in Chinese and an indicator of effective needling, included numbness, swelling, tingling, and a feeling of muscle weakness. At the same time, acupuncturists also could feel local muscle contracted and wrapped the silver needle. Acupuncture treatment was given 3 times a week, 4 weeks as a course. The interval between the two courses was 2 weeks of rest, with a total of 4 courses in 6 months.

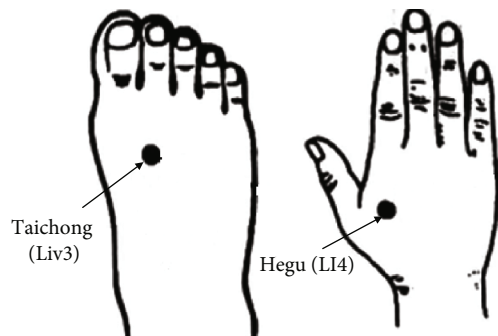


FIGURE 1: Location of acupoints used in the experiment.

2.3. MRI Data Acquisition. MRI data were obtained using a 3.0-Tesla scanner (Trio, Siemens, Erlangen, Germany). All participants were asked to lie supine with a headset to insulate scanner noise, hold still, and keep their eyes closed. Foam paddings were employed to reduce head motion. First, the routine head MRI scans were completed, including axial T1-weighted images scans, T2-weighted images scans, fluid-attenuated inversion recovery scans, diffusion-weighted imaging scans, and coronal and sagittal T1-weighted images scans. The parameters used to acquire 3D T1-weighted anatomical images and resting-state fMRI images were identical to those reported previously [17]. Resting-state functional MRI images were acquired using an echo-planar imaging (EPI) sequence: repetition time (TR) = 2000 ms, echo time (TE) = 40 ms, flip angle (FA) = 90°, field of view (FOV) = 256 × 256 mm², matrix = 64 × 64, 28 axial slices, slice thickness/gap = 4/1 mm, bandwidth = 2232 Hz/pixel, and number of repetitions = 239. The 3D T1-weighted anatomical images were acquired with a magnetization-prepared rapid gradient echo (MPRAGE) method with the following parameters: TR = 1900 ms, TE = 2.2 ms, inversion time (TI) = 900 ms, FA = 9°, bandwidth = 199 Hz/pixel, matrix = 256 × 224, FOV = 256 × 224 mm², 176 sagittal slices, and slice thickness = 1 mm.

2.4. MRI Data Preprocessing and Functional Connectivity Analysis. Resting-state fMRI data were preprocessed with the statistical parametric mapping software SPM12 (<https://www.fil.ion.ucl.ac.uk/spm>), and seed-to-voxel correlation analysis was performed using the functional connectivity (CONN) toolbox v17f [18]. After discarding the first 10 functional images, the remaining 229 images of each individual subject underwent slice-timing correction and realignment. All subjects included in the present study exhibited head motion less than 3.0 mm in any of the *x*, *y*, or *z* directions and less than 3.0° of any angular dimension. The resulting images were spatially normalized to the Montreal Neurological Institute (MNI) space with a resampled resolution of 2 × 2 × 2 mm³ and smoothed with a 4 mm full width at half maximum (FWHM) isotropic Gaussian kernel. After preprocessing, images were band-pass filtered to 0.008 ~ 0.09 Hz to reduce the influence of noise. Further denoising steps included regression of the six motion parameters, regression of white matter, and cerebrospinal fluid (CSF) signals and a linear detrending.

The bilateral hippocampi were defined using the Automated Anatomical Labeling (AAL) templates. The correlation maps were generated by computing the Pearson correlation coefficients between the seed voxels and all other brain voxels. For group analyses, the correlation coefficients were converted to *z* value using Fisher's *r*-to-*z* transformation to improve normality. To consider the influence of volumetric difference in HP between aMCI and HC, we compared gray matter volume of the HP between the aMCI and HC groups.

Due to the particularity of acupuncture treatment, this study adopted a randomized, single-blind study. According to the previous study [15, 19], the estimated sample size was 30. The randomized digital table method combined with the random number remainder grouping method was used to randomly group the patients by a specialized statistical expert. The acupuncture treatment group and the blank control group were, respectively, 15 cases. Because the aMCI control group received no intervention, the patients in this study were not blind, but the functional magnetic resonance data analysts and the scale assessment experts that assessing outcomes were not aware of the treatment. Therefore, this study was a randomized, single-blind study.

2.5. Statistical Analysis. Demographic data and neuropsychological measures were analyzed using SPSS 22. Student's *t*-tests were conducted for continuous variables, including age, years of education, and neuropsychological test scores, and chi-squared tests were used to examine the differences in gender composition between groups.

In the random effect analysis of imaging data, we determined the voxel-wise FC patterns of bilateral hippocampi within each group, using one-sample *t*-test. Two-sample *t*-tests were performed to assess the differences in HP-FC between aMCI and HC subjects at the baseline. The significance threshold was set to $p < 0.05$ corrected for false discovery rate (FDR), with age, years of education, gender, and gray matter volume of the HP as covariates. Brain regions that showed significant differences in hippocampal FC were selected as ROIs and interregional FC values of the seeds were extracted. Two-sample *t*-tests were performed to investigate the differences of the FC changes between the aMCI acupuncture group and aMCI control group.

In addition, we employed a 2 (time: baseline versus follow-up) × 2 (group: aMCI acupuncture group versus aMCI control group) flexible factorial analysis, with 4 conditions—the aMCI acupuncture group at baseline (aMCI acupuncture1), the aMCI acupuncture group at follow-up (aMCI acupuncture2), the aMCI control group at baseline (aMCI control1), and the aMCI control group at follow-up (aMCI control2). The time by group interaction reflected the effects of acupuncture treatment on aMCI subject. The significance threshold was set to $p < 0.05$, FDR corrected, with age, years of education, and gender as covariates. Increased FC of HP in the aMCI acupuncture group after acupuncture relative to the aMCI control group was evaluated by [(aMCI acupuncture2 > aMCI acupuncture1) > (aMCI control2 > aMCI control1)] and decreased FC of HP in the aMCI acupuncture group after acupuncture

TABLE 1: Scoring results of neuropsychological scale.

	aMCI control group			aMCI acupuncture group			Changes (follow-up vs. baseline)		
	Baseline	Follow-up	<i>p</i> value	Baseline	Follow-up	<i>p</i> value	aMCI control	aMCI acupuncture	<i>p</i> value
CDR	0.5	0.5		0.5	0.5				1
MMSE	25.4 ± 3.7	24.0 ± 4.0	0.01	25.0 ± 3.1	25.8 ± 2.9	0.29	-1.4 ± 1.7	0.8 ± 2.6	0.02
MoCA	22.1 ± 4.2	21.0 ± 5.2	0.09	20.5 ± 3.7	19.9 ± 3.6	0.31	-1.1 ± 2.2	-0.6 ± 2.1	0.59
AVLT-immediate	6.5 ± 1.8	5.6 ± 1.5	0.14	6.3 ± 0.9	6.0 ± 1.8	0.40	-0.8 ± 2.1	-0.3 ± 1.2	0.40
AVLT-delay	4.5 ± 3.0	2.6 ± 2.1	0.01	3.1 ± 3.4	3.8 ± 3.9	0.37	-1.9 ± 2.1	0.6 ± 2.4	0.01
AVLT-recognition	7.2 ± 4.1	7.9 ± 3.6	0.48	6.8 ± 2.8	7.2 ± 3.8	0.75	0.6 ± 3.4	0.4 ± 4.5	0.86

Values represent the means ± SD. aMCI: mild cognitive impairment due to Alzheimer’s disease; Lt.: left; Rt.: right; HP: hippocampus; CDR: clinical dementia rate; MMSE: mini mental state examination; MoCA: Montreal Cognitive Assessment; AVLT: auditory verbal learning test.

relative to the aMCI control group was evaluated by $[(\text{aMCI acupuncture}_2 > \text{aMCI acupuncture}_1) < (\text{aMCI control}_2 > \text{aMCI control}_1)]$.

The regions showing a significant interaction effect were defined as ROIs, and the FC values were extracted for *post hoc* pairwise comparisons and correlations analysis using SPSS 22. Independent-sample *t*-tests were applied to compute the group differences of FC between the aMCI acupuncture and aMCI control groups at baseline and follow-up separately. Paired-sample *t*-tests were performed to explore the longitudinal FC changes within each group at follow-up, as compared to baseline.

Finally, to identify the distinct FC biomarkers and predictor of treatment effects, partial correlations were computed between the FC strength at baseline and changes in neuropsychological scores (post- vs. pretreatment), with adjustment for age, gender, and years of education in the aMCI acupuncture group. In addition, Pearson’s correlations were conducted between the FC alterations and neuropsychological score changes (post- vs. pretreatment) to evaluate the relationship between the effect of acupuncture and FC changes. Statistical significance was set at $p < 0.05$, Bonferroni corrected for multiple comparisons.

3. Results

3.1. Scoring Results of Neuropsychological Scale. Eighty including 30 aMCI and 50 HC participants were recruited. Two aMCI patients refused to complete the baseline examination after the numbering, so a total of 28 patients and 50 HC were enrolled at baseline. The data of one aMCI control patient and two aMCI acupuncture patients were discarded because of excessive head movements in the scanner at follow-up. There were no significant differences in age, gender, and years of education between the aMCI and HC groups. Compared to HC, aMCI exhibited significantly smaller HP volume, higher CDR scores, and lower MMSE, MoCA, and AVLT scores, in confirmation of episodic memory impairment (Supplementary Table 1). Randomly divided into two groups, the aMCI acupuncture group and aMCI control group did not show significant differences in age, gender, years of education, CDR, MMSE, MoCA, or AVLT score (Supplementary Table 1).

3.2. Effects of Acupuncture on Cognitive Assessment in aMCI. As shown in Table 1, as compared with baseline measures, MMSE scores increased in the aMCI acupuncture group after acupuncture treatment, whereas the scores of the aMCI control group have continuously declined. At the same time, the scores of AVLT delayed recall changed in the same pattern; AVLT delayed recall scores increased in the aMCI acupuncture group, whereas the scores of the aMCI control group declined. The comparison between the score changes was significant.

3.3. Hippocampal FC: Within-Group Analysis. In the HC group, there were significant FC between the bilateral hippocampi and several cognitive-related regions including the temporal lobe, precuneus, cingulate gyrus, frontal lobe, and some subcortical nuclei (Supplementary Figure 1). In the aMCI group, similar FC patterns of bilateral hippocampi were revealed with relatively smaller cluster sizes, mainly including the temporal lobe, precuneous cortex, cingulate gyrus, and some subcortical nuclei (Supplementary Figures 2–6).

3.4. Between-Group Hippocampal FC Analysis at Baseline. Compared to HC, the aMCI patients showed a significantly weakened FC of the right HP to the right inferior/middle temporal gyrus (ITG/MTG), the left amygdala, and the right fusiform. Significantly enhanced FC was found between the right HP and bilateral caudates (Table 2, Figure 2). On the contrary, no significant FC changes of the left HP were found.

3.5. Effects of Acupuncture on HP-FC in the aMCI Acupuncture Group: ROI Analysis. To explore the effect of acupuncture on HP-FC in the aMCI acupuncture group after the whole treatment course, the abovementioned brain regions were defined as seeds and the FC values were extracted. Two-sample *t*-tests were performed to investigate the differences in the longitudinal HP-FC changes between the two groups and a significant result was found in the right HP to the right ITG/MTG. The weakened right HP-FC to the right ITG/MTG significantly enhanced at follow-up in the aMCI acupuncture group, while that of the aMCI control group continued to decline (Figure 3(a)). On the contrary, the trends of the right HP-FC changes in the other brain regions were similar

TABLE 2: Significant between-group differences in functional connectivity of the right hippocampus.

Contrast	Region	Cluster size (voxel)	MNI			T value
			x	y	z	
HC > aMCI	Rt. MTG/ITG	320	54	-12	-24	6.21
	Lt. amygdala	188	-32	2	-18	4.45
	Rt. fusiform	95	30	0	-48	4.39
HC < aMCI	Lt. caudate	90	-2	6	6	4.25
	Rt. caudate	100	16	20	8	4.04
(aMCI acupuncture2 > aMCI acupuncture1) > (aMCI control2 > aMCI control1)	Lt. MTG	71	-50	-18	-18	5.14
	Rt. ITG	66	54	-64	-12	4.86

Between-group results were thresholded at cluster-level $p < 0.05$ (FDR corrected). The anatomical localization was implemented by using xjView software. HC: healthy control; aMCI: amnesic mild cognitive impairment; aMCI acupuncture1: aMCI acupuncture group at baseline; aMCI acupuncture2: aMCI acupuncture group at follow-up; aMCI control1: aMCI control group at baseline; aMCI control2: aMCI control group at follow-up; MNI: Montreal Neurological Institute; Lt.: left; Rt.: right; MTG: middle temporal gyrus; ITG: inferior temporal gyrus.

between the aMCI acupuncture and aMCI control groups, which showed no significant difference.

3.6. Effects of Acupuncture on HP-FC in the aMCI Acupuncture Group: Whole Brain Analysis. For time by group interaction effect, the right HP showed significant enhanced FC with the right ITG and the left MTG in the aMCI acupuncture group in contrast to the aMCI control group. *Post hoc* pairwise comparisons showed that (1) at baseline, there was no significant between-group differences in FC of the right HP and right ITG ($p = 0.1618$) and the left MTG ($p = 0.1688$); (2) at follow-up, compared with the aMCI control group, the FC of the right HP and the right ITG ($p = 0.0126$) and the left MTG ($p < 0.0001$) were significantly increased in the aMCI acupuncture group; (3) compared with baseline, the FC between the right HP and the right ITG ($p = 0.0043$) and left MTG ($p = 0.0018$) were both significantly increased in the aMCI acupuncture at follow-up; (4) compared with baseline, the FC of the right HP and the left MTG ($p < 0.0001$) was significantly reduced in the aMCI control group at follow-up. These results showed that after acupuncture, the abnormal right HP-FC to the right ITG (Figure 3(b)) and the left MTG (Figure 3(c)) enhanced in the aMCI acupuncture group, while those of the aMCI control group continued to decline, verifying our hypothesis that abnormal HP-FC in the aMCI group would show a recovery after acupuncture therapy.

3.7. Correlations between HP-FC and Clinical Performance in the aMCI Acupuncture Subjects. In the aMCI acupuncture subjects, partial correlation analysis, adjusting for age, gender, and education years, revealed that the FC value of the right HP to the right ITG at baseline was negatively related with the longitudinal changes of MoCA scores ($p = 0.004$, $r = -0.767$), suggesting that patients with lower FC value at baseline will present stronger acupuncture treatment effect (Figure 3(d)). On the other hand, no significant relationship was found between FC values at baseline and other clinical changes except MoCA in the partial correlation analysis and there is no obvious correlation between FC changes and clinical alterations.

4. Discussion

We evaluated the long-term effects of acupuncture treatment on aMCI by investigating the longitudinal changes of neuropsychological tests and hippocampal FC. The results showed that acupuncture could slow down cognitive decline and enhance the FC of the right HP to the right ITG and the left MTG, which may associate with the efficacy of acupuncture treatment on aMCI. Further, predicting the longitudinal changes of MoCA scores, FC of the right HP-ITG might be a biomarker indicating acupuncture treatment for patients with aMCI.

Recently, a tau-positron emission tomography (PET) study revealed that individuals with preclinical AD and positive beta-amyloid presented higher tau-PET in the ITG, MTG, precuneus, amygdala, superior temporal sulcus, fusiform gyrus, entorhinal cortex, and inferior parietal cortex. [20] Gray matter atrophy and hypometabolism in the cognitive networks were also reported in MCI patients [21]. In functional network analysis, aMCI patients showed decreased connectivity between hippocampal subfields and the right fusiform gyrus [22]. An fMRI study also demonstrated significant alteration of connectivity patterns in a memory-related subnetwork, including part of the HP, amygdala, fusiform gyrus, ITG, and MTG at the late stage of MCI and the deficits propagated to the rest of the brain as disease progressed. [23] Granger causality analysis revealed that directed FC between the HP and the temporal lobe, frontal lobe, and cingulate cortex were significantly changed in MCI [24]. On the other hand, increased spontaneous brain activities and FC have also been revealed in the frontal and temporal cortex in aMCI patients [25, 26]. These enhancements were thought to function as compensatory mechanisms due to cognitive deficits in aMCI. The caudate nucleus has been reported to be larger in AD that possibly serving as a mechanism for temporary compensation [27]. In the present study, at baseline, aMCI patients as compared with HC showed significantly weakened FC of the right HP with the right ITG/MTG, the left amygdala, and right fusiform and increased FC with bilateral caudates. These findings were consistent with previous studies suggesting that neural impairment and compensation may coexist in aMCI.

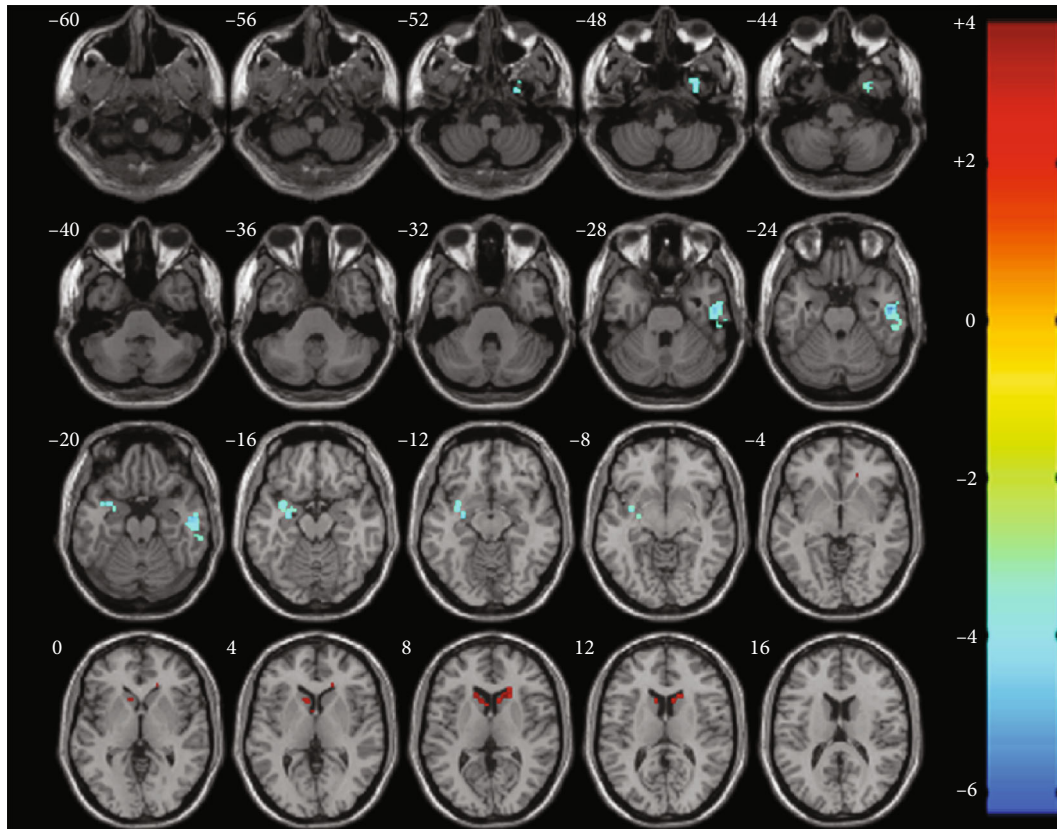


FIGURE 2: Brain regions showing altered connectivity to the right hippocampus in the aMCI group comparing to HC at baseline. Numbers in the figure indicate the Z coordinate in MNI space. The color scale represents t values. Warm color represents increased connectivity; cold color represents decreased connectivity.

Acupuncture is growing in popularity worldwide for its therapeutic effects on age-related cognitive decline [28]. Since the theory of traditional Chinese medicine cannot be explained by contemporary science, we regard its traditional Chinese medicine therapeutic mechanism as a black box. The key points are to find objective evidences of its efficacy and potential imaging markers to predict the curative effects. Acupuncture at the four gate acupoints is widely used in China to treat dementia. Jiang et al. reported in a rodent model of AD that acupuncture treatment on four gate acupoints improved learning and memory, along with decrease in the hippocampal amyloid-beta 42 immunoactivity and interleukin-1 (IL-1) beta content and upregulation of the hippocampal IL-2 [29]. In our previous study, we investigated the instantaneous effects of acupuncture at the four gate acupoints and found that acupuncture could activate cognition-related regions, including bilateral fusiform gyrus, right MTG, right parahippocampus gyrus, and frontal cortex in MCI and AD subjects [14, 30]. Moreover, bilateral MTG, left ITG, and fusiform gyrus showed enhanced hippocampal connectivity after acupuncture [5]. These results revealed that acupuncture at four gate acupoints modulate intrinsic brain activity and functional connectivity in MCI and AD patients.

After 6 months of acupuncture treatment, ROI analysis revealed that the weakened FC between the right HP and

the right MTG/ITG were upregulated in the aMCI acupuncture group while the aMCI control group continued to decline. Whole brain analysis with bilateral hippocampi as the seeds confirmed this result. Compared with previous studies focused on instantaneous effects of acupuncture, the brain regions showing increased FC were much smaller in the present study. This discrepancy may be related with difference between instantaneous effects and the long-term effects of acupuncture. The latter has excluded the effects of pain and irritation during acupuncture that cannot be ignored in the instantaneous effect studies. The ITG and MTG are important components of the default mode network [31]. Amyloid deposits, hypometabolism, and atrophy have been consistently reported in these brain regions in MCI [32–34]. Furthermore, metabolic levels in the right ITG and MTG are significantly correlated with the speed of conversion to dementia [35], and 18F 3H-2-fluoro-2-deoxy-D-glucose (FDG) uptake reduction in ITG and MTG could significantly predict overall cognition impairment as assessed by MMSE score [36]. In resting-state fMRI, aMCI patients showed disrupted connectivity between the right HP subregion and the MTG, which is closely correlated with reduced capacity of episodic memory [37]. All the above-mentioned studies suggested that destroyed ITG and MTG functions play an important role in cognition impairment. On the other hand, a recent study revealed less extended

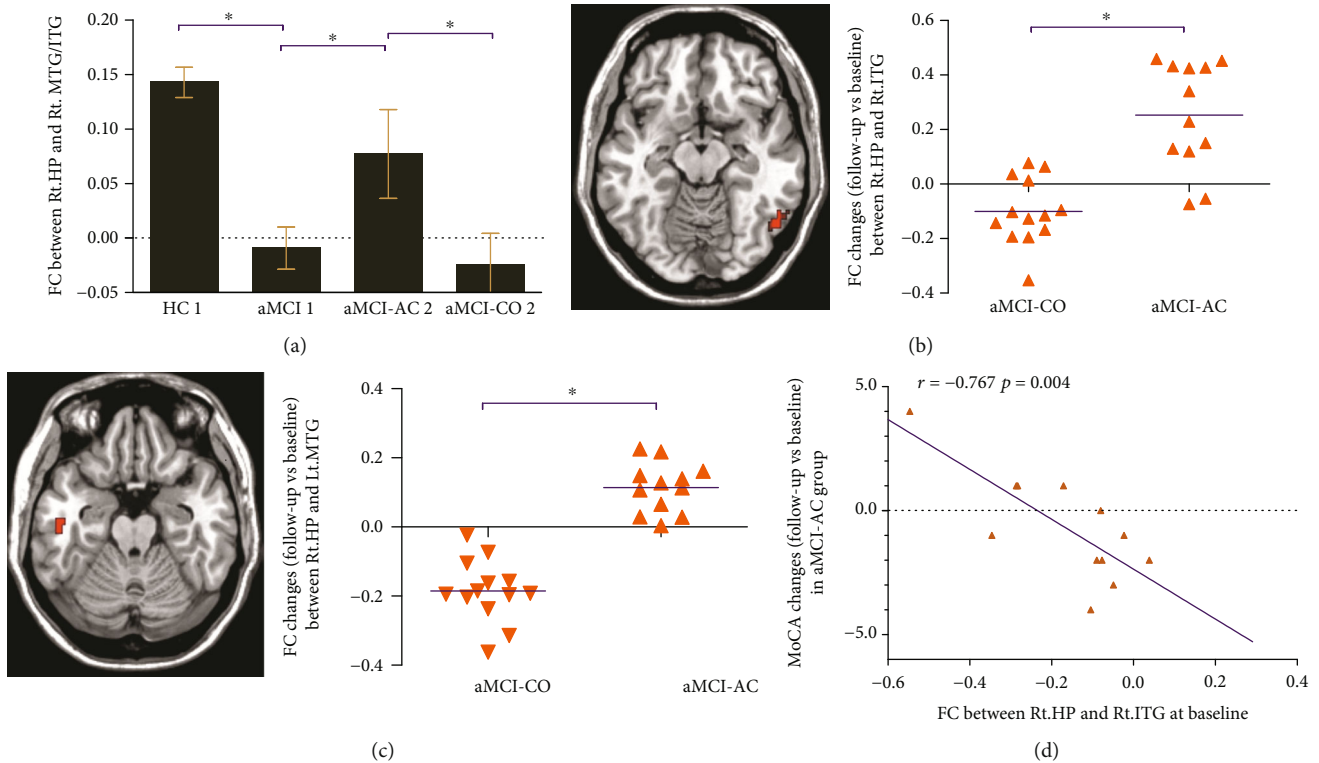


FIGURE 3: (a) The value of FC between the right HP and right MTG/ITG in HC at baseline, aMCI at baseline, aMCI acupuncture at follow-up, and aMCI control at follow-up. (b) Increased FC between the right HP and right ITG in aMCI acupuncture subjects as compared to aMCI control at follow-up vs. baseline (interaction effect). (c) Increased FC between the right HP and left MTG in aMCI acupuncture subjects as compared to aMCI control at follow-up vs. baseline (interaction effect). (d) Linear correlation of longitudinal changes in MoCA scores and the FC between the right HP and the right ITG at baseline in aMCI acupuncture subjects. HC 1: healthy control participants at baseline; aMCI: amnesic mild cognitive impairment; aMCI 1: all aMCI subjects at baseline; aMCI-AC 2: aMCI acupuncture group at follow-up; aMCI-CO 2: aMCI control group at follow-up; FC: functional connectivity; HP: hippocampus; Lt.: left; Rt.: right; MTG: middle temporal gyrus; ITG: inferior temporal gyrus; * indicates cluster-level $p < 0.05$, FDR corrected.

and severe hypometabolism in ITG and MTG in late-converter MCI patients as compared with those with typically progressing MCI, suggesting that ITG and MTG may represent sites of resilience to slow the disease progression despite harboring the primary risk factors [38]. In the present study, the aMCI acupuncture group showed cognitive improvement and increased HP-MTG/ITG FC after continuous regular acupuncture treatment. We suggested that acupuncture probably could enhance the resilience in ITG and MTG to resistant against neurodegeneration and alleviate disease progression.

We also found that the changes in neuropsychological performances in the aMCI acupuncture group were significantly different from those of the aMCI control group and the longitudinal changes of MoCA scores were negatively correlated with the FC between the right HP and the right ITG at baseline in the aMCI acupuncture group, suggesting that subjects with lower FC values would present stronger acupuncture therapeutic effect at the aMCI stage. This similarly negative relationship has been reported in healthy cognitive aging and participants who were worse at baseline benefit from physostigmine treatment, while those with better baseline performance either did not show such benefits or showed poorer memory [39]. At the same time, no significant correlation was

found between the FC changes and the neuropsychological assessment changes, which might suggest that acupuncture played a therapeutic role by regulating the whole brain FC of the hippocampus rather than a separate brain region-related FC.

Several limitations need to be considered. First, the sample size of the study was relatively small, and studies with a larger sample will be needed to confirm the current findings and elucidate the long-term effects of acupuncture on aMCI. Second, without access to PET examination and cerebrospinal fluid analysis [40], the aMCI patients have been chosen to include only those with hippocampal atrophy on MRI. It is well known that these patients with morphological changes will have very high chance of converting to AD. Based on this, the criteria used in the present study suggested an intermediate level of certainty that the aMCI syndrome is due to AD and the effect of acupuncture on AD-related pathological status is explored. Third, sham acupoint acupuncture intervention was not used in the aMCI control group and should be included in the future study.

5. Conclusions

In summary, acupuncture treatment at four gate acupoints significantly alleviated the progression of cognitive

decline and enhanced the resilience to resistant against neurodegeneration by modulating the FC strength of the HP-MTG/ITG. The FC strength of right HP-ITG at baseline was significantly associated with neuropsychological changes. The findings confirmed the therapeutic roles of acupuncture treatment and provided objective evidences with the application of fMRI.

Abbreviations

aMCI:	Amnesic mild cognitive impairment
AD:	Alzheimer's disease
HC:	Healthy control
aMCI-AC:	aMCI acupuncture group
MCI-CO:	aMCI control group
fMRI:	Functional magnetic resonance imaging
FC:	Functional connectivity
HP:	Hippocampus
ITG:	Inferior temporal gyrus
MTG:	Middle temporal gyrus.

Data Availability

The datasets analyzed during the current study are not publicly available due to the unfinished study of the whole project but are available from the corresponding author on reasonable request.

Disclosure

The abstract was presented at Alzheimer's Association International Conference Monday Poster Abstract (<https://alz-journals.onlinelibrary.wiley.com/doi/10.1016/j.jalz.2019.06.1241>).

Conflicts of Interest

All authors declare no conflict of interest.

Acknowledgments

This work was supported partly by grants from the National Natural Science Foundation of China (81471649, 81571648, 81370037, and 81873892), the Clinical Medicine Development Special Funding from the Beijing Municipal Administration of Hospital (ZYLX201609), the Key Projects in the National Science and Technology Pillar Program during the Twelfth Five-Year Plan Period (2012BAI10B04), the Beijing Municipal Science and Technology Commission (Z171100000117001), and the NIH (United States) grant R21MH113134.

Supplementary Materials

All the figures are the results of one-sample *T*-tests of each group at baseline or at follow-up and the table is the clinical characteristics of subjects with amnesic mild cognitive impairment (aMCI) and healthy control (HC) at baseline. Supplementary Table 1: clinical characteristics of subjects with amnesic mild cognitive impairment (aMCI) and healthy control (HC). (*Supplementary Materials*)

References

- [1] R. C. Petersen, "Mild cognitive impairment," *The New England Journal of Medicine*, vol. 364, no. 23, pp. 2227–2234, 2011.
- [2] R. C. Petersen, R. O. Roberts, D. S. Knopman et al., "Prevalence of mild cognitive impairment is higher in men. The Mayo Clinic Study of Aging," *Neurology*, vol. 75, no. 10, pp. 889–897, 2010.
- [3] S. Gauthier, B. Reisberg, M. Zaudig et al., "Mild cognitive impairment," *The Lancet*, vol. 367, no. 9518, pp. 1262–1270, 2006.
- [4] T. T. Tan, D. Wang, J. K. Huang et al., "Modulatory effects of acupuncture on brain networks in mild cognitive impairment patients," *Neural Regeneration Research*, vol. 12, no. 2, pp. 250–258, 2017.
- [5] Z. Wang, P. Liang, Z. Zhao et al., "Acupuncture modulates resting state hippocampal functional connectivity in Alzheimer disease," *PLoS One*, vol. 9, no. 3, article e91160, 2014.
- [6] R. Sun, Y. Yang, Z. Li, Y. Li, S. Cheng, and F. Zeng, "Connectomics: a new direction in research to understand the mechanism of acupuncture," *Evidence-Based Complementary and Alternative Medicine*, vol. 2014, Article ID 568429, 9 pages, 2014.
- [7] S.-W. Yu, S. H. Lin, C. C. Tsai et al., "Acupuncture effect and mechanism for treating pain in patients with Parkinson's disease," *Frontiers in Neurology*, vol. 10, 2019.
- [8] J. Guo, S. Yu, C. Liu, G. Wang, and B. Li, "Acupuncture for patients with insomnia disorder using resting-state functional magnetic resonance imaging: a protocol for a randomized controlled trial," *Trials*, vol. 20, article 685, no. 1, 2019.
- [9] Y. Feng, L. Bai, Y. Ren et al., "fMRI connectivity analysis of acupuncture effects on the whole brain network in mild cognitive impairment patients," *Magnetic Resonance Imaging*, vol. 30, no. 5, pp. 672–682, 2012.
- [10] S. Chen, L. Bai, M. Xu et al., "Multivariate granger causality analysis of acupuncture effects in mild cognitive impairment patients: an fMRI study," *Evidence-Based Complementary and Alternative Medicine*, vol. 2013, Article ID 127271, 12 pages, 2013.
- [11] L. Bai, M. Zhang, S. Chen et al., "Characterizing acupuncture de qi in mild cognitive impairment: relations with small-world efficiency of functional brain networks," *Evidence-based Complementary and Alternative Medicine*, vol. 2013, Article ID 304804, 8 pages, 2013.
- [12] S. Chen, M. Xu, H. Li et al., "Acupuncture at the Taixi (KI3) acupoint activates cerebral neurons in elderly patients with mild cognitive impairment," *Neural Regeneration Research*, vol. 9, no. 11, pp. 1163–1168, 2014.
- [13] B. Jia, Z. Liu, B. Min et al., "The effects of acupuncture at real or sham acupoints on the intrinsic brain activity in mild cognitive impairment patients," *Evidence-Based Complementary and Alternative Medicine*, vol. 2015, Article ID 529675, 9 pages, 2015.
- [14] Z. Wang, B. Nie, D. Li et al., "Effect of acupuncture in mild cognitive impairment and Alzheimer disease: a functional MRI study," *PLoS One*, vol. 7, no. 8, article e42730, 2012.
- [15] W. Zheng, Z. Su, X. Liu et al., "Modulation of functional activity and connectivity by acupuncture in patients with Alzheimer disease as measured by resting-state fMRI," *PLoS One*, vol. 13, no. 5, article e196933, 2018.

- [16] M. S. Albert, S. T. Dekosky, D. Dickson et al., "The diagnosis of mild cognitive impairment due to Alzheimer's disease: recommendations from the National Institute on Aging-Alzheimer's Association workgroups on diagnostic guidelines for Alzheimer's disease," *Alzheimers & Dementia*, vol. 7, no. 3, pp. 270–279, 2011.
- [17] H. Li, X. Jia, Z. Qi et al., "Altered functional connectivity of the basal nucleus of Meynert in mild cognitive impairment: a resting-state fMRI study," *Frontiers in Aging Neuroscience*, vol. 9, 2017.
- [18] S. Whitfield-Gabrieli and A. Nieto-Castanon, "Conn: a functional connectivity toolbox for correlated and anticorrelated brain networks," *Brain Connectivity*, vol. 2, no. 3, pp. 125–141, 2012.
- [19] Y. Zou, W. Tang, X. Li, M. Xu, and J. Li, "Acupuncture reversible effects on altered default mode network of chronic migraine accompanied with clinical symptom relief," *Neural Plasticity*, vol. 2019, Article ID 5047463, 10 pages, 2019.
- [20] S. A. Schultz, B. A. Gordon, S. Mishra et al., "Widespread distribution of tauopathy in preclinical Alzheimer's disease," *Neurobiology of Aging*, vol. 72, pp. 177–185, 2018.
- [21] M. Montembeault, S. M. Brambati, F. Lamari et al., "Atrophy, metabolism and cognition in the posterior cortical atrophy spectrum based on Alzheimer's disease cerebrospinal fluid biomarkers," *NeuroImage: Clinical*, vol. 20, pp. 1018–1025, 2018.
- [22] X. Wang, Y. Yu, W. Zhao et al., "Altered whole-brain structural covariance of the hippocampal subfields in subcortical vascular mild cognitive impairment and amnesic mild cognitive impairment patients," *Frontiers in Neurology*, vol. 9, p. 342, 2018.
- [23] J. Rasero, C. Alonso-Montes, I. Diez et al., "Group-level progressive alterations in brain connectivity patterns revealed by diffusion-tensor brain networks across severity stages in Alzheimer's disease," *Frontiers in Aging Neuroscience*, vol. 9, p. 215, 2017.
- [24] J. Xue, H. Guo, Y. Gao et al., "Altered directed functional connectivity of the hippocampus in mild cognitive impairment and Alzheimer's disease: a resting-state fMRI study," *Frontiers in Aging Neuroscience*, vol. 11, p. 326, 2019.
- [25] Z. Qi, X. Wu, Z. Wang et al., "Impairment and compensation coexist in amnesic MCI default mode network," *NeuroImage*, vol. 50, no. 1, pp. 48–55, 2010.
- [26] N. Cera, R. Esposito, F. Cieri, and A. Tartaro, "Altered cingulate cortex functional connectivity in normal aging and mild cognitive impairment," *Frontiers in Neuroscience*, vol. 13, p. 857, 2019.
- [27] K. Persson, V. D. Bohbot, N. Bogdanovic, G. Selbaek, A. Braekhus, and K. Engedal, "Finding of increased caudate nucleus in patients with Alzheimer's disease," *Acta Neurologica Scandinavica*, vol. 137, no. 2, pp. 224–232, 2018.
- [28] U. Ghafoor, J. H. Lee, K. S. Hong, S.-S. Park, J. Kim, and H.-R. Yoo, "Effects of acupuncture therapy on MCI patients using functional near-infrared spectroscopy," *Frontiers in Aging Neuroscience*, vol. 11, p. 237, 2019.
- [29] M. C. Jiang, J. Liang, Y. J. Zhang et al., "Effects of acupuncture stimulation of bilateral "Hegu" (LI 4) and "Taichong" (LR 3) on learning-memory ability, hippocampal AP 42 expression and inflammatory cytokines in rats with Alzheimer's disease," *Zhen Ci Yan Jiu*, vol. 41, no. 2, pp. 113–118, 2016.
- [30] Y. Shan, J. J. Wang, Z. Q. Wang et al., "Neuronal specificity of acupuncture in Alzheimer's disease and mild cognitive impairment patients: a functional MRI study," *Evidence-Based Complementary and Alternative Medicine*, vol. 2018, Article ID 7619197, 10 pages, 2018.
- [31] R. L. Buckner, J. R. Andrews-Hanna, and D. L. Schacter, "The brain's default Network," *Annals of the New York Academy of Sciences*, vol. 1124, no. 1, pp. 1–38, 2008.
- [32] A. Maass, S. Landau, S. L. Baker et al., "Comparison of multiple tau-PET measures as biomarkers in aging and Alzheimer's disease," *Neuroimage*, vol. 157, pp. 448–463, 2017.
- [33] K. Li, W. Chan, R. S. Doody, J. Quinn, S. Luo, and the Alzheimer's Disease Neuroimaging Initiative, "Prediction of conversion to Alzheimer's disease with longitudinal measures and time-to-event data," *Journal of Alzheimers Disease*, vol. 58, no. 2, pp. 361–371, 2017.
- [34] J. Cha, H. J. Jo, H. J. Kim et al., "Functional alteration patterns of default mode networks: comparisons of normal aging, amnesic mild cognitive impairment and Alzheimer's disease," *European Journal of Neuroscience*, vol. 37, no. 12, pp. 1916–1924, 2013.
- [35] S. Morbelli, M. Bauckneht, D. Arnaldi et al., "18F-FDG PET diagnostic and prognostic patterns do not overlap in Alzheimer's disease (AD) patients at the mild cognitive impairment (MCI) stage," *European Journal of Nuclear Medicine and Molecular Imaging*, vol. 44, no. 12, pp. 2073–2083, 2017.
- [36] K. Chiotis, L. Saint-Aubert, E. Rodriguez-Vieitez et al., "Longitudinal changes of tau PET imaging in relation to hypometabolism in prodromal and Alzheimer's disease dementia," *Molecular Psychiatry*, vol. 23, no. 7, pp. 1666–1673, 2018.
- [37] H. Li, X. Jia, Z. Qi et al., "Disrupted functional connectivity of Cornu Ammonis subregions in amnesic mild cognitive impairment: a longitudinal resting-state fMRI study," *Frontiers in Human Neuroscience*, vol. 12, 2018.
- [38] M. Bauckneht, A. Chincarini, R. Piva et al., "Metabolic correlates of reserve and resilience in MCI due to Alzheimer's disease (AD)," *Alzheimer's Research & Therapy*, vol. 10, no. 1, p. 35, 2018.
- [39] J. Kukolja, C. M. Thiel, and G. R. Fink, "Cholinergic stimulation enhances neural activity associated with encoding but reduces neural activity associated with retrieval in humans," *Journal of Neuroscience*, vol. 29, no. 25, pp. 8119–8128, 2009.
- [40] C. R. Jack, D. A. Bennett, K. Blennow et al., "NIA-AA Research Framework: Toward a biological definition of Alzheimer's disease," *Alzheimer's & Dementia*, vol. 14, no. 4, pp. 535–562, 2018.

Research Article

Changes in the Fluorescence Tracking of NaV1.6 Protein Expression in a BTBR T+Itpr3tf/J Autistic Mouse Model

Musaad A. Alshammari,^{1,2} Mohammad R. Khan,¹ Fawaz Alasmari ¹,
Abdulaziz O. Alshehri,¹ Rizwan Ali,³ Mohamed Boudjelal,³ Khalid A. Alhosaini,^{1,2}
Abdurahman A. Niazy,^{2,4} and Tahani K. Alshammari ^{1,2}

¹Department of Pharmacology and Toxicology, College of Pharmacy, King Saud University, Saudi Arabia

²Prince Naif Bin Abdulaziz Health Research Center (PNHRC), King Saud University, Saudi Arabia

³Medical Research Core Facilities & Platforms, King Abdullah International Medical Research Center, Saudi Arabia

⁴Department of Oral Medicine and Diagnostic Sciences, College of Dentistry, King Saud University, Saudi Arabia

Correspondence should be addressed to Tahani K. Alshammari; talshammari@ksu.edu.sa

Received 20 September 2019; Revised 28 October 2019; Accepted 6 November 2019; Published 17 December 2019

Guest Editor: Tommaso Schirinzi

Copyright © 2019 Musaad A. Alshammari et al. This is an open access article distributed under the Creative Commons Attribution License, which permits unrestricted use, distribution, and reproduction in any medium, provided the original work is properly cited.

The axon initial segment (AIS), the site of action potential initiation in neurons, is a critical determinant of neuronal excitability. Growing evidence indicates that appropriate recruitment of the AIS macrocomplex is essential for synchronized firing. However, disruption of the AIS structure is linked to the etiology of multiple disorders, including autism spectrum disorder (ASD), a condition characterized by deficits in social communication, stereotyped behaviors, and very limited interests. To date, a complete understanding of the molecular components that underlie the AIS in ASD has remained elusive. In this research, we examined the AIS structure in a BTBR T+Itpr3tf/J mouse model (BTBR), a valid model that exhibits behavioral, electrical, and molecular features of autism, and compared this to the C57BL/6J wild-type control mouse. Using Western blot studies and high-resolution confocal microscopy in the prefrontal frontal cortex (PFC), our data indicate disrupted expression of different isoforms of the voltage-gated sodium channels (NaV) at the AIS, whereas other components of AIS such as ankyrin-G and fibroblast growth factor 14 (FGF14) and contactin-associated protein 1 (Caspr) in BTBR were comparable to those in wild-type control mice. A Western blot assay showed that BTBR mice exhibited a marked increase in different sodium channel isoforms in the PFC compared to wild-type mice. Our results provide potential evidence for previously undescribed mechanisms that may play a role in the pathogenesis of autistic-like phenotypes in BTBR mice.

1. Introduction

Autism spectrum disorder (ASD) refers to a heterogeneous and indistinctly defined neurodevelopmental and neurobehavioral disorder involving deficits in social interaction, impairments in communication, and repetitive stereotyped patterns of behaviors and interests. However, the exact cause of ASD is not yet known. Genetic, epigenetic, or environmental factors are thought to underlie the pathogenesis of ASD and are currently being investigated [1]. The use of animal models of ASD will, therefore, provide important knowl-

edge of behavioral phenotypes, underlying pathophysiology, molecular motives, and therapeutic developments [1, 2].

Phenotypic variations of this disorder have been identified in several mouse models parallel to the different mutations present in human ASD, including pharmacologically induced mice, valproic acid-induced mice, Shank3B mutant mice, and BTBR T+Itpr3tf/J (BTBR). Following the discovery of an association between prenatal exposure to valproic acid (VPA) and an elevated risk of ASD, the VPA-induced model has been utilized preclinically as an ASD model [3]. Conversely, SHANK3 mutations are highly prevalent in ASD

patients, and the Shank3B mouse model has been extensively studied. In molecular terms, these mice exhibit deficits in neurotransmission, synaptic plasticity, and neuronal wiring. Behaviorally, they display core features of autistic-like behavior such as compulsive stereotyped repetitive behavior and reduced sociability [4]. In addition to the pharmacologically induced VPA model and the Shank3B genetic model, the BTBR inbred mouse strain is another valid model of ASD that has been used to represent idiopathic autism. The BTBR model displays various genetic, neuroanatomic, and molecular irregularities [5], including altered neurotrophic brain-derived factor (BDNF), the absence of the corpus callosum, and an imbalance in the excitatory/inhibitory (E/I) ratio [6]. Furthermore, the BTBR exhibits three unique and vigorous behavioral features that characterize ASD: deficits in social communication among both the young and adults, an uncommon ultrasonic utterance in newborns, and recurring fixed grooming behaviors [7–10]. Neuroimaging studies also indicate that altered neuronal activation and cognitive capacity evident in the BTBR mouse model may indicate a decreased cerebral blood flow and metabolism of cerebral oxygen [11]. These factors suggest that BTBR is a valid pre-clinical model that can be used to investigate the pathology of ASD.

Previously, it has been suggested that the developmental deregulation of neuronal networks due to postnatal events, including cell differentiation, synaptic formation, and plasticity, promotes autistic behavior in humans [12–15]. However, our understanding of the molecular neurobiological mechanisms that underlie ASD is far from complete [16].

The axon initial segment (AIS) is a very small subcellular structure that originates at a transient length from the neuronal soma immediately after the axon hillock [17]. It is enriched with scaffold proteins and voltage-gated sodium channels (NaV). It has been shown that different isoforms of NaV type 1 α subunits (NaV1) are concentrated in the AIS [18, 19]. This provides an increased flow rate of sodium ions (Na^+) and a decreased action potential threshold [20]. NaV channels are distributed differentially at the AIS; for example, the NaV1.6 is localized in the distal part of the AIS, whereas the NaV1.2 is located at the proximal part of the AIS [21]. Altered structure and/or function of NaV1 α subunits in the AIS can also result in severe CNS disabilities. For instance, it has been found that missense alterations in the gene that encodes the NaV1.1 (SCN1A) may lead to serious severe epilepsy in infants due to imperfections at the level of the AIS [22]. Similarly, mutations in NaV1.2 (SCN2A) and NaV β 1 (SCN1B) can lead to generalized epilepsies [23, 24]. Increased levels of expression of the NaV1.6 and ankyrin-G have also been reported at the AIS in an epileptic animal model [25]. Any alteration in intrinsic membrane proteins at the AIS might also aggravate the pathophysiological process of Angelman syndrome in a mouse model [26]. Notably, mutations and dysfunctions in genes encoding sodium channel isoforms are risk factors for ASD [27, 28].

Ankyrin-G protein has a significant physiological role in modulating the structure and function of ion channels in different types of cells [29]. The cytoskeletal scaffold protein ankyrin-G is a master organizer of membrane proteins in

many types of cells [30]. Ankyrin-G (ANK3) has a pivotal role in ion channel targeting within neuronal populations [31]. In neurons, ankyrin-G is restricted to the AIS [32]. In vitro studies have shown that AIS proteins and ion channels not anchored by ankyrin-G are removed from the membrane by endocytosis [33]. Thus, the clustering of AIS membrane proteins depends on ankyrin-G [34]. Indeed, a lack of ankyrin-G expression in mice disrupts many accessory proteins clustering at the AIS, such as NaV channels [35, 36]. Therefore, all the AIS proteins are anchored directly or indirectly to the scaffold made of the cytoskeletal network, and as a result, ankyrin-G organizes the subcellular polarity of these protein molecules [37]. Genome-wide studies have also identified links between mutations in the gene encoding ankyrin-G, ANK3 gene, and ASD [38–41]. This implies that an alteration in AIS components is a molecular signature in the pathophysiology of ASD.

Abundant evidence has demonstrated that secreted fibroblast growth factors and their FGF tyrosine-kinase receptors (FGFRs) are essential in proper brain development, and for that reason, it is implicated in the pathology of various brain disorders. Secreted FGF2 is considered to be an indicator of allostatic load. It plays several roles in cell proliferation, differentiation, growth, survival, and angiogenesis [42, 43]. In a recent study, the level of FGF2 was reduced in the serum of ASD patients [44]. However, whether other nonsecreted members of the same gene family play a role in this process is not completely understood. In contrast to secreted FGFs, FGF14 belongs to the intracellular FGF group (iFGF) iFGF11 subfamily. This set of FGF members does not act through FGFRs [45, 46]. However, iFGFs control neuronal excitability and synaptic transmission by interacting intracellularly with the carboxy-terminal tail of NaV channels, axonal trafficking proteins (MAP kinase scaffolding protein, IB2 (MAPK8IP2)), and microtubules [47]. FGF14 is found in a range of neuronal tissues and present in gradient form in the AIS of the cultured hippocampal neurons [46]. It has been found to interact with NaV1.1, NaV1.2, and NaV1.6 channels directly via NaV C-termini [46, 48, 49]. Moreover, selected deletion of FGF14 has been implicated in deficits in neuronal excitability [50], immature dentate gyrus endophenotypes [51], and cognitive functions [52].

Although behavioral phenotypes of BTBR as an ASD animal model are well documented, at the molecular level, there are gaps in our knowledge [6, 7, 53–55], especially regarding the AIS structure. In this study, we examined different components of AIS in the prefrontal cortex brain region in the BTBR mouse model using high-resolution confocal imaging, image analysis, and Western blot studies. Our findings provide clear insights into the neuroaxonal structure and improve our understanding of the mechanisms of ASD.

2. Material and Methods

2.1. Animals. BTBR and C57BL/6J (wild-type) (obtained from Jackson Laboratory, Bar Harbor, ME, USA) male mice were maintained through an inbred background of backcrossing to littermate mating. Adult male mice at 2–4 months of age were used in this study. They were maintained at 25

$\pm 2^{\circ}\text{C}$ in a 12 h light/dark cycle, housed in a hygienic environment, and fed with a Purina standard rodent chow diet (Grain Silos and Flour Mills Organization, Riyadh, Saudi Arabia). The mice were housed $n \leq 4-6$ per cage and provided with water *ad libitum*. We utilized 4-6 per group. All experimental procedures were performed in accordance with the guidelines of the King Saud University Institutional Research Ethics Committee (REC).

2.2. Preparation of Brain Sections. Preparation and staining of mouse brain sections were previously described in [56]. In brief, the mice were deeply anesthetized with 10:1 mixture of ketamine 50 mg/ml (Tekam) and xylazine 20 mg/ml (Seton) (dose 0.1 ml/10 gm i.p.) diluted in 1X phosphate-buffered saline (PBS, pH = 7.4) (1X PBS) and then briefly perfused intracardially (flow rate: 8-10 ml/min for 2-5 min) with 1X PBS. This was followed by 10 min of 4% paraformaldehyde freshly prepared (Sigma-Aldrich) or commercially available 4% formaldehyde (a dilution of 37% formaldehyde solution, Sigma-Aldrich, in 1X PBS); all solutions were adjusted to pH 7.4. To ensure complete tissue fixation, brains were removed carefully and postfixed into the same fixative for 1 h at 4°C and then cryopreserved in 20-30% sucrose/PBS at 4°C in preparation for sectioning. Brains were then embedded in OCT compound (Tissue-Tek[®], Ted Pella, Inc.) and sectioned sagittally into 14-20 μm thick slices at -20°C using a Leica CM3050 S cryostat (Leica Microsystems). They were then mounted on glass slides (Fisher Scientific) and stored at -80°C for further use in cresyl and immunofluorescence studies. The second group of brains was gently dissected to isolate the frontal cortex according to the mouse brain atlas [57], and the samples were stored at -80°C for a Western blotting assay.

2.3. Immunofluorescence. Sagittal brain sections were washed with 1X PBS, incubated with a permeabilizing agent (1X Triton, 0.5X Tween in PBS, or -20°C acetone), then washed extensively with 1X PBS, and incubated with 5% normal goat serum NGS (Sigma-Aldrich) in 1X TBS containing 0.3% Triton X-100 for 1 h. This was followed by overnight incubation at 4°C with primary antibodies in 3% bovine serum albumin (BSA, Sigma-Aldrich) and 1X PBS containing 0.1% Tween 20. The primary antibodies used were mouse anti-FGF14 (1:300, NeuroMab, catalog number 75-096), mouse anti-ankyrin-G (1:1000, NeuroMab, catalog number 75-146), guinea pig anti-NeuN (1:750, Synaptic System, catalog number 266 004), mouse anti-NaV1.1 (1:500, NeuroMab, catalog number 75-023), mouse anti-NaV1.2 (1:300, NeuroMab, catalog number 75-024), mouse anti-NaV1.6 (1:300, NeuroMab, catalog number 75-026), mouse anti-Caspr (1:500, NeuroMab, catalog number 75-001), and mouse anti-PanNaV1 (1:300, NeuroMab, catalog number 75-405). After 12 hours of incubation, the sections were washed with 1X PBS and then incubated with appropriate secondary antibodies (1:250, Invitrogen) for 1 h in a 1X PBS solution containing 3% BSA and 0.1% Tween 20. Following incubation with secondary antibodies, the tissue was washed five more times with 1X PBS buffer solution. Finally, the glass slides were placed in an oven at $30-32^{\circ}\text{C}$ for

10-15 min to dry and then coverslipped using Fisherfinest[®] Premium Cover Glass (Fisher Scientific) with ProLong[®] Gold antifade or ProLong[®] Gold antifade mountant with DAPI reagents (Life Technologies, catalog number P36941).

2.4. Confocal Microscopy. Confocal images were acquired using a Zeiss LSM-780 confocal microscope with a Plan Apochromat (63x/1.46 oil) objective. Multitrack acquisition was performed with excitation lines at 488 nm for Alexa 488, 543 nm for Alexa 568/594, and 633 nm for Alexa 633. Z-series stack confocal images were taken at fixed intervals with the same pinhole setting for all the three channels; the frame size was 1024×1024 pixels. Laser intensity and gain were kept constant for all the experimental groups.

2.5. Image Acquisition and Analysis. All confocal images were analyzed using ImageJ (NIH, USA, <http://imagej.nih.gov/ij>). For soma fluorescence intensity analysis, Z-stacks of confocal images were sum-projected, an ROI corresponding to soma was highlighted using an intensity threshold method, and mean fluorescence intensity was quantified. Quantification of the fluorescence intensities of AIS staining was performed using a method previously described in [47]. In brief, the fluorescence intensity of the AIS was analyzed by drawing a segmented line of 6 pixels in width along the AIS, starting from the soma and using anti-ankyrin-G or FGF14 staining as a marker of AIS location on the overlay image.

2.6. Western Blot. Western immunoblotting was performed as previously described in [58]. This involved homogenizing 50 mg of PFC from the brain tissues of BTBR and wild-type mice ($n = 4-5$ mice per group) in 0.32 M sucrose solution in the presence of protease and phosphatase inhibitors. For the Western blot, protein concentrations of samples from brain tissue homogenate were measured using a NanoDrop[™] 8000 Spectrophotometer (Thermo Fisher Scientific), then prepared with 4X sodium dodecyl sulfate (SDS) and tris(2-carboxyethyl)phosphine (TCEP) (1:20), denatured for 10 min at 95°C , and then ran on 7.5% SDS-PAGE gel. The proteins were electrophoretically transferred from a gel onto a nitrocellulose membrane. Membranes were then blocked with 5% nonfat dry milk in TBS-T for 30 min and probed with the following primary antibodies in a blocking solution: anti-PanNaV1 (1:500, NeuroMab), anti-NaV1.1 (1:500, NeuroMab), anti-NaV1.2 (1:500, NeuroMab), anti-NaV1.6 (1:500, NeuroMab), mouse anti-ankyrin-G (1:500, NeuroMab), mouse anti-FGF14 (1:500, NeuroMab), and anti-Caspr (1:500, NeuroMab). This was followed by treatment with horseradish peroxidase-conjugated secondary antibodies and ECL Western blotting detection reagents. The signals were detected and measured with a luminescent image analyzer (ChemiDoc[™] MP, Bio-Rad). ImageJ was used to measure the intensity of the proteins of interest.

2.7. Statistical Analysis. The data were presented as the mean \pm standard error of the mean (SEM). The statistical significance of observed differences among groups was determined using two-sample Student's *t*-test or the corresponding nonparametric test, Mann-Whitney rank sum, based on the distribution of the samples underlying the populations. A

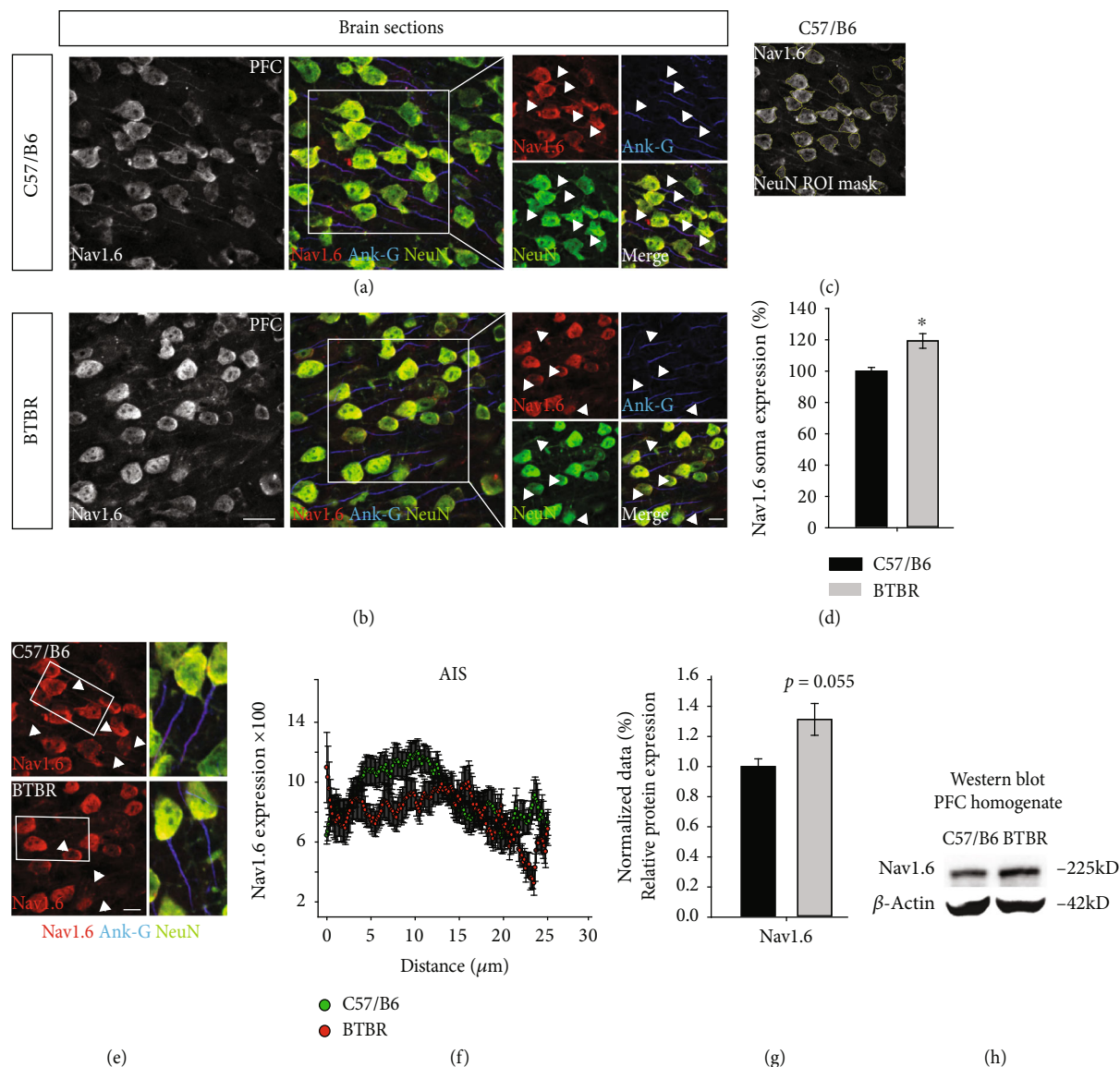


FIGURE 1: Altered NaV1.6 expression and distribution in the PFC of the BTBR mouse model. (a, b) The red channel represents confocal images of NaV1.6 (antisodium channel), the blue channel represents ankyrin-G (Ank-G), and the green channel represents NeuN immunofluorescence in the PFC of C57BL/6J and BTBR mice. (c) The mask ROI was used to detect NaV1.6 expression within the NeuN soma. (d) The quantification of NaV1.6 immunofluorescence expression within the soma of C57BL/6J and BTBR mice. $n = 3$ mice per group. (e) Representative confocal images of NaV1.6 (red) at the AIS in C57BL/6J and BTBR mice. (f) AIS tracking analysis of NaV1.6 in C57BL/6J and BTBR mice. $n = 3$ mice per group. (g) NaV1.6 protein levels in PFC lysates from C57BL/6J and BTBR mice and the Western blot bands. The protein expression was normalized with β -actin. $n = 4-5$ mice per group. Data represent mean \pm SEM; statistical differences were assessed using Student's t -test ($*p < 0.05$). Scale bars represent $20 \mu\text{m}$ in (b) and $10 \mu\text{m}$ in the white box (zoom images in (b)) and (e).

level of $p < 0.05$ was considered statistically significant. Statistical analysis was performed using InStat, GraphPad Software, Inc., and SigmaPlot 12 (Systat Software, San Jose, CA). The data were tabulated in Microsoft Excel.

3. Results

3.1. Voltage-Gated Sodium Channel (NaV1.6, NaV1.2, and NaV1.1) Immunoreactivity and Expression in the BTBR Mouse PFC. We then examined NaV1.6 in the PFC—layer III—of BTBR, where immunofluorescence studies indicated

that fluorescence expression in the soma of BTBR significantly increased compared to that of the wild-type mice (Figure 1(a)–(d), $119.25\% \pm 4.66$ in BTBR vs. $100\% \pm 2.33$ in wild type, $p < 0.05$, $n = 3$). Similarly, the Western blot analysis of the total protein homogenate of PFC indicated that NaV1.6 protein expression was elevated, albeit not significantly, in BTBR compared to the wild-type mice (Figure 1(g) and (h), 1.31 ± 0.105 in BTBR vs. 1.00 ± 0.051 in wild type, $p = 0.056$, $n = 4-5$). In the fluorescence tracking of axonal expression using ankyrin-G as an axonal marker, we found an aberrant pattern of distribution through the

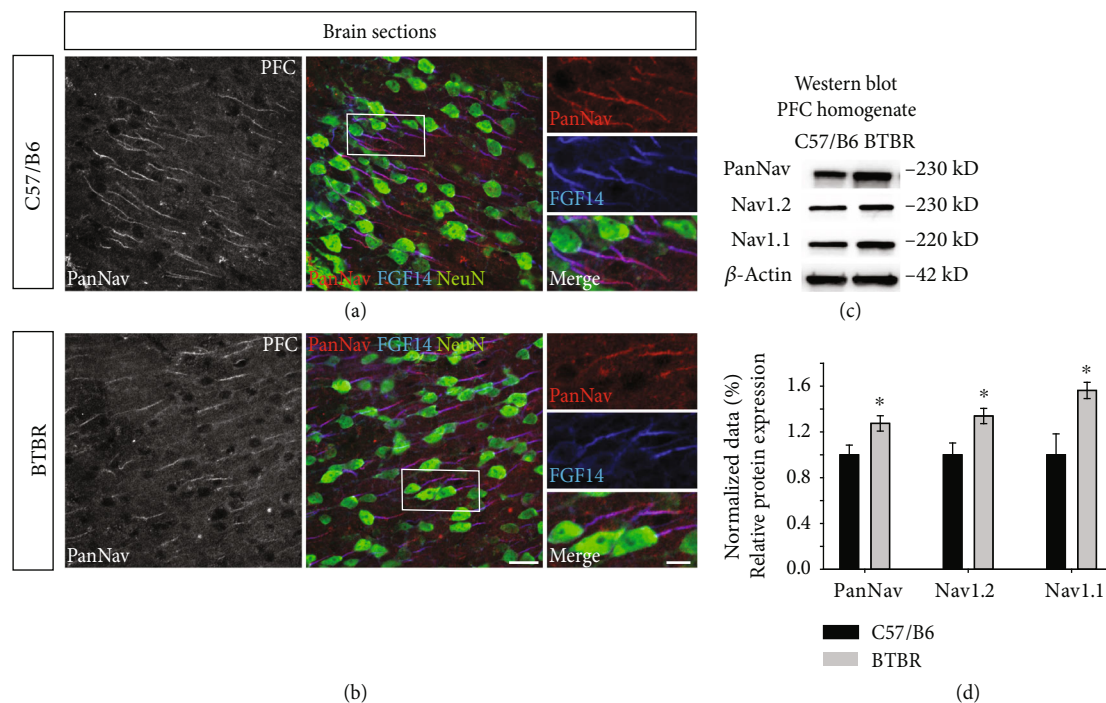


FIGURE 2: PanNaV, NaV1.1, and NaV1.2 expression in the PFC of the BTBR mouse model. (a, b) High-resolution confocal images where the red channel represents confocal images of PanNaV, the blue channel represents FGF14, and the green channel represents NeuN immunofluorescence in the PFC of C57BL/6J and BTBR mice. (c) Western blot analysis for PanNaV, NaV1.1, and NaV1.2 was performed on PFC homogenate and quantified. (d) The upregulation of PanNaV, NaV1.1, and NaV1.2. The protein expression was normalized with β -actin. Data represent mean \pm SEM; statistical differences were assessed using Student's *t*-test ($*p < 0.05$, $n = 4-5$ mice per group). Scale bars represent 20 μ m in (b) and 10 μ m in zoom images in (b).

AIS structure (Figure 1(e) and (f)). Although it is difficult to anticipate the consequences of these molecular changes since the cortical circuitry is fairly complex [59], these findings indicate that NaV1.6 functionality could be altered in BTBR mice. This led us to investigate other isoforms of NaV1 α subunits. Thus, we examined NaV1.1 and NaV1.2 using the Western blot and found that, in the PFC of BTBR, both isoforms were elevated significantly compared to the wild type controls. In support of these findings, the expression of PanNaV increased in the PFC of BTBR compared to wild-type mice (Figure 2(c) and (d), 1.27 ± 0.067 in BTBR vs. 1.00 ± 0.085 in wild type, $p < 0.05$, for PanNaV; 1.33 ± 0.066 in BTBR vs. 1.00 ± 0.103 in wild type, $p < 0.05$, for NaV1.2; and 1.56 ± 0.071 in BTBR vs. 1.00 ± 0.183 in wild type, $p < 0.05$, for NaV1.1; $n = 4-5$ per group). These results showed a disruption in NaV1.6, NaV1.2, and NaV1.1 expressions, which could be implicated in altered firing and the synaptic wiring in ASD.

3.2. Ankyrin-G Expression in the BTBR Mouse PFC. To explore the expression of the AIS scaffold protein ankyrin-G, we examined ankyrin-G in the soma of matured neurons in the PFC of BTBR and found that immunostaining appeared to have not been altered (Figure 3(a)–(d), $97.31\% \pm 3.203$ in BTBR vs. $100\% \pm 3.573$ in wild type, $p = 0.512$, $n = 3$ per group). To validate this finding, we examined the PFC total protein homogenate expression, consistent with immunofluorescence studies from layer III, and found that

ankyrin-G was unchanged in the BTBR mouse model compared to the wild-type mice (Figure 3(g) and (h), $1.00\% \pm 0.206$ in BTBR vs. 1.00 ± 0.158 in wild type, $p = 0.991$, $n = 4-5$ per group). The tracking of the AIS structure indicated that the ankyrin-G expression pattern is upregulated in the proximal part of the AIS (Figure 3(e) and (f)). These findings suggest that the cytoskeleton structure in BTBR mice might be unaffected.

3.3. Fibroblast Growth Factor 14 (FGF14) Expression in BTBR. Because most NaV1 α isoforms were disrupted, we continued with our studies and examined FGF14, a key regulator of NaV channels. The immunohistochemical staining examinations indicated that FGF14 expression was comparable in both types of mice (Figure 4(a) and (b)). These results were confirmed by Western blot analysis (Figure 4(d) and (e), 1.23 ± 0.332 in BTBR vs. 1.00 ± 0.499 in wild type, $p = 0.705$, $n = 4-5$ per group). The tracking of the AIS structure indicated an increase in FGF14 expression in the distal part of PFC neurons (Figure 4(c)). These results suggest that the increase in NaV1.6 expression in the AIS is accompanied by an increase in FGF14 in AIS.

3.4. Examination of the Node of Ranvier in the BTBR Mouse Model. We then examined a vital component of the node of Ranvier by analyzing the expression of Caspr in the PFC of BTBR mice. The Caspr immunoreactivity analysis of the PFC homogenate revealed nonsignificant Caspr expression

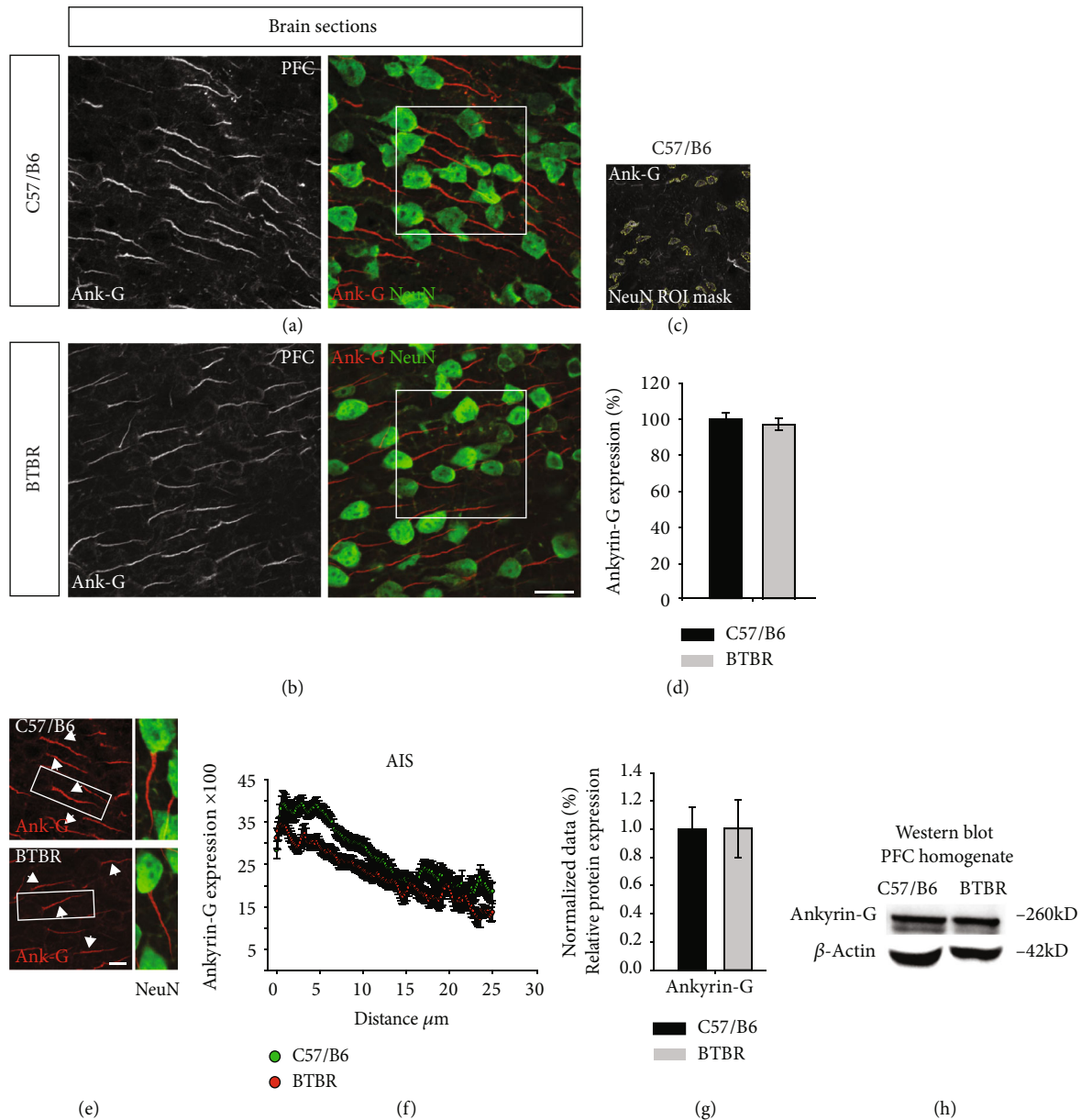


FIGURE 3: Ankyrin-G expression in the PFC of the BTBR mouse model. (a, b) High-resolution confocal images acquired from the PFC of C57BL/6J and BTBR: ankyrin-G (grey and red) and NeuN (green). (c) The ROI mask used to quantify ankyrin-G. (d) The quantification of ankyrin-G immunofluorescence. $n = 3$ mice per group. (e) Representative high-resolution confocal images of AIS in C57BL/6J and BTBR mice. (f) The AIS tracking analysis of ankyrin-G in C57BL/6J and BTBR mice. $n = 3$ mice per group. (g) Ankyrin-G protein levels in PFC lysates from C57BL/6J and BTBR mice and the Western blot bands. The protein expression was normalized with β -actin. $n = 4-5$ mice per group. Data represent mean \pm SEM; statistical differences were assessed using Student's t -test ($*p < 0.05$). Scale bars represent $20 \mu\text{m}$ in (b) and $10 \mu\text{m}$ in (e).

in BTBR compared to wild-type mice (Figure 5(c) and (d), 1.12 ± 0.087 in BTBR vs. 1.00 ± 0.127 in wild type, $p = 0.453$, $n = 4-5$ per group). These results suggest that the node of Ranvier may be unaffected in the BTBR mouse model.

4. Discussion

Although studies have shown that ASD is characterized by a reduced excitation and inhibition ratio, examination of the AIS molecules may reveal the possible mechanism and etiol-

ogy of ASD and therapeutic targets for its improvement [60]. The AIS-specific proteins play an essential role in the physiology and the function of neuronal populations [61].

In the current study, our aim was to ascertain whether the disruption of AIS accessory proteins is observed in BTBR mice, as this feature could be a molecular signature of ASD pathogenesis. Our results showed that the expression of different NaV1 α isoforms was reduced and that the AIS accessory scaffold protein ankyrin-G was not altered. Additionally, FGF14 expression was comparable in BTBR

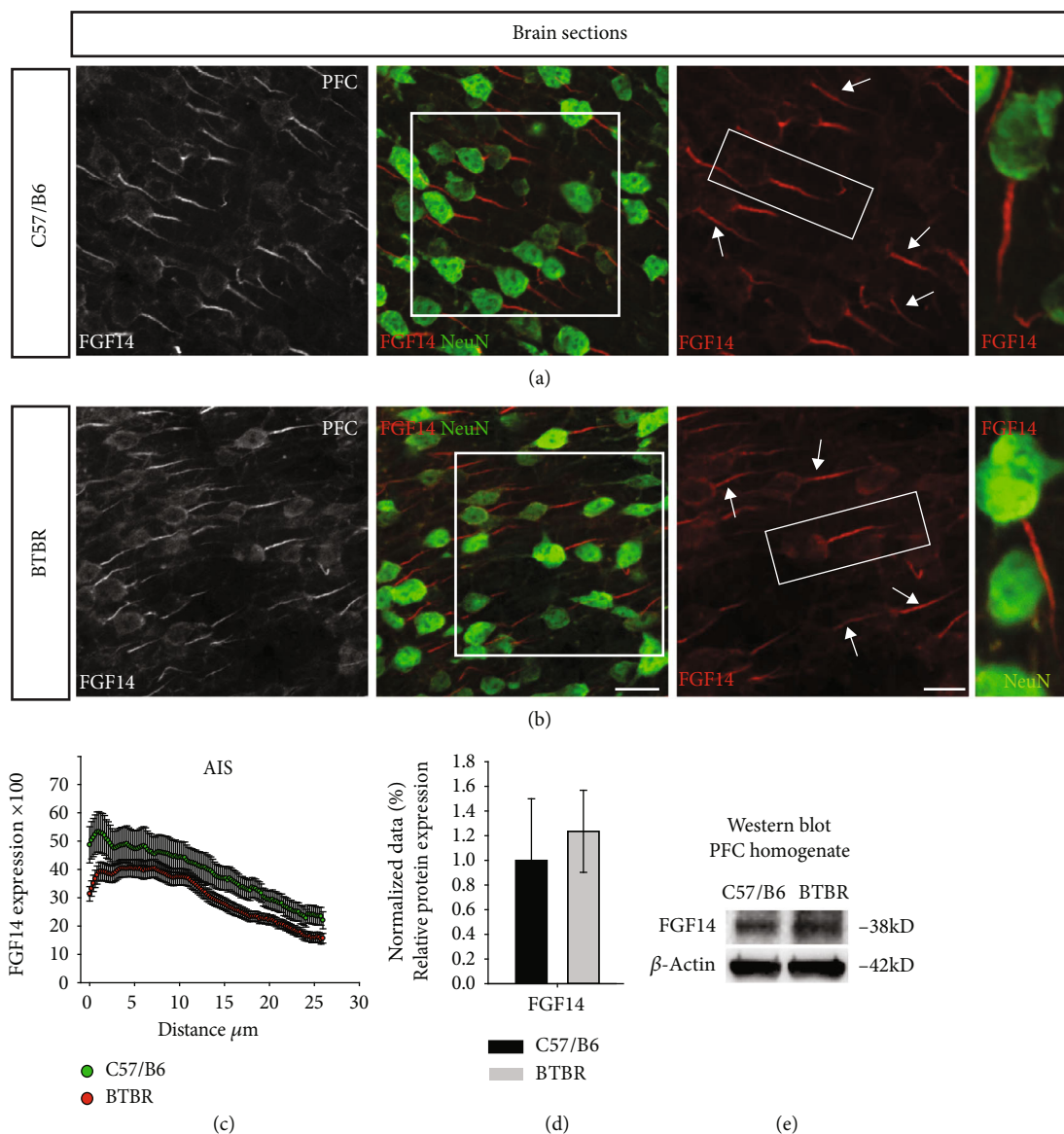


FIGURE 4: FGF14 expression in the AIS of the BTBR mouse PFC. (a, b) Representative confocal images of FGF14 (grey and red) and NeuN (green) from the PFC of C57BL/6J and BTBR; FGF14 (grey and red) and NeuN (green) arrows represent AIS. (c) The expression of FGF14 across the AIS. $n = 3$ mice per group. (d, e) Immunoblot detection of FGF14 in the PFC homogenate from C57BL/6J and BTBR and the quantitative Western blot analysis. $n = 4-5$ mice per group. Data represent mean \pm SEM; statistical differences were assessed using Student's t -test ($*p < 0.05$). Scale bars represent $20 \mu\text{m}$ in (b).

and wild-type controls. Besides, the expression level of Caspr, a key molecule of the node of Ranvier, was not altered in BTBR compared to the wild-type controls, indicating that neuronal firing could be affected in this model.

The BTBR was derived from the inbred strain Black and Tan Brachyury (BTBR), which carries mutations in a couple of genes including *Itr3* (inositol 1,4,5-trisphosphate receptor 3) and *T* (brachyury) genes [62]. This strain has exhibited most of the behavioral disabilities observed in ASD. Therefore, these mice could result as a valid model in investigating the role played by the structural proteins of AIS in the cortical tissue of the autistic brain.

In our experimental setup, we conducted the immunofluorescence studies in layer III of the prefrontal cor-

tex, while the Western blotting analysis was performed on the whole homogenate of the prefrontal cortex. This route was taken because, based on our experimental experience, most AIS were condensed and easily detected in layer III of the prefrontal cortex. Additionally, it was reported that within the cortex, the deep III layer was characterized by the existence of condensed axonal projections [63].

There is a high degree of enrichment and subcellular polarity for NaV channels at the AIS, which facilitates high Na^+ current density and a low action potential threshold [20]. NaV1.6 is the major NaV1 α subunit, which is expressed either with NaV1.1/NaV1.2 or alone in different subdomains of AIS in different neurons [21, 64, 65].

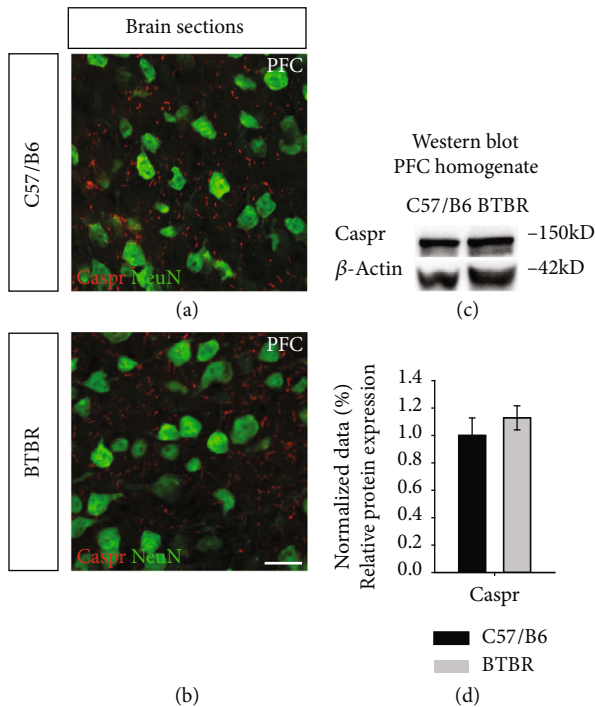


FIGURE 5: Caspr expression in the PFC of the BTBR mouse model. (a, b) Representative high-resolution confocal images of the PFC of BTBR and C57BL/6 control mice immunostained for Caspr (red) in combination with NeuN (green). (c) Immunoblot detection of Caspr in the PFC homogenate from C57BL/6J and BTBR mice. (d) The quantitative Western blot analysis normalized with β -actin. $n = 4-5$ mice per group. Data represent mean \pm SEM; statistical differences were assessed using Student's t -test. Scale bars represent $20 \mu\text{m}$ in (b).

Nav1.6 is a prime voltage-gated sodium channel in the brain [66]. The AIS is enriched by this isoform, which enables it to modulate the initiation of action potentials [67]. It is also concentrated at the nodes of Ranvier and other subcellular structures, including the soma and the dendrites [66].

Nav1.6 plays a critical role in the generation of persistent and resurgent cellular currents. Thus, altered expression in this protein could have serious consequences [66]. Mutations in genes encoding different isoforms of sodium channels will result in ASD in humans, and different single-nucleotide polymorphisms (SNPs) have been found to be associated with ASD [68]. In this research, we found that the expression of Nav1.6 increased in the soma and the AIS, suggesting that both persistent and resurgent currents could be altered. It is quite difficult to relate alterations in some sodium channel isoforms to system-level dysfunction of neural wiring. It is for future studies to characterize the axonal structure of inhibitory interneurons and analyze the functional characteristics of neuronal populations using electrophysiological recordings.

The accumulation of Nav1.2 at the proximal AIS promotes action potential propagation to the soma and sets the action potential threshold of the somatodendritic region of the neuron. The Nav1.2 channel may control action poten-

tial backpropagation because of its high density at the proximal AIS. Our findings demonstrated an alteration in the expression of Nav1.2 channels in the AIS of the cortical neurons of BTBR mice, suggesting that this may contribute to the functional alterations observed in ASD [21]. Mutations in Nav1.2 may cause common epilepsies [23]. Similarly, a recent genomic study indicates that mutations in the Nav1.2 gene (SCN2A) in ASD are a consistent finding and may be considered an ASD risk factor [27]. Small changes in the density of Nav channels could change the excitability of a neuron, and reduced integrity of the AIS barrier would be expected to affect the normal distribution of axonal and somatodendritic proteins in the cell [34]. The increased expression of Nav1.2 observed in our studies may not necessarily indicate that more excitation is taking place. It may be a compensatory mechanism as the increased production of protein could be attributed to either improper positions, lack of function, or even a deficit in maintenance. Importantly, alterations of the functioning of Nav channels at the AIS may cause severe CNS dysfunction. A recent study indicated that variants in the Nav1.2-encoding gene lead to a gain in function and an increase in neuronal excitability: these result in an imbalance in the excitation/inhibition (E/I) ratio and seizures [27].

In addition to altered Nav1.2 and Nav1.6, our analysis indicated an increase in Nav1.1, suggesting that the inhibitory current is also altered [69]. Increased Nav1.1 was previously reported in the dorsal root ganglion following nerve injury, indicating that it could be a mechanism in modulating neuropathic pain [70]. The Nav1.1 (SCN1A) locus was identified as indicating susceptibility to autism during genome-wide association studies [71, 72]. The mutations in the Nav1.1 gene were identified in individuals with familial autism by genome sequencing [68]. The missense mutations in the gene encoding Nav1.1 can lead to severe epilepsy in infants due to defects at the level of the AIS [22]. It has also been reported that heterozygous mice with a missense mutation in the Nav1.1 channel develop hyperactivity, autistic traits, cognitive deficits, anxiety, social interaction deficits, and excessive stereotyped behaviors. These cognitive and behavioral deficits are caused by reduced action potential firing in GABAergic interneurons [73].

The molecular mechanisms that modulate the composite configuration of the Nav1 α subunit in the AIS are complex. An altered excitation over inhibition ratio is a unified hypothesis underlying ASD and related disorders. Strong evidence suggests that an increase in the ratio between excitation and inhibition, leading to the hyperexcitability of cortical circuits, is implicated in ASD. This circuitry imbalance leads to a deficit in learning and cognitive capacity as well as sociability [60].

We then moved on to examine ankyrin-G. The cytoskeletal adaptor protein ankyrin-G has a binding site for Nav1 α subunits. Therefore, we investigated whether BTBR mice would also exhibit altered Ank-G expression. We found that ankyrin-G immunostaining in the mature neurons of BTBR mice was comparable to that of wild-type mice. It has previously been reported that the cytoskeletal scaffold protein ankyrin-G is a principal architect of membrane proteins

and subcellular polarity in different types of cells [32, 74–76]. In neurons, ankyrin-G is concentrated on the AIS and NaV channels that bind to ankyrin-G [32, 33]. The silencing of ankyrin-G gene expression by RNA interference in mice interferes with the assembly of NaV channels at the AIS [35, 36]. This suggests that mutations harbored in BTBR mice do not affect the initial steps in AIS assembly; however, they do affect the localization and recruitment of subsequent proteins, including sodium channels, at the AIS [31].

In this research, we found that FGF14 is prominently expressed in the AIS of mature cortical neurons. FGF14 and NaV immunostaining was disrupted in the AIS of cortical neurons in BTBR mice, indicating a regulatory interaction among these proteins. Similarly, a recent study showed that FGF14 plays a regulatory role in the localization of NaV1 α subunits in the Purkinje neuron in the AIS, and the expression of NaV1.6 was found to decrease over the length of the AIS of the Purkinje neuron [77].

The node of Ranvier has clear links to demyelinating diseases [78, 79]. It also has a common molecular organization to the AIS, probably because the node of Ranvier evolved from the AIS [34]. The genes that are translated into Caspr, which are enriched at the node of Ranvier, have been classified as a prime locus of susceptibility for autism spectrum disorders, bipolar disorder, and mental retardation [80, 81].

The mutation in the inositol triphosphate receptor is a key component in dysfunctional phenotypes observed in BTBR. Inositol triphosphate modulates various physiological processes by promoting cellular calcium signals [82]. A mutation in the inositol triphosphate receptor in BTBR might be responsible for the deficit in the trafficking of AIS components, leading to the molecular phenotypes observed in this study. In line with this evidence, a previous study has implicated Wnt/Ryk calcium signaling in the regulation of axonal outgrowth, axonal development, and guidance [83].

5. Conclusion and Future Directions

These results provide novel insights into the etiology of ASD and favor the notion that alterations in architectural proteins in the AIS of growing neurons are significant in the development of the autistic brain in BTBR mice. Future studies might be needed to address whether other components of AIS such as FGF-13, FGF-12, neurofascin, and β IV spectrin are altered in BTBR mice. It would also be useful to shed light on the functionality of voltage-gated sodium channel α subunits in the cortical region of the ASD model and characterize their electrophysiological features. This would help determine the functional architecture of AIS and establish neuronal polarity.

Data Availability

The datasets used and/or analyzed during the current study are available from the corresponding author on reasonable request.

Conflicts of Interest

The authors declare no conflict of interest or affiliations that may affect the objectivity of this review.

Authors' Contributions

M.A.A., M.R.K., and T.K.A. contributed to the design of the work, acquisition, analysis, and interpretation of the data and drafted the manuscript. M.A.A. performed tissue cryo-sectioning, immunohistochemistry, confocal imaging, and image analysis. M.A.A. and M.R.K. prepared and perfused mouse tissue and supervised and maintained the animal colony and animal genotyping in the laboratory. M.R.K. and F.F.A. performed the Western blot. A.O.A. maintained the animal colony and conducted animal genotyping in K.A.A.'s laboratory where the IHC experiments were performed by K.A.A. R.A. and M.B. contributed to the editing of the manuscript, and confocal imaging was performed in their laboratory. A.A.N. contributed to the editing of the manuscript.

Acknowledgments

The authors extend their appreciation to the Deanship of Scientific Research at King Saud University for funding this work through Project No. R17-02-17.

References

- [1] L. R. Fenlon, S. Liu, I. Gobius et al., "Formation of functional areas in the cerebral cortex is disrupted in a mouse model of autism spectrum disorder," *Neural Development*, vol. 10, no. 1, p. 10, 2015.
- [2] H. Wei, Y. Ma, C. Ding et al., "Reduced glutamate release in adult BTBR mouse model of autism spectrum disorder," *Neurochemical Research*, vol. 41, no. 11, pp. 3129–3137, 2016.
- [3] A. Ornoy, L. Weinstein-Fudim, and Z. Ergaz, "Prevention or amelioration of autism-like symptoms in animal models: will it bring us closer to treating human ASD?," *International Journal of Molecular Sciences*, vol. 20, no. 5, article 1074, 2019.
- [4] M. A. Rhine, J. M. Parrott, M. N. Schultz, T. M. Kazdoba, and J. N. Crawley, "Hypothesis-driven investigations of diverse pharmacological targets in two mouse models of autism," *Autism Research*, vol. 12, no. 3, pp. 401–421, 2019.
- [5] K. Z. Meyza and D. C. Blanchard, "The BTBR mouse model of idiopathic autism – current view on mechanisms," *Neuroscience & Biobehavioral Reviews*, vol. 76, Part A, pp. 99–110, 2017.
- [6] C. M. Daimon, J. M. Jasien, W. H. Wood et al., "Hippocampal transcriptomic and proteomic alterations in the BTBR mouse model of autism spectrum disorder," *Frontiers in Physiology*, vol. 6, p. 324, 2015.
- [7] H. G. McFarlane, G. K. Kusek, M. Yang, J. L. Phoenix, V. J. Bolivar, and J. N. Crawley, "Autism-like behavioral phenotypes in BTBR T+tf/J mice," *Genes, Brain and Behavior*, vol. 7, no. 2, pp. 152–163, 2008.
- [8] R. L. H. Pobbe, B. L. Pearson, E. B. Defensor, V. J. Bolivar, D. C. Blanchard, and R. J. Blanchard, "Expression of social behaviors of C57BL/6J versus BTBR inbred mouse strains in

- the visible burrow system,” *Behavioural Brain Research*, vol. 214, no. 2, pp. 443–449, 2010.
- [9] M. L. Scattoni, S. U. Gandhi, L. Ricceri, and J. N. Crawley, “Unusual repertoire of vocalizations in the BTBR T+tf/J mouse model of autism,” *PLoS One*, vol. 3, no. 8, article e3067, 2008.
- [10] D. T. Stephenson, S. M. O’Neill, S. Narayan et al., “Histopathologic characterization of the BTBR mouse model of autistic-like behavior reveals selective changes in neurodevelopmental proteins and adult hippocampal neurogenesis,” *Molecular Autism*, vol. 2, no. 1, p. 7, 2011.
- [11] D. Abookasis, D. Lerman, H. Roth, M. Tfilin, and G. Turgeman, “Optically derived metabolic and hemodynamic parameters predict hippocampal neurogenesis in the BTBR mouse model of autism,” *Journal of Biophotonics*, vol. 11, no. 3, article e201600322, 2018.
- [12] A. C. Bender, R. P. Morse, R. C. Scott, G. L. Holmes, and P.-P. Lenck-Santini, “SCN1A mutations in Dravet syndrome: impact of interneuron dysfunction on neural networks and cognitive outcome,” *Epilepsy & Behavior*, vol. 23, no. 3, pp. 177–186, 2012.
- [13] S. Berghs, D. Aggujaro, R. Dirckx Jr. et al., “ β IV spectrin, a new spectrin localized at axon initial segments and nodes of Ranvier in the central and peripheral nervous system,” *The Journal of Cell Biology*, vol. 151, no. 5, pp. 985–1002, 2000.
- [14] P. Imbrici, D. C. Camerino, and D. Tricarico, “Major channels involved in neuropsychiatric disorders and therapeutic perspectives,” *Frontiers in Genetics*, vol. 4, p. 76, 2013.
- [15] F. Sicca, P. Imbrici, M. C. D’Adamo et al., “Autism with seizures and intellectual disability: possible causative role of gain-of-function of the inwardly-rectifying K^+ channel Kir4.1,” *Neurobiology of Disease*, vol. 43, no. 1, pp. 239–247, 2011.
- [16] L. de la Torre-Ubieta, H. Won, J. L. Stein, and D. H. Geschwind, “Advancing the understanding of autism disease mechanisms through genetics,” *Nature Medicine*, vol. 22, no. 4, pp. 345–361, 2016.
- [17] A. Dufflocq, F. Chareyre, M. Giovannini, F. Couraud, and M. Davenne, “Characterization of the axon initial segment (AIS) of motor neurons and identification of a para-AIS and a juxtapara-AIS, organized by protein 4.1B,” *BMC Biology*, vol. 9, no. 1, p. 66, 2011.
- [18] A. Lorincz and Z. Nusser, “Molecular identity of dendritic voltage-gated sodium channels,” *Science*, vol. 328, no. 5980, pp. 906–909, 2010.
- [19] A.-H. Song, D. Wang, G. Chen et al., “A selective filter for cytoplasmic transport at the axon initial segment,” *Cell*, vol. 136, no. 6, pp. 1148–1160, 2009.
- [20] M. H. P. Kole, S. U. Ilschner, B. M. Kampa, S. R. Williams, P. C. Ruben, and G. J. Stuart, “Action potential generation requires a high sodium channel density in the axon initial segment,” *Nature Neuroscience*, vol. 11, no. 2, pp. 178–186, 2008.
- [21] W. Hu, C. Tian, T. Li, M. Yang, H. Hou, and Y. Shu, “Distinct contributions of $Na_v1.6$ and $Na_v1.2$ in action potential initiation and backpropagation,” *Nature Neuroscience*, vol. 12, no. 8, pp. 996–1002, 2009.
- [22] I. Ogiwara, H. Miyamoto, N. Morita et al., “ $Na_v1.1$ localizes to axons of parvalbumin-positive inhibitory interneurons: a circuit basis for epileptic seizures in mice carrying an *Scn1a* gene mutation,” *Journal of Neuroscience*, vol. 27, no. 22, pp. 5903–5914, 2007.
- [23] M. Gardiner, “Genetics of idiopathic generalized epilepsies,” *Epilepsia*, vol. 46, no. s9, pp. 15–20, 2005.
- [24] P. W. Spratt, R. Ben-Shalom, C. M. Keeshen et al. et al., “The autism-associated gene *Scn2a* plays an essential role in synaptic stability and learning,” *bioRxiv*, vol. 366781, 2018.
- [25] Z. Chen, S. Chen, L. Chen et al., “Long-term increasing colocalization of SCN8A and ankyrin-G in rat hippocampal cornu ammonis 1 after pilocarpine induced status epilepticus,” *Brain Research*, vol. 1270, pp. 112–120, 2009.
- [26] H. Kaphzan, S. A. Buffington, J. I. Jung, M. N. Rasband, and E. Klann, “Alterations in intrinsic membrane properties and the axon initial segment in a mouse model of Angelman syndrome,” *Journal of Neuroscience*, vol. 31, no. 48, pp. 17637–17648, 2011.
- [27] R. Ben-Shalom, C. M. Keeshen, K. N. Berrios, J. Y. An, S. J. Sanders, and K. J. Bender, “Opposing effects on $Na_v1.2$ function underlie differences between SCN2A variants observed in individuals with autism spectrum disorder or infantile seizures,” *Biological Psychiatry*, vol. 82, no. 3, pp. 224–232, 2017.
- [28] M. Rubinstein, A. Patowary, I. B. Stanaway et al., “Association of rare missense variants in the second intracellular loop of $Na_v1.7$ sodium channels with familial autism,” *Molecular Psychiatry*, vol. 23, no. 2, pp. 231–239, 2018.
- [29] P. Agre, E. P. Orringer, and V. Bennett, “Deficient red-cell spectrin in severe, recessively inherited spherocytosis,” *The New England Journal of Medicine*, vol. 306, no. 19, pp. 1155–1161, 1982.
- [30] V. Bennett and D. N. Lorenzo, “An adaptable spectrin/ankyrin-based mechanism for long-range organization of plasma membranes in vertebrate tissues,” in *Current Topics in Membranes*, pp. 143–184, Elsevier, 2016.
- [31] S. M. Jenkins and V. Bennett, “Ankyrin-G coordinates assembly of the spectrin-based membrane skeleton, voltage-gated sodium channels, and L1 CAMs at Purkinje neuron initial segments,” *The Journal of Cell Biology*, vol. 155, no. 5, pp. 739–746, 2001.
- [32] E. Kordeli, S. Lambert, and V. Bennett, “Ankyrin_G. A new ankyrin gene with neural-specific isoforms localized at the axonal initial segment and node of Ranvier,” *Journal of Biological Chemistry*, vol. 270, no. 5, pp. 2352–2359, 1995.
- [33] M.-P. Fache, A. Moussif, F. Fernandes, P. Giraud, J. J. Garrido, and B. Dargent, “Endocytotic elimination and domain-selective tethering constitute a potential mechanism of protein segregation at the axonal initial segment,” *The Journal of Cell Biology*, vol. 166, no. 4, pp. 571–578, 2004.
- [34] M. N. Rasband, “The axon initial segment and the maintenance of neuronal polarity,” *Nature Reviews Neuroscience*, vol. 11, no. 8, pp. 552–562, 2010.
- [35] K. L. Hedstrom, X. Xu, Y. Ogawa et al., “Neurofascin assembles a specialized extracellular matrix at the axon initial segment,” *The Journal of Cell Biology*, vol. 178, no. 5, pp. 875–886, 2007.
- [36] D. Zhou, S. Lambert, P. L. Malen, S. Carpenter, L. M. Boland, and V. Bennett, “AnkyrinG is required for clustering of voltage-gated Na channels at axon initial segments and for normal action potential firing,” *The Journal of Cell Biology*, vol. 143, no. 5, pp. 1295–1304, 1998.
- [37] S. L. Jones and T. M. Svitkina, “Axon initial segment cytoskeleton: architecture, development, and role in neuron polarity,” *Neural Plasticity*, vol. 2016, Article ID 6808293, 19 pages, 2016.

- [38] C. Bi, J. Wu, T. Jiang et al., "Mutations of ANK3 identified by exome sequencing are associated with autism susceptibility," *Human Mutation*, vol. 33, no. 12, pp. 1635–1638, 2012.
- [39] Z. Iqbal, G. Vandeweyer, M. van der Voet et al., "Homozygous and heterozygous disruptions of ANK3: at the crossroads of neurodevelopmental and psychiatric disorders," *Human Molecular Genetics*, vol. 22, no. 10, pp. 1960–1970, 2013.
- [40] L. Shi, X. Zhang, R. Golhar et al., "Whole-genome sequencing in an autism multiplex family," *Molecular Autism*, vol. 4, no. 1, p. 8, 2013.
- [41] S. J. Sanders, M. T. Murtha, A. R. Gupta et al., "De novo mutations revealed by whole-exome sequencing are strongly associated with autism," *Nature*, vol. 485, no. 7397, pp. 237–241, 2012.
- [42] M. Ford-Perriss, H. Abud, and M. Murphy, "Fibroblast growth factors in the developing central nervous system," *Clinical and experimental pharmacology & physiology*, vol. 28, no. 7, pp. 493–503, 2001.
- [43] C. A. Turner, S. J. Watson, and H. Akil, "The fibroblast growth factor family: neuromodulation of affective behavior," *Neuron*, vol. 76, no. 1, pp. 160–174, 2012.
- [44] E. Esnafoglu and S. N. Ayyildiz, "Decreased levels of serum fibroblast growth factor-2 in children with autism spectrum disorder," *Psychiatry Research*, vol. 257, pp. 79–83, 2017.
- [45] S. K. Olsen, M. Garbi, N. Zampieri et al., "Fibroblast growth factor (FGF) homologous factors share structural but not functional homology with FGFs," *The Journal of Biological Chemistry*, vol. 278, no. 36, pp. 34226–34236, 2003.
- [46] F. Laezza, B. R. Gerber, J. Y. Lou et al., "The *FGF14*^{F145S} mutation disrupts the interaction of FGF14 with voltage-gated Na⁺ channels and impairs neuronal excitability," *Journal of Neuroscience*, vol. 27, no. 44, pp. 12033–12044, 2007.
- [47] M. K. Bosch, Y. Carrasquillo, J. L. Ransdell, A. Kanakamedala, D. M. Ornitz, and J. M. Nerbonne, "Intracellular FGF14 (iFGF14) is required for spontaneous and evoked firing in cerebellar Purkinje neurons and for motor coordination and balance," *The Journal of Neuroscience*, vol. 35, no. 17, pp. 6752–6769, 2015.
- [48] F. Laezza, A. Lampert, M. A. Kozel et al., "FGF14 N-terminal splice variants differentially modulate Nav1.2 and Nav1.6-encoded sodium channels," *Molecular and Cellular Neuroscience*, vol. 42, no. 2, pp. 90–101, 2009.
- [49] J.-Y. Lou, F. Laezza, B. R. Gerber et al., "Fibroblast growth factor 14 is an intracellular modulator of voltage-gated sodium channels," *The Journal of Physiology*, vol. 569, no. 1, pp. 179–193, 2005.
- [50] Q. Wang, M. E. Bardgett, M. Wong et al., "Ataxia and paroxysmal dyskinesia in mice lacking axonally transported FGF14," *Neuron*, vol. 35, no. 1, pp. 25–38, 2002.
- [51] M. A. Alshammari, T. K. Alshammari, M. N. Nenov, F. Scala, and F. Laezza, "Fibroblast growth factor 14 modulates the neurogenesis of granule neurons in the adult dentate gyrus," *Molecular Neurobiology*, vol. 53, no. 10, pp. 7254–7270, 2016.
- [52] T. K. Alshammari, M. A. Alshammari, M. N. Nenov et al., "Genetic deletion of fibroblast growth factor 14 recapitulates phenotypic alterations underlying cognitive impairment associated with schizophrenia," *Translational Psychiatry*, vol. 6, no. 5, article e806, 2016.
- [53] D. H. Ebert and M. E. Greenberg, "Activity-dependent neuronal signalling and autism spectrum disorder," *Nature*, vol. 493, no. 7432, pp. 327–337, 2013.
- [54] J. M. Jasien, C. M. Daimon, R. Wang, B. K. Shapiro, B. Martin, and S. Maudsley, "The effects of aging on the BTBR mouse model of autism spectrum disorder," *Frontiers in Aging Neuroscience*, vol. 6, p. 225, 2014.
- [55] D. M. Jones-Davis, M. Yang, E. Rider et al., "Quantitative trait loci for interhemispheric commissure development and social behaviors in the BTBR T⁺*tf/J* mouse model of autism," *PLoS One*, vol. 8, no. 4, article e61829, 2013.
- [56] M. A. Alshammari, T. K. Alshammari, and F. Laezza, "Improved methods for fluorescence microscopy detection of macromolecules at the axon initial segment," *Frontiers in Cellular Neuroscience*, vol. 10, p. 5, 2016.
- [57] K. B. J. Franklin and G. Paxinos, *Paxinos and Franklin's the Mouse Brain in Stereotaxic Coordinates*, vol. 1, Academic Press, an imprint of Elsevier, Amsterdam, Fourth edition. ed edition, 2013.
- [58] F. Tempia, E. Hoxha, G. Negro et al., "Parallel fiber to Purkinje cell synaptic impairment in a mouse model of spinocerebellar ataxia type 27," *Frontiers in Cellular Neuroscience*, vol. 9, p. 205, 2015.
- [59] M. D. Tang-Schomer, P. Davies, D. Graziano, A. E. Thurber, and D. L. Kaplan, "Neural circuits with long-distance axon tracts for determining functional connectivity," *Journal of Neuroscience Methods*, vol. 222, pp. 82–90, 2014.
- [60] S. B. Nelson and V. Valakh, "Excitatory/inhibitory balance and circuit homeostasis in autism spectrum disorders," *Neuron*, vol. 87, no. 4, pp. 684–698, 2015.
- [61] B. D. Clark, E. M. Goldberg, and B. Rudy, "Electrogenic tuning of the axon initial segment," *The Neuroscientist*, vol. 15, no. 6, pp. 651–668, 2009.
- [62] K. C. Kim, E. L. Gonzales, M. T. Lázaro et al., "Clinical and neurobiological relevance of current animal models of autism spectrum disorders," *Biomolecules & Therapeutics*, vol. 24, no. 3, pp. 207–243, 2016.
- [63] H. Barbas and B. Zikopoulos, "The prefrontal cortex and flexible behavior," *The Neuroscientist*, vol. 13, no. 5, pp. 532–545, 2007.
- [64] A. Duflocq, B. le Bras, E. Bullier, F. Couraud, and M. Davenne, "Nav1.1 is predominantly expressed in nodes of Ranvier and axon initial segments," *Molecular and Cellular Neuroscience*, vol. 39, no. 2, pp. 180–192, 2008.
- [65] A. Lorincz and Z. Nusser, "Cell-type-dependent molecular composition of the axon initial segment," *Journal of Neuroscience*, vol. 28, no. 53, pp. 14329–14340, 2008.
- [66] D. Pal, J. M. Jones, S. Wisidagamage, M. H. Meisler, and G. A. Mashour, "Reduced Na_v1.6 sodium channel activity in mice increases *in vivo* sensitivity to volatile anesthetics," *PLoS One*, vol. 10, no. 8, article e0134960, 2015.
- [67] M. Royeck, M.-T. Horstmann, S. Remy, M. Reitze, Y. Yaari, and H. Beck, "Role of axonal Na_v1.6 sodium channels in action potential initiation of CA1 pyramidal neurons," *Journal of Neurophysiology*, vol. 100, no. 4, pp. 2361–2380, 2008.
- [68] L. A. Weiss, A. Escayg, J. A. Kearney et al., "Sodium channels *SCN1A*, *SCN2A* and *SCN3A* in familial autism," *Molecular Psychiatry*, vol. 8, no. 2, pp. 186–194, 2003.
- [69] C. S. Cheah, F. H. Yu, R. E. Westenbroek et al., "Specific deletion of Na_v1.1 sodium channels in inhibitory interneurons causes seizures and premature death in a mouse model of

- Dravet syndrome,” *Proceedings of the National Academy of Sciences of the United States of America*, vol. 109, no. 36, pp. 14646–14651, 2012.
- [70] W. Wang, F. Atianjoh, E. B. Gauda, M. Yaster, Y. Li, and Y.-X. Tao, “Increased expression of sodium channel subunit Nav1.1 in the injured dorsal root ganglion after peripheral nerve injury,” *Anatomical Record*, vol. 294, no. 8, pp. 1406–1411, 2011.
- [71] C. Pescucci, R. Caselli, S. Grosso et al., “2q24-q31 deletion: report of a case and review of the literature,” *European Journal of Medical Genetics*, vol. 50, no. 1, pp. 21–32, 2007.
- [72] N. Ramoz, G. Cai, J. G. Reichert, J. M. Silverman, and J. D. Buxbaum, “An analysis of candidate autism loci on chromosome 2q24-q33: evidence for association to the *STK39* gene,” *American Journal of Medical Genetics Part B: Neuropsychiatric Genetics*, vol. 147B, no. 7, pp. 1152–1158, 2008.
- [73] S. Han, C. Tai, R. E. Westenbroek et al., “Autistic-like behaviour in *Scn1a*^{+/-} mice and rescue by enhanced GABA-mediated neurotransmission,” *Nature*, vol. 489, no. 7416, pp. 385–390, 2012.
- [74] V. Bennett and A. J. Baines, “Spectrin and ankyrin-based pathways: metazoan inventions for integrating cells into tissues,” *Physiological Reviews*, vol. 81, no. 3, pp. 1353–1392, 2001.
- [75] M. S. Grubb and J. Burrone, “Activity-dependent relocation of the axon initial segment fine-tunes neuronal excitability,” *Nature*, vol. 465, no. 7301, pp. 1070–1074, 2010.
- [76] O. Durak, F. C. de Anda, K. K. Singh et al., “Ankyrin-G regulates neurogenesis and Wnt signaling by altering the subcellular localization of β -catenin,” *Molecular Psychiatry*, vol. 20, no. 3, pp. 388–397, 2015.
- [77] M. Xiao, M. K. Bosch, J. M. Nerbonne, and D. M. Ornitz, “FGF14 localization and organization of the axon initial segment,” *Molecular and Cellular Neurosciences*, vol. 56, pp. 393–403, 2013.
- [78] K. Susuki and M. N. Rasband, “Molecular mechanisms of node of Ranvier formation,” *Current Opinion in Cell Biology*, vol. 20, no. 6, pp. 616–623, 2008.
- [79] J. L. Salzer, P. J. Brophy, and E. Peles, “Molecular domains of myelinated axons in the peripheral nervous system,” *Glia*, vol. 56, no. 14, pp. 1532–1540, 2008.
- [80] M. C. Inda, J. DeFelipe, and A. Munoz, “Voltage-gated ion channels in the axon initial segment of human cortical pyramidal cells and their relationship with chandelier cells,” *Proceedings of the National Academy of Sciences of the United States of America*, vol. 103, no. 8, pp. 2920–2925, 2006.
- [81] C. Zweier, E. K. de Jong, M. Zweier et al., “*CNTNAP2* and *NRXN1* are mutated in autosomal-recessive Pitt-Hopkins-like mental retardation and determine the level of a common synaptic protein in *Drosophila*,” *American Journal of Human Genetics*, vol. 85, no. 5, pp. 655–666, 2009.
- [82] M. J. Berridge, “Inositol trisphosphate and calcium signalling,” *Nature*, vol. 361, no. 6410, pp. 315–325, 1993.
- [83] B. I. Hutchins, L. Li, and K. Kalil, “Wnt/calcium signaling mediates axon growth and guidance in the developing corpus callosum,” *Developmental Neurobiology*, vol. 71, no. 4, pp. 269–283, 2011.